Detection of cross-contamination and strong mitonuclear discordance in two species groups of sawfly genus *Empria* (Hymenoptera, Tenthredinidae)

Marko Prous[a,b,*,#], Kyung Min Lee[c,#], Marko Mutanen[c]

[a] Senckenberg Deutsches Entomologisches Institut, Eberswalder Straße 90, 15374 Müncheberg, Germany
[b] Department of Zoology, Institute of Ecology and Earth Sciences, University of Tartu, Vanemuise 46, 51014, Tartu, Estonia
[c] Ecology and Genetics Research Unit, University of Oulu, PO Box 3000, FI-90014, University of Oulu, Finland

[*] Corresponding author at: Senckenberg Deutsches Entomologisches Institut, Eberswalder Straße 90, 15374 Müncheberg, Germany.
E-mail address: mprous@ut.ee (M. Prous).

[#] Joint first authorship.

Keywords:
COI barcoding
DNA barcode sharing
Phylogenomics
Species delimitation

Abstract

In several sawfly taxa strong mitonuclear discordance has been observed, with nuclear genes supporting species assignments based on morphology, whereas the barcode region of the mitochondrial COI gene suggesting different relationships. As previous studies were based on only few nuclear genes, the causes and the degree of mitonuclear discordance remain ambiguous. Here, we obtain genomic-scale ddRAD data together with Sanger sequencing of mitochondrial COI and two to three nuclear protein coding genes to investigate species limits and mitonuclear discordance in two closely related species groups within the sawfly genus *Empria*. As found previously based on nuclear ITS and mitochondrial COI sequences, species are in most cases supported as monophyletic based on previous and new nuclear data reported here, but not based on mitochondrial COI. This mitonuclear discordance can be explained by occasional mitochondrial introgression with little or no nuclear gene flow, a pattern that might be common in haplodiploid taxa with slowly evolving mitochondrial genomes. Some species in *E. immersa* group are not recovered as monophyletic also based on nuclear data, but this could partly be because of unresolved taxonomy. Preliminary analyses of ddRAD data did not recover monophyly of *E. japonica* within *E. longicornis* group (three Sanger sequenced nuclear genes strongly supported monophyly), but closer examination of the data and additional Sanger sequencing suggested that both specimens were substantially (possibly 10–20% of recovered loci) cross-contaminated. A reason could be due to specimen identification tag jumps during sequencing library preparation of pooled specimens that in previous studies have been shown to affect up to 2.5% of the sequenced reads. We provide an R script to examine patterns of identical loci among the specimens and estimate that cross-contamination rate is not unusually high for our ddRAD dataset as a whole (based on counting identical sequences between *immersa* and *longicornis* groups that are well separated from each other and probably do not hybridise). The high rate of cross-contamination for both *E. japonica* specimens might be explained by small number of recovered loci (~1000)

compared to most other specimens (>10 000 in some cases) because of poor sequencing results. We caution drawing unexpected biological conclusions when closely related specimens are pooled before sequencing and tagged only at one end of the molecule or at both ends using unique combination of limited number of tags (less than the number of specimens).

1. Introduction

Continuing developments in high-throughput sequencing technologies and falling of prices makes it increasingly easier to collect genome-scale data for many non-model organisms. The large amount of data that could be obtained with high-throughput next generation sequencing methods makes it possible to answer many biological questions simultaneously (in phylogeny, population genetics, evolutionary ecology etc.) and in higher resolution than would be possible with more traditional methods (e.g. Sanger sequencing of one or few markers, genotyping by microsatellites etc.). However, the large amount of data that is generated with next generation sequencing methods introduces its own problems that are hardly relevant when only few markers are analysed. Genome-scale or phylogenomic datasets are plagued mainly by two types or errors: data errors and systematic errors (Philippe et al., 2017). Data errors, such as assembly and alignment artefacts or contaminants for example, are easy to control for in single-gene scale datasets, but prohibitive in genome-scale datasets if done manually. Because automated methods of dataset assembly are not (yet) perfect, some data errors are nearly always introduced in phylogenomic datasets. Even if the dataset is perfectly assembled (all contaminants and non-homologous alignments excluded), one still has to consider systematic errors (e.g. biases in nucleotide or amino acid composition, unequal rates of evolution) which only increase with dataset size and therefore could seriously mislead phylogenomic analyses, although this problem becomes critical only when dealing with ancient divergences (tens and more millions of years ago) (Philippe et al., 2017, 2005; Tarver et al., 2016).

DNA barcoding of single molecular marker for the purpose of species identification can also benefit from high-throughput sequencing, as hundreds or thousands individuals could be sequenced simultaneously (e.g. Cruaud et al., 2017; Hebert et al., 2018; Meier et al., 2016). For animals, a ~650 bp fragment from 5' end of the mitochondrial cytochrome c oxidase I (COI) has been chosen as the standard barcoding marker (Hebert et al., 2003), which by now has been sequenced from more than five million individuals according to Barcode of Life (BOLD) database (www.boldsystems.org). Although this short mitochondrial fragment seems to be suitable in most species rich groups, such as Coleoptera and Lepidoptera (Mutanen et al., 2016; Pentinsaari et al., 2017; Zahiri et al., 2017), rampant mitochondrial introgression is also known in some groups (Sloan et al., 2017). In some cases the usefulness of COI sequences is not clear due to lack of sequencing efforts and / or taxonomic research. For example, while large-scale COI sequencing efforts have been applied also to many hyperdiverse insect groups, congruence with sufficiently informative nuclear genes and / or morpho-taxonomy has not always been evaluated (Alex Smith et al., 2013; Hebert et al., 2016). Nevertheless, some theoretical considerations can give indications in which cases mitonuclear discordances could be expected at increased rate (Ivanov et al., 2018; Sloan et al., 2017). Particularly, Patten et al. (2015) found recently through theoretical modelling that haplodiploid species may be especially prone to biased mitochondrial introgression, which could be amplified by several other adaptive and non-adaptive conditions (reviewed by Sloan et al., 2017). The most species rich group (at least in terms of described species) of haplodiploid animals is Hymenoptera (sawflies, ants, bees, and wasps) and could therefore be a good candidate for investigating mitochondrial introgression and utility of mitochondrial barcodes. Besides haplodiploidy, mutation rate of mitochondrial DNA (mtDNA) could also be a factor affecting rate of mitochondrial introgression. Sloan et al. (2017) suggested that lower mutation rates promote adaptive mitochondrial introgression while higher rates lead more likely to compensatory co-

evolution and mitonuclear incompatibilities. As mitochondrial genomes of Apocrita (the bulk of hymenopteran species) evolve faster than those of basal hymenopterans (Kaltenpoth et al., 2012; Ma et al., 2019; Niu et al., 2019; Tang et al., 2019), mitochondrial introgression might be less common in Apocrita compared to sawflies. Within the sawflies, Xyeloidea, Pamphilioidea, and Tenthredinoidea have the slowest evolving mtDNA, while Cephoidea, Orussoidea, Siricoidea, and possibly Anaxyleoidea (which are more closely related to Apocrita), have intermediate or fast evolutionary rate (Ma et al., 2019; Niu et al., 2019; Tang et al., 2019). While we are not aware of cases of large-scale discordance between mitochondrial barcodes and species boundaries in Apocrita, there are several such cases among sawflies, particularly among Tenthredinoidea (Linnen and Farrell, 2007; Schmidt et al., 2017). However, in all those cases discordance were identified based on morphology and COI barcodes or morphology plus few nuclear genes and COI barcodes, and it is likely that in some cases operational factors, such as over-splitting of species, are involved too (cf. Mutanen et al., 2016).

Here we investigate based on genome-scale data the phylogeny and species limits in two closely related species groups (divergence probably not more than few million years) within the sawfly genus *Empria* Lepeletier & Serville, 1828 (Hymenoptera, Tenthredinidae). The genus includes at least 60 species, several of which are still undescribed (Prous, 2012). Most species in the genus are externally rather similar to each other, which makes species identification difficult. However, the differences in the structure of ovipositors and penis valves are often very clear even between closely related species (Prous, 2012).

Taxonomic and limited phylogenetic studies on the genus have revealed two species complexes (*longicornis* and *immersa* groups) where species delimitation has been especially problematic (Prous, 2012; Prous et al., 2014, 2011b). Based on morphology, the main evidence indicating the presence of more than one species in both of the groups, is the structure of the female ovipositor, which often shows clear differences between species and which correlates with host plant use (Prous, 2012; Prous et al., 2011b). Species in *longicornis* group specialise on different herbaceous genera in Rosaceae (specifically in subfamily Rosoideae and genus *Dryas*) and species in *immersa* group on *Betula* or *Salix*. Differences in other morphological characters (including male genitalia) are rather weak between the species, but can nevertheless be helpful in species identification. While sequencing of mitochondrial COI gene did not reveal any correlation with species boundaries defined based on morphological and ecological data, nuclear ITS (internal transcribed spacers 1 and 2) sequence data did (Prous, 2012; Prous et al., 2011b). Discord between mitochondrial and morphological plus nuclear ITS data in these groups is quite remarkable: different species frequently have identical COI barcodes (658 bp) or even complete (1536 bp) COI gene (Prous et al., 2011b), while at the same time different specimens of the same species can diverge by 3.3% in the barcoding region. To better understand this discord and to test species boundaries in *longicornis* and *immersa* groups, we collected genome-wide data using double digest RADseq (Lee et al., 2018; Peterson et al., 2012) and sequenced long fragments of two to three nuclear protein coding genes.

Results showed that in some cases there were substantial amount of cross-contamination in RADseq data, which might have escaped detection without the knowledge of the organisms involved (based on morphological, ecological and single gene data) and initial manual checks. This cross-contamination had significant impact on the phylogenetic tree building and population admixture analyses. We developed a workflow to detect possible cases of cross-contamination that could be excluded from downstream analyses.

2. Materials and methods

2.1. DNA extraction

For most specimens, DNA had been extracted as described in Prous et al. (2011b). New DNA extractions for this study were obtained with an EZNA Tissue DNA Kit (Omega Bio-tek) according to the manufacturer's protocol and stored at -20 °C for later use. Typically, the middle right leg was used for DNA extraction, but for males the whole genital capsule was often additionally used to increase DNA yield and to free penis valves from muscles for photography. Specimens that were selected for sequencing are listed in Table 1.

Table 1. Collecting data of *Empria* specimens selected for sequencing. CMH – Private collection of Mikk Heidemaa (Tartu, Estonia); DEI - Senckenberg Deutsches Entomologisches Institut, Müncheberg, Germany; ISEA - Institute of Systematics and Ecology of Animals, Russian Academy of Sciences, Novosibirsk, Russia; IZBE - Estonian University of Life Sciences, Tartu, Estonia; LOENNV - Private collection Ole Lønnve, Oslo, Norway; TUZ - University of Tartu, Tartu, Estonia; UOG - University of Guelph, Guelph, Canada; USNM - Smithsonian Institution, National Museum of Natural History, Washington DC, USA; ZIN - Zoological Institute, Russian Academy of Sciences, Saint Petersburg, Russia.

Specimen ID	Group	Species	Sex	Country	Decimal coordinates	Collecting date	Collected by	Collection
DEI-GISHym20706	immersa	E. camtschatica	male	Sweden	62.435N 13.835E	2013-06-07	Liston, Prous & Taeger	DEI
DEI-GISHym80070	immersa	E. camtschatica	female	Sweden	67.212N 23.497E	2014-06-10	A. Taeger	DEI
BIOUG00998-E05	immersa	E. fletcheri	male	Canada	58.754N 93.997W	2010-06-17	J. Wang	UOG
BIOUG17274-F06	immersa	E. fletcheri	male	Canada	60.714N 137.432W	2014-07-02	C. Wong	UOG
DEI-GISHym31039	immersa	E. fletcheri	male	Sweden	66.035N 22.16E	2014-05-28	A. Liston & M. Prous	DEI
TUZ615113	immersa	E. fletcheri	male	UK	56.99237N 3.50222W	2010-06-04	M. Prous	TUZ
TUZ615334	immersa	E. fletcheri	male	Estonia	59.1028N 25.4983E	2011-05-22	M. Prous	TUZ
DEI-GISHym80045	immersa	E. immersa	male	Sweden	66.166N 23.495E	2014-06-01	A. Liston & M. Prous	DEI
DEI-GISHym80071	immersa	E. immersa	male	Sweden	66.534N 19.721E	2014-06-11	A. Taeger	DEI
TUZ615623	immersa	E. immersa	male	Finland	65.078N 25.482E	2012-06-22	M. Prous	TUZ
BIOUG00998-B05	immersa	E. improba	female	Canada	58.626N 94.229W	2010-06-16	J. Wang	UOG
BIOUG00998-D05	immersa	E. improba	male	Canada	58.626N 94.229W	2010-06-13	J. Wang	UOG
BIOUG00998-D06	immersa	E. improba	female	Canada	58.626N 94.229W	2010-06-13	J. Wang	UOG
BIOUG00998-C05	immersa	E. plana	male	Canada	58.754N 93.997W	2010-06-28	J. Wang	UOG
DEI-GISHym15478	immersa	E. plana	female	Sweden	62.435N 13.835E	2013-06-07	Liston, Prous & Taeger	DEI
TUZ615181	immersa	E. plana	female	Japan	43.4166N 142.68066E	2009-06-24	A. Shinohara	TUZ
DEI-GISHym80142	longicornis	E. alector	male	Germany	48.908N 10.008E	2016-05-07	SDEI	DEI
TUZ615036	longicornis	E. alector	male	Estonia	57.774N 26.339E	2008-05-03	M. Prous	TUZ
TUZ615121	longicornis	E. alector	male	Estonia	59.22889N 25.31694E	2009-05-17	M. Prous	TUZ
TUZ615220	longicornis	E. alector	female	Estonia	58.884N 22.636E	2008-05-31	M. Prous	TUZ
DEI-GISHym15214	longicornis	E. alpina	male	Sweden	68.362N 18.723E	2012-07-05	A.D. Liston & A. Taeger	DEI
DEI-GISHym80011	longicornis	E. alpina	male	Russia	52.80771N 93.28815E	2011-06-20	E. V. Borisova	ISEA
DEI-GISHym80106	longicornis	E. alpina	male	Sweden	68.409N 18.639E	2016-07-01	A. Liston & M. Prous	DEI
DEI-GISHym14890	longicornis	E. basalis	female	Slovakia	48.9695N 19.65E	2005-06-22	A. Taeger	DEI
OL10-02	longicornis	E. basalis	male	Norway	59.95N 9.03333E	2010-05-24/2010-07-14	O. Lonnve	LOENNV

TUZ615083	longicornis	E. basalis	female	Estonia	57.653N 26.242E	2008-05-03	M. Prous	TUZ
TUZ615141	longicornis	E. basalis	male	UK	56.5253N 4.2911W	2010-06-05	M. Prous	TUZ
TUZ615625	longicornis	E. basalis	female	Finland	65.0775N 25.4915E	2012-06-22	M. Prous	TUZ
TUZ615162	longicornis	E. japonica	female	Japan	43.647N 142.791E	2008-06-22	A. Shinohara	TUZ
USNM2051678_003	longicornis	E. japonica	male	Japan	43.6667N 143.1E	2008-06-06/2008-06-27	A. Ueda	USNM
USNM2051678_038	longicornis	E. japonica	male	Japan	43.6667N 143.1E	2008-06-06/2008-06-27	A. Ueda	USNM
TUZ615180	longicornis	E. loktini	female	Japan	43.647N 142.791E	2008-06-22	A. Shinohara	TUZ
DEI-GISHym14886	longicornis	E. longicornis	male	Slovakia	49.01183N 19.823E	2005-06-19	A. Taeger	DEI
TUZ615022	longicornis	E. longicornis	male	France	45.587N 2.824E	2008-05-22	M. Prous	TUZ
TUZ615057	longicornis	E. longicornis	larva [b]	Estonia	58.444N 26.653E	2006-05-25	M. Prous	TUZ
DEI-GISHym21189	longicornis	E. minuta	female	Sweden	65.82N 24.033E	2014-06-03	A. Liston & M. Prous	DEI
IZBE0350001	longicornis	E. minuta	male	Estonia	58.329N 26.94E	2009-04-19/2009-05-02	O. Kurina	IZBE
MH10-01	longicornis	E. minuta	male	Estonia	58.41N 26.5511E	2010-04-12/2010-04-30	M. Heidemaa	CMH
DEI-GISHym80040	longicornis	E. montana	male	Russia	52.80771N 93.28815E	2011-06-20	E. V. Borisova	ISEA
ZIN_Hym_1796001 [a]	longicornis	E. montana	male	Russia	61.9N 149.5E	1987-07-09/1987-07-15	A. Zinovjev	ZIN
ZIN_Hym_1796002 [a]	longicornis	E. montana	female	Russia	61.9N 149.5E	1987-07-09/1987-07-15	A. Zinovjev	ZIN
USNM2051678_040	longicornis	E. sp11	male	Japan	43.6667N 143.1E	2008-06-06/2008-06-27	A. Ueda	USNM
DEI-GISHym15231	longicornis	E. sp14	female	Austria	47.52299N 13.69299E	2011-06-30	Blank, Liston & Taeger	DEI
MH11-01	longicornis	E. sp14	male	France	42.74333N 0.09339E	2011-05-28	M. Heidemaa	CMH
DEI-GISHym20872	longicornis	E. tridens	larva	Germany	49.61689N 7.91258E	2013-07-05	K. B„hner	DEI
TUZ615023	longicornis	E. tridens	larva [b]	Estonia	58.483N 26.483E	2007-05-13	M. Prous	TUZ
TUZ615027	longicornis	E. tridens	larva [b]	Estonia	59.208N 25.571E	2006-05-07	M. Prous	TUZ
TUZ615037	longicornis	E. tridens	male	France	45.587N 2.824E	2008-05-22	M. Prous	TUZ
TUZ615165	longicornis	E. tridens	male	Switzerland	46.091N 9.013E	2009-05-27	M. Prous	TUZ
TUZ615624	longicornis	E. tridens	male	Finland	65.078N 25.482E	2012-06-22	M. Prous	TUZ
USNM2057434_19	longicornis	E. tridens	male	Japan	43.0667N 142.6833E	2009-06-05/2009-06-25	A. Ueda	USNM
DEI-GISHym86125 [a]	outgroup	E. gelida	female	Russia	43.694N 132.168E	2016-05-19	Kramp, Prous & Taeger	DEI
TUZ615182	outgroup	E. tridentis	male	Japan	43.647N 142.791E	2008-06-22	A. Shinohara	TUZ

[a] – For these specimens no attempt to obtain ddRAD data was made.
[b] – Collecting data is of the female, from which the larva was reared.

2.2. Sanger sequencing

To test congruence between mitochondrial and nuclear gene trees and to compare results based on Sanger sequencing of small number of genes with the genome-scale ddRAD sequencing, we initially amplified fragments of three genes, one mitochondrial and two nuclear. The mitochondrial gene used is complete (amplified and sequenced as described in Prous et al., 2011b) or partial cytochrome oxidase subunit I (COI). For most specimens, the sequenced fragment is at least 1078 bp. One specimen (BIOUG00998-B05, GenBank accession JX830389) had only the 658 bp fragment corresponding to the standard barcode region of the animal kingdom (Hebert et al., 2003). Complete or partial COI barcode sequences of three specimens (BIOUG17274-F06, BIOUG00998-D06, BIOUG00998-B05) were available in BOLD (http://www.boldsystems.org/), two of which were extended to 1078 bp by doing new DNA extractions, amplifications, and sequencing. The two nuclear markers are fragments of sodium/potassium-transporting ATPase subunit alpha (NaK) and DNA dependent RNA polymerase II subunit RPB1 (POL2). The NaK fragment used is a nearly complete sequence of its longest exon, 1654 bp. The POL2 fragment used is composed of two partial exons and one short intron that did not vary in length (87 bp) in the specimens studied here, altogether 2494–2710 bp, depending on the primer set used. After the first analyses of ddRAD data, we suspected cross-contamination in *Empria japonica*. To test this, we selected two variable candidate RAD loci that we suspected to be contaminated in *E. japonica* and designed primers to amplify and re-sequence these regions. One of the selected loci turned out to be a fragment of the zinc finger CCCH domain-containing protein 14 (ZC3H14) for which we designed additional primers to amplify its longest exon (containing also the ddRAD locus), varying between 1582–1639 bp in the studied specimens. For the second candidate locus (anonymous), quite a similar (around 80%) match was found only among the WGS (whole genome shotgun) contigs of *Neodiprion lecontei* (scaffold_346, GenBank accession LGIB01000346). This locus might be non-coding because of apparent frame-shifting indels in some ddRAD sequences, but was of the same length in the PCR amplified specimens, 138 bp. Primers used for amplification and sequencing are listed in Table 2. New POL2 and ZC3H14 primers (Table 2) were designed based on WGS contigs of four sawfly genomes (GenBank accessions AOFN01001568, LGIB01000323, AMWH01001469, AZGP01005167, AOFN02000929, LGIB01000132, AMWH01002139, AZGP02000664), sawfly transcriptomes published by Misof et al. (2014) and Peters et al. (2017), and based on POL2 sequences published by Malm and Nyman (2015). Numbers in the new POL2 and ZC3H14 primer names refer to the binding position of the primer's 3' end in the coding region of *Athalia rosae* mRNA (accessions XM_012395805 and XM_012401276). Primers for the anonymous locus were designed based on our ddRAD data.

PCR reactions were carried out in a total volume of 15–30 µl containing 1–2 µl of extracted DNA, 1.0–3.0 µl (5.0–15 pmol) of primers and 7.5–15 µl of 2x Multiplex PCR Plus Master mix (QIAGEN). The PCR protocol consisted of an initial DNA polymerase (HotStar Taq) activation step at 95 °C for 5 min, followed by 38–40 cycles of 30 s at 95 °C, 90 s at 49–59 °C depending on the primer set used, and 60–180 s (depending on the amplicon size) at 72 °C; the last cycle was followed by a final 30 min extension step at 68 °C. 3 µl of PCR product was visualised on a 1.4% agarose gel and then purified with FastAP and Exonuclease I (Thermo Scientific). 1.0–2.0 U of both enzymes were added to 12–27 µl of PCR solution and incubated for 15 min at 37 °C, followed by 15 min at 85 °C. 3–5 µl of purified PCR product per primer in a total volume of 10 µl (5–7 µl of sequencing primer at concentration 5 pmol/µl) were sent to Macrogen (Netherlands) for sequencing. Ambiguous positions (i.e. double peaks in chromatograms) due to heterozygosity or heteroplasmy were coded using IUPAC symbols. Sequences reported here have been deposited in the GenBank (NCBI) database (accession numbers MK299849–MK299982).

Table 2. Primers used for PCR and sequencing (preferred primers in bold), with information provided on respective gene fragment, primer name, direction (forward, F or reverse, R), primer sequence, standard PCR annealing temperature, utilization (PCR/ sequencing), and reference. Primer annealing temperatures used for sequencing at Macrogen were 47°C for COI and 50°C for nuclear genes.

Gene Region	Primer name	F/ R	Primer sequence 5′–3′	PCR annealing temperature (°)	PCR/ Sequencing	Reference
COI	**SymF1**	F	TTTCAACWAATCATAAARAYATTGG	47	PCR, seq	(Prous et al., 2016)
COI	**Sym-C1-J1718**	F	GGAGGATTTGGAAAYTGAYTAGTWCC	49	PCR, seq	(Nyman et al., 2006)
COI	**symC1-J1751**	F	GGAGCNCCTGATATAGCWTTYCC	47	Seq	(Prous et al., 2016)
COI	**SymR1**	R	TAAACTTCWGGRTGICCAAARAATC	47	PCR, seq	(Prous et al., 2016)
COI	SymR2	R	TAAACTTCTGGRTGTCCAAARAATCA	47	PCR, seq	(Prous et al., 2016)
COI	**A2590**	R	GCTCCTATTGATARWACATARTGRAAATG	49	PCR, seq	(Normark et al., 1999)
NaK	**NaK_263F**	F	CTYAGCCAYGCRAARGCRAARGA	59	PCR, seq	(Prous et al., 2017)
NaK	**NaK_809F**	F	GCWTTYTTCTCNACSAAYGCSGTNGARGG	55	PCR, seq	(Prous et al., 2017)
NaK	**NaK_907Ri**	R	TGRATRAARTGRTGRATYTCYTTIGC	54	PCR, seq	(Prous et al., 2017)
NaK	NaK_910R	R	TGRATRAARTGRTGRATYTCYTT	50	PCR, seq	(Prous et al., 2017)
NaK	**NaK_1250Fi**	F	ATGTGGTTYGAYAAYCARATYATIGA	56	PCR, seq	(Prous et al., 2017)
NaK	**NaKRev475**	R	TCGATRATYTGRTTRTCRAACCACAT	56	seq	(Leppänen et al., 2012)
NaK	**NaK_1498R**	R	ACYTGRTAYTTGTTNGTNGARTTRAA	52	PCR, seq	This study
NaK	**NaK_1918R**	R	GATTTGGCAATNGCTTTGGCAGTDAT	59	PCR, seq	(Prous et al., 2017)
POL2	POL2_104Fi	F	GYATGTCAGTYACNGATGGIGG	59	PCR, seq	This study
POL2	**POL2_104Fv2**	F	CGNATGTCNGTNACNGAYGGIGG	60	PCR, seq	This study
POL2	**POL2_574R**	R	TCYTCRTTNACRTGYTTCCAYTCNGC	59	seq	This study
POL2	POL2_599F	F	GARTGGAARCAYGTVAAYGARGA	54	PCR, seq	This study
POL2	**POL2_797F**	F	ATGTAYGGNTCNGCNAARAAYCARGA	58	PCR, seq	This study
POL2	POL2_889R	R	TGRAAYTGYARCATYTTWATRTTYTC	52	PCR, seq	This study
POL2	**POL2_928R**	R	GGCATNCCNGGCATRTCRTTRTCNAC	59	PCR, seq	This study
POL2	**POL2_1388F**	F	CAYAARATGAGTATGATGGG	51	PCR, seq	This study
POL2	POL2_1459R	R	TTCATYTCRTCNCCRTCRAARTC	52	PCR, seq	This study
POL2	**POL2_1706F**	F	TGGGAYGGNAARATGCCNCA	60	PCR, seq	This

			RCC			study
			ATCATRTTNACRTTNCCNGGD			This
POL2	POL2_1759R	R	ATDAT	55	PCR, seq	study
			GTRCTGTGIGTYCKDATCATRT			This
POL2	**POL2_1777Ri**	R	T	55	PCR, seq	study
						(Malm and
			ACNCACAGYACNCAYCCNGA			Nyman,
POL2	POL2 hym 3F	F	YGA	56	Seq	2015)
			CATTTYATHAARGAYGAYTAY			This
POL2	POL2_2423F	F	GG	51	Seq	study
			TTNACRGCRGTATCRATNAGA			This
POL2	**POL2_2509R**	R	CCYTC	60	PCR, seq	study
			GGATCRAAYTTRAAYTTYTTY			This
POL2	POL2_2725R	R	TC	50	PCR, seq	study
ZC3H1			TAGAGYGCNATYCGNGCNAA			This
4	**ZC3H14_59F**	F	RCT	58	PCR, seq	study
ZC3H1			TTYGTNGANTGGCTNCAYGAY			This
4	**ZC3H14_212F**	F	CARGT	60	Seq	study
ZC3H1			ATYCTNGGYTTRTTNACRCTN			This
4	**ZC3H14_838R**	R	GAYTT	55	PCR, seq	study
ZC3H1			AARTCNAGYGTNAAYAARCC			This
4	**ZC3H14_863F**	F	NAGRAT	55	PCR, seq	study
ZC3H1			GGYCTNGGNGTNACDATNAC			This
4	**ZC3H14_1696R**	R	YTTRCT	60	Seq	study
ZC3H1			ACVACNGAYTGRTTNGCYTCN			This
4	**ZC3H14_1780R**	R	GCRAC	60	PCR, seq	study
anony			ACACGTGATCAATAATAACGA			This
mous	Nlec346F	F	CT	55	PCR, seq	study
anony			ATCGTACAATGATTCGGGACT			This
mous	Nlec346R	R	AT	55	PCR, seq	study

2.3. ddRADseq library preparation and bioinformatics

The quantity of genomic DNA (gDNA) was checked using PicoGreen kit (Molecular Probes). To reach sufficient gDNA quality and quantity, whole genome amplification was performed using REPLI-g Mini kit (Qiagen) due to the low concentrations of gDNA. The ddRADseq library was implemented following protocols described in (Lee et al., 2018) with an exception: the size distribution and concentration of the pools were measured with Bioanalyzer (Agilent Technologies). The de-multiplexed *Empria* fastq data are archived in the NCBI SRA: PRJNA505249 (Lee, 2018).

Raw paired-end reads were demultiplexed with no mismatches tolerated using their unique barcode and adapter sequences using *ipyrad* v.0.7.23 (Eaton and Overcast, 2016). All *ipyrad* defaults were used, with the following exceptions: the minimum depth at which majority rule base calls are made was set to 3, the clustering threshold was set to 0.95, the minimum number of samples that must have data at a given locus for it to be retained was set to 4, and the assembly method was set to denovo and reference for independent testing. The reference assembly method is mapped reads to *Athalia rosae* genome sequences (GenBank, GCA_000344095) with BWA using the default bwa-mem setting (Li, 2013) based on 95% of sequence similarity.

2.4. Phylogenetic analysis

Maximum likelihood (ML) trees were inferred in RAxML v.8.2.0 or v8.2.10 (Stamatakis, 2014), with bootstrap support estimated by a 1,000 replicates rapid bootstrap analysis from the unpartitioned GTR+GAMMA model. We visualized the resulting phylogeny and assessed bootstrap support using FigTree v.1.4.2 (Rambaut, 2015).

Maximum parsimony (MP) analyses were conducted using PAUP* 4.0b10 program (Swofford, 2003). All heuristic searches were performed with 1,000 replicates, employed the

random addition of taxa, retained only the best tree, held 10 trees at each step using tree bisection-reconnection (TBR) branch swapping, collapsed zero-length branches, and using MULTREES. Bootstrap values were calculated using 1,000 replicates with the following options selected: heuristic search, TBR branch swapping, collapse of zero-length branches, and random-sequence-addition with one replicate.

Pairwise sequence divergence based on K2P distances were calculated using MEGA6 (Tamura et al., 2013) and the proportion of missing data was calculated using Mesquite (Maddison and Maddison, 2017). Net synonymous divergence between species was calculated with MEGA7 (Kumar et al., 2016).

2.5. Population structure and admixture

An admixture analysis was implemented in STRUCTURE v.2.3.1 (Pritchard et al., 2000) using SNP frequency data to better visualize genomic variation between individuals. Ten replicates were run at each value of *K* between 2 and 5 for *E. immersa* group and *K*=9 for *E. longicornis* group. Each run had a burn-in of 10K generations followed by 20K generations of sampling. We used StrAuto to automate Structure processing of samples (Chhatre and Emerson, 2017). Replicates were permuted in the program CLUMPP (Jakobsson and Rosenberg, 2007) according to the ad hoc ΔK statistics (Evanno et al., 2005), which is the second-order rate of change of the likelihood function. Structure results were visualized using the program DISTRUCT (Rosenberg, 2004).

We used four-taxon D-statistics (Durand et al., 2011) for introgression analysis. For the test, 1,000 bootstrap replicates were performed to measure the standard deviation of the D-statistics. Significance was evaluated by converting the Z-score (which represents the number of standard deviations from zero from D-statistics) into two tailed P-values, and using α=0.01 as a conservative cut-off for significance after correcting for multiple comparisons using Holm-Bonferroni correction. All D-statistics were calculated in pyRAD v.3.0.64 (Eaton, 2014). In order to run interactive data analysis, the Python Jupyter notebooks (http://jupyter.org) were used.

2.6. Cross-contamination detection

To detect identical loci between specimens or groups of specimens in ddRAD data, an R (R Core Team, 2017) script requiring a package *ape* (Paradis and Schliep, 2018) was written. The script takes as an input a text file containing alignments of ddRAD loci (output from *ipyrad*). A table is produced for every locus (rows) and specimen (columns) where cells contain list of specimens that are identical to a specimen indicated in the column (the cell is empty if there are no identical specimens for a particular specimen and locus). Additional columns are added to get information per locus about identical specimens between two groups, the number of specimens, maximum, median and mean divergence. The two groups examined are *longicornis* (including *E. tridentis*, which taxonomically is not a member of the group, but closely related) and *immersa* groups. For both groups and for every locus, specimens are recorded that are identical to any member in the other group while different from specimens in its own group. The second table produced by the script lists the specimens in the dataset, the number of loci, and the normalised number of loci per specimen. Normalised numbers of loci were calculated as half of the maximum number of loci divided by the number of loci of a particular specimen in the dataset. Then the script proceeds to produce bar plots (output as pdf) for every specimen showing percent of loci and normalised percent of loci that are identical to a particular specimen while different from all others. Two additional bar plots are produced for *longicornis* and *immersa* groups to show percent of loci of a particular specimen that are identical to any specimen in the wrong group while different from specimens in its own group. The script and the dataset with 19 413 loci (Supplementary Data S4, S11) are available on Figshare (http://dx.doi.org/10.6084/m9.figshare.7605404).

3. Results

3.1. Detection of divergent loci and cross-contamination

In the initial RAxML analysis of the dataset assembled with a clustering threshold of 80% similarity (29 859 loci, 5 945 539 bp; including *E. immersa* group) in the process of exploring RAD data, *E. japonica* did not form a monophyletic group, as the specimen USNM2051678-003 (hereafter as USNM003) was even outside of the *longicornis* group, forming a sister group to *E. tridentis* and the rest of *E. longicornis* group (Supplementary Data S1). Manual examination of the alignment regions present in at least one of the *E. japonica* specimens (about 600 000 bp) revealed that there were about 20 markers that contained regions that were not homologous to other specimens (divergence roughly 5–10 times higher than the average among the other specimens), mostly apparently because of mis-association of paired-end reads (Supplementary Data S2). In one case we also noticed that *E. japonica* specimen USNM003 was identical (when disregarding one indel in the middle of the locus, which can be explained by different lengths of quality trimmed paired-end reads) to *E. immersa* DEI-GISHym80071 while clearly different from all other specimens, indicating possible cross-contamination (p-distance to other *immersa* group specimens 0.6–3.4%, distance to *longicornis* group specimens 8.6–11.2%; Supplementary Data S3). Because most of the loci containing non-homologous regions could be detected with the criterion maximum p-distance more than 0.2, we created a dataset with these loci removed (19 413 loci, 3 517 320 bp). Except for within species relationships, the topology of ML tree based on this smaller dataset was identical to the initial tree (Supplementary Data S4).

Because the phylogenetic position of *E. japonica* specimen USNM003 did not change when the divergent loci were removed, we aimed next to detect possible cross-contamination in the smaller dataset. For this, we identified pairs of specimens that were identical to each other while different from the rest. In addition, to specifically get an idea about the level of cross-contamination between *immersa* and *longicornis* groups, we identified loci in which a particular specimen was identical to any member from the group it does not belong to, e.g. *E. japonica* specimen USNM003 being identical to at least one specimen in *immersa* group while different from the others in *longicornis* group (if present).

Clear outlier with regard to cross-contamination between *immersa* and *longicornis* groups was *E. japonica* USNM003, with 26.7% of its loci (out of 1015) identical to one or more specimens in *immersa* group (Fig. 1a). The cross-contamination in USNM003 seems to be caused by *E. immersa* DEI-GISHym80071 (Fig. 1b) which alone contributes 8.4% of the sequences of USNM003 (there were only two other *immersa* group specimens, both with only one sequence (0.1%) identical to USNM003). The other specimens with possibly significant amount of cross-contamination were *E. tridens* TUZ615037 (5.6% of loci identical to *E. tridentis* TUZ615182, which is not a member of *immersa* or *longicornis* groups), *E. immersa* DEI-GISHym80045 (5.1% identical to any in *longicornis* group), *E. fletcheri* TUZ615334 (4.7% identical to any in *longicornis* group), *E. plana* TUZ615181 (4.4% identical to any in *longicornis* group). For the other specimens these percentages are less than 2.5% and in most cases less than 1% (Supplementary Data S5).

It is more problematic to estimate level of cross-contamination within the *immersa* and *longicornis* groups themselves, because of higher degree of relatedness and at least occasional hybridisations between the species cannot be excluded. Nevertheless, for *longicornis* group it seems that in most cases the specimens are free of cross-contamination. For most specimens, the proportions of loci that were identical to a particular specimen belonging to a different species were less than 2.5% (Supplementary Data S5). Clear exception was *E. japonica* USNM2051678-038 (hereafter as USNM038) with 12.3% of its loci identical to *E. minuta* MH10-01 and 5.1% identical to *E. loktini*

(Fig. 1c). The other exception was pair of *E. longicornis* TUZ615057 (4.8% of its loci identical to TUZ615023) and *E. tridens* TUZ615023 (2.9% of its loci identical to TUZ615057), but this might be genuine because these species are closely related and the specimen TUZ615023 seems to be highly heterozygous (0.48% of two-fold degenerate positions; Supplementary Data S6) which increases the chance for sequences to be identified as identical.

For *E. japonica* USNM038, however, the high amount of loci that were identical to *E. loktini* (5.1%) and especially to a particular specimen of *E. minuta* MH10-01 (12.3%) was suspicious. From a morphological perspective, *Empria japonica* is not expected to be specifically related to *E. loktini* or *E. minuta*, but is very similar to *E. tridens* and *E. longicornis*. Indication of cross-contamination is also the fact that practically only one *E. minuta* specimen from Estonia contributed the identical sequences. The other two *E. minuta* specimens from Estonia and Sweden both contributed only one (0.1%) identical locus. To further check the possibility of contamination, we selected two candidate ddRAD loci of USNM038 to see if the results can be replicated using PCR and Sanger sequencing. In the ddRAD alignments, one of the selected sequences of USNM038 was identical to *E. loktini* while clearly different from other species, and the other had seven ambiguous positions (two Ns and five two-fold degenerate positions), which made it identical to 9 (out of 23) other specimens, including *E. loktini* and *E. minuta* MH10-01. In both cases, the Sanger sequencing revealed that *E. japonica* specimens were identical to each other and different from all other specimens, confirming the pattern found in the other Sanger sequenced nuclear markers (Supplementary Data S7). For the other sequenced specimens, the Sanger sequencing results were found to be consistent with the ddRAD data (no substitution differences), but in some cases there were indel differences, which can at least partly be explained by length differences of quality trimmed paired-end reads, because at least some of them were in the middle of the locus and different ddRAD assemblies produced different lengths (Supplementary Data S7).

It is more difficult to recognise possible cross-contamination within *E. immersa* group, because of small number of specimens and unresolved taxonomy. Nevertheless, based on morphology and ecology, *E. fletcheri* can be reliably separated from the others in *immersa* group. At least the two European specimens of *E. fletcheri* (from Estonia and Sweden) do not share significant amount of identical loci with a particular specimen from the other species (for each of these specimens the contribution is less than 2.2%; Supplementary Data S5). However, the *E. fletcheri* specimen from Canada (BIOUG17274-F06), which genetically seems to have little in common with the European counterpart, might be somewhat contaminated because the largest contributor of identical loci and in quite a large amount (3.4%; Supplementary Data S5) is *E. camtschatica* from Sweden (DEI-GISHym80070). For other cases in *immersa* group it is difficult to evaluate if it is a genuine signal or cross-contamination. For example *E. plana* DEI-GISHym15478 has 7.8% of its loci identical to *E. camtschatica* DEI-GISHym80070 (Supplementary Data S5), but both are from Sweden and could be the same species despite of some differences in the saws (ovipositors).

We subsequently analysed *immersa* and *longicornis* groups separately using datasets assembled with clustering threshold of 95% similarity (both, *de novo* and reference assembly), which decreases the chance of introducing highly divergent regions (Tables 3 and 4). Because both *E. japonica* specimens were apparently substantially more cross-contaminated than the other specimens, we decided to exclude them from final analyses, but also examined the effects of including one or both of them in different analyses. We excluded also apparently the third most contaminated specimen *E. tridens* TUZ615037 from the final analyses (5.6% of loci identical to *E. tridentis* TUZ615182, which is not a member of *immersa* or *longicornis* groups), although its inclusion had almost no effect on the results.

Table 3. Summary statistics of ddRAD and mitochondrial COI barcode data sets from *E. longicornis* and *E. immersa* group.

	E. longicornis group			*E. immersa* group		
	ddRAD_dn	ddRAD_ref	mtDNA	ddRAD_dn	ddRAD_ref	mtDNA
Number of taxa	22	22	22	10	10	10
Assembly method	De novo	Reference	–	De novo	Reference	–
Loci	20,871	943	1	9,362	551	1
SNPs	145,512	4,549	129	44,573	1,359	68
PIS	45,463	1,405	47	14,308	332	45
Alignment length (bp)	3,733,285	161,903	1,536	1,714,773	97,793	1,536
Missing (%)	70.1	67.7	7.7	47.6	53.1	32.1
Base frequency (C/G)	0.21590/ 0.21513	0.23849/ 0.23731	0.14303/ 0.12937	0.21581/ 0.21615	0.23943/ 0.22707	0.14031/ 0.13571
Number of MP trees	1	–	3	1	–	1
MP tree length	156210	–	169	45200	–	71
Consistency index (CI)	0.856	–	0.799	0.881	–	0.972
Retention index (RI)	0.612	–	0.815	0.644	–	0.971

Note: PIS, parsimony informative SNPs; MP, maximum parsimony.

Table 4. Specimens of *Empria* analysed in this study and a summary of the ddRAD data in *de novo* and reference assembly.

Species	Sample ID	Total reads (million)	*de novo* assembly				Reference assembly				
			Clusters at 95%[a]	Mean depth	Retained loci [b]	Recovered loci	Mapped reads	Clusters total	Clusters depth	Reads consensus	Recovered loci in assembly
(a) *Empria longicornis* group											
E. alector	ealec_DEI_GISHym80142	4.78	227253	20.1	59694	13725	28997	8165	14.9	2699	618
E. alector	ealec_TUZ615036	0.34	14426	11.3	4576	2139	2163	422	26.6	133	70
E. alector	ealec_TUZ615121	4.81	146273	31.1	42238	13311	17241	5081	17.6	1782	620
E. alector	ealec_TUZ615220	2.18	39319	51.6	11234	4894	1	1	4.0	1	NA
E. alpina	ealpi_DEI_GISHym80106	4.24	154599	26.2	45944	6777	19941	5475	17.1	2029	430
E. basalis	ebasa_DEI_GISHym14890	0.72	41354	15.4	16358	6920	2166	1245	5.8	437	267
E. basalis	ebasa_OL10_02	1.01	22225	34.5	4675	1628	718	520	2.9	124	62
E. basalis	ebasa_TUZ615083	0.09	9336	8.9	2817	1354	487	284	2.4	72	47
E. basalis	ebasa_TUZ615141	0.86	50972	15.4	18278	8815	3397	1805	5.9	630	362
E. loktini	elokt_TUZ615180	3.73	87639	38.4	29215	3204	9162	2681	13.7	1049	230
E. longicornis	elong_TUZ615022	2.35	26206	74.4	5274	1888	2710	362	6.7	158	77
E. longicornis	elong_TUZ615057	7.94	169150	43.4	60811	12411	27292	5494	34.5	2648	624
E. minuta	eminu_DEI_GISHym21189	0.47	15693	23.2	8430	1701	2245	615	13.9	321	110
E. minuta	eminu_IZBE0350001	0.99	17678	50.7	7576	1712	678	129	37.7	95	63
E. minuta	eminu_MH10_01	2.47	67598	35.0	30890	5477	8133	2266	16.3	1280	366
E. sp. 11	esp11_USNM2051678_040	0.34	10506	23.1	4687	904	542	337	3.1	137	39
E. sp. 14	esp14_MH11_01	1.34	47172	26.7	23470	6544	3217	857	31.0	495	287
E. tridens	etrid_TUZ615023	2.46	88462	27.0	42207	14400	12408	4209	14.0	2184	732
E. tridens	etrid_TUZ615027	2.23	81560	26.5	36613	12705	13373	3713	19.5	1919	645
E. tridens	etrid_TUZ615165	7.32	87708	65.9	29019	10128	7056	2643	10.4	1257	507
E. tridens	etrid_TUZ615624	1.18	25886	42.8	9701	3738	1815	896	8.8	407	169
E. tridentis	etridt_TUZ615182	2.93	71026	34.6	28846	2866	5943	2607	8.9	1308	270
	AVERAGE	**2.49**	**68275**	**33.0**	**23752**	**6238**	**7713**	**2264**	**14.3**	**962**	**314**
(b) *Empria immersa* group											
E. camtschatica	ecamt_DEI_GISHym80070	1.22	48116	24.2	17103	6835	3061	1591	4.9	562	311
E. fletcheri	eflet_BIOUG17274_F06	11.77	162626	68.7	26945	3803	3008	1474	9.1	415	227
E. fletcheri	eflet_DEI_GISHym31039	0.51	30181	14.6	10985	4306	2333	1131	8.0	398	215
E. fletcheri	eflet_TUZ615334	0.27	28908	9.2	9900	3805	1735	1083	4.2	306	187
E. immersa	eimme_DEI_GISHym80045	0.98	53371	17.1	20648	7866	4804	2265	14.3	823	429
E. immersa	eimme_DEI_GISHym80071	4.09	124234	30.7	41156	8318	13554	4017	21.5	1697	470
E. immersa	eimme_TUZ615623	2.96	79575	34.0	33109	8058	8117	2695	22.8	1231	453
E. improba	eimpr_BIOUG00998_D06	0.39	12918	27.2	4762	1414	668	379	3.2	146	69

E. plana	eplan_DEI_GISHym15478	1.84	24812	29.4	9043	2594	1374	488	8.6	268	110
E. plana	eplan_TUZ615181	0.58	20249	26.3	8695	2109	2226	599	10.1	275	93
	AVERAGE	**2.46**	**58499**	**28.1**	**18235**	**4911**	**4088**	**1572**	**10.7**	**612**	**256**

[a]Clusters that passed filtering for 6x minimum coverage.
[b]Loci retained after passing coverage and paralog filters.
NA, not applicable.

3.2. Empria longicornis group

All species with more than one individual sampled are found to be monophyletic and in most cases strongly supported in maximum likelihood trees reconstructed from ddRAD datasets based on *de novo* and reference assemblies (Figs 2a and 3a). Monophyly of only *E. tridens* is moderately supported based on reference assembly (Fig. 3a). There are some differences in tree topology above the species level based on reference and *de novo* assembly (phylogenetic positions of *E. sp11* and *E. loktini*), but these differences are poorly supported, particularly in the smaller dataset based on the reference assembly (Figs 2a and 3a).

Monophyly of most species defined based on morphology is also well supported by concatenated analysis of three nuclear protein coding genes obtained by Sanger sequencing (Fig. 4d). Of the species for which more than one individual was sampled, only *E. tridens* is not monophyletic according to three-gene tree. The species for which only one individual was sampled (*E. alpina*, *E. loktini*, sp11) are well separated from the other species as well as from each other based both on ddRAD and Sanger data, supporting their species status (Figs 2a, 3a, 4d). For *E. montana* Koch, 1984 we were not able to obtain enough ddRAD data to be included in the analyses (Supplementary Data S8), but based on Sanger sequencing of three specimens, we can confirm that it belongs to *longicornis* group (Supplementary Data S9 and S10). *Empria montana* was not recognised by Prous et al. (2011b) as a member of *longicornis* group because of divergent penis valve (only holotype male was known at the time). Two of the studied specimens of *E. montana* (http://dx.doi.org/10.6084/m9.figshare.7447847; http://dx.doi.org/10.6084/m9.figshare.7447874) were reared from *Dasiphora fruticosa*, which was previously unknown. Based on current genetic sampling of three *E. montana* specimens (two from Magadan oblast, one from Krasnoyarsk Krai, Russia), this species is monophyletic according to mitochondrial COI (Supplementary Data S10). Partial fragments of three nuclear genes used here are available for only one *E. montana* specimen, based on which this species groups together with *E. alpina*, *E. minuta*, and sp11, but in unresolved position (Supplementary Data S9).

Distance calculations of ddRAD data (*de novo* assembly) are also consistent with species limits defined based on morphology (Table 5). Mean within species divergence varies between 0.18–0.92%, while distances among species are about twice as high, 1.05–1.87%.

Table 5. Mean pairwise distances of ddRAD (below diagonal) and mtDNA data (above diagonal) within (grey shaded cells; ddRAD de novo assembly data/mtDNA) and between the species.

(a) *E. longicornis* group and *E. tridentis*

	alec	alpi	basa	lokt	long	minu	sp11	sp14	trid	tridt
alecor	0.35/1.20	0.74	1.54	1.82	1.00	1.07	1.82	1.80	1.36	5.07
alpina	1.78	NA	1.58	1.76	0.79	0.59	1.76	1.67	1.21	5.01
basalis	1.08	1.70	0.50/1.01	1.58	0.93	1.51	1.90	1.90	0.94	5.26
loktini	1.87	1.83	1.77	NA	1.53	1.50	0	1.95	1.66	4.56
longicornis	1.24	1.77	1.13	1.80	0.18/1.24	0.99	1.53	1.63	0.74	5.05
minuta	1.73	1.70	1.61	1.85	1.69	0.52/0.79	1.50	1.49	1.33	4.87
sp.11	1.82	1.60	1.72	1.73	1.87	1.69	NA	1.95	1.66	4.56
sp.14	1.55	1.60	1.53	1.84	1.52	1.75	1.79	NA	1.86	5.34
tridens	1.17	1.73	1.05	1.84	1.09	1.74	1.84	1.52	0.92/0.97	5.23
tridentis	2.08	2.07	1.99	1.99	2.10	2.10	2.02	2.08	2.01	NA

(b) *E. immersa* group

	camt	flet	imme	impr	plan
camtschatica	NA	2.30	1.90	2.74	1.42

fletcheri	1.14	0.94/2.88	1.99	2.24	2.39
immersa	0.88	1.34	0.49/1.21	2.68	2.47
improba	1.18	1.31	1.42	NA	3.72
plana	1.02	1.31	1.22	1.17	1.15/2.02

NA, not applicable because of single specimen.

Based on nuclear NaK, POL2, and ZC3H14 (altogether 5646 bp), net synonymous divergences among most of the species (7 species for which more than one individual was sampled) were between 2.3–9.4%, suggesting that these species are well separated (Roux et al., 2016). Divergence between only *E. basalis* and *E. tridens* (1.5%) falls within the grey zone of speciation according to Roux et al. (2016).

Phylogenies based on ddRAD and combined data of three nuclear protein coding genes (NaK, POL2, and ZC3H14) were largely congruent when considering well supported relationships (bootstrap support more than 70%). Moderately supported differences involved relationships among *E. minuta*, *E. alpina*, and sp11, which formed a clade based on the three-gene dataset (Fig. 4d), but not based on ddRAD data (Figs 2a and 3a). There are some strongly or moderately supported phylogenetic differences among the three protein coding genes. According to the gene tree of POL2 (Fig. 4b), *E. longicornis* and *E. japonica* form strongly supported clade, which is absent in the other two gene trees (NaK and ZC3H14) (Figs 4a and 4c). The second, moderately supported difference is non-monophyly of sp14 according to ZC3H14 (Fig. 4c), contrary to POL2 (Fig. 4b) (according to NaK it is unresolved). Another, moderately supported difference is between NaK and ZC3H14 on one hand and POL2 on the other. According to NaK and ZC3H14 (Figs 4a and 4c), *E. alpina*, *E. minuta*, and sp11 form a clade (although relationships among these three species differ, but without strong support), but *E. minuta* is weakly supported as basal to all other *longicornis* group species in POL2 tree (Fig. 4b). These differences between single genes can be expected in closely related species complexes because of incomplete lineage sorting, which can cause incompatibilities between gene and species trees even without hybridisations.

Admixture analysis with STRUCTURE at K=9 (the number of species based on morphology, excluding *E. japonica*) supports most species as largely separate populations from each other (Fig. 2a). Best supported are *E. alector*, *E. basalis*, *E. longicornis*, *E. minuta* and sp11, which appear to have very little or no contribution from other species (Fig. 2a). Reasonably well supported are *E. loktini* and sp14, while *E. tridens* and *E. alpina* apparently have significant contributions from some other species (Fig. 2a). However, there are inconsistencies among different STRUCTURE analyses. When both *E. japonica* specimens are included (at K=10), *E. alpina* is better supported, while *E. longicornis* receives less support, as it seems to have a large contribution from *E. basalis* (Supplementary Data S11).

The results of four-taxon D-statistic tests suggest numerous cases of introgressions between different species. The most strongly supported case involves *E. minuta* and sp14 (Table 6), but curiously this receives (almost) no support from STRUCTURE analyses (Fig. 2a, Supplementary Data S11). In contrast to STRUCTURE (Fig. 2a) and D-statistic tests (Table 6), the counting of the number of identical loci between the specimens suggests the largest contributor as *E. alpina* (1.5%) in case of sp14 (*E. minuta* contributes 0.5%, Supplementary Data S5), which finds some support in the STRUCTURE analysis when both *E. japonica* specimens are included (Supplementary Data S11). There are numerous other inconsistencies among the four-taxon D-statistic tests, different STRUCTURE analyses and the counting of identical loci.

Table 6. Four-taxon D-statistic tests results showing significant replicates for introgression in *Empria*.

Test	P1[1]	P2	P3	O	Range Z[2]	nSig/n[3]	nSig/n (%)[4]
(a) *E. longicornis* group (28 cases out of 44)							
a1	T	T	L	Tt	0.1 – **15.9**	5/11	45.5
a2	T	T	B	Tt	0.3 – **15.4**	7/23	30.4
a3	T	T	Ac	Tt	0.0 – **10.2**	4/17	23.5
a4	T	T	Sp14	Tt	0.1 – **17.5**	2/5	40.0
a5	T	T	Sp11	Tt	0.3 – **9.4**	2/5	40.0
a6	T	T	M	Tt	0.0 – **20.8**	6/17	35.3
a7	T	T	Ap	Tt	0.0 – **6.9**	1/5	20.0
a8	T	T	Lt	Tt	0.1 – **5.6**	2/5	40.0
a9	L	L	B	Tt	1.5 – **3.3**	1/3	33.3
a10	L	L	M	Tt	0.5 – **18.8**	1/3	33.3
a11	B	B	T	Tt	0.0 – **13.6**	2/23	8.7
a12	B	B	L	Tt	0.0 – **3.5**	1/11	9.1
a13	B	B	Ac	Tt	0.0 – **8.2**	3/17	17.6
a14	B	B	sp14	Tt	0.2 – **13.3**	3/5	60.0
a15	B	B	sp11	Tt	0.0 – **3.5**	1/5	20.0
a16	B	B	M	Tt	0.5 – **6.4**	1/5	20.0
a17	B	B	Lt	Tt	0.0 – **10.2**	4/17	23.5
a18	Ac	Ac	B	Tt	0.0 – **4.6**	1/11	9.1
a19	M	M	T	Tt	0.0 – **17.2**	2/11	18.2
a20	M	M	L	Tt	0.2 – **3.8**	1/5	20.0
a21	M	M	B	Tt	0.1 – **12.3**	3/11	27.3
a22	M	M	Ac	Tt	0.0 – **3.9**	2/8	25.0
a23	M	M	Sp14	Tt	17.8 – **38.5**	3/3	100.0
a24	M	M	Sp11	Tt	0.0 – **10.0**	1/3	33.3
a25	(T+L)	(T+L)	B	Tt	0.0 – **15.3**	26/59	44.1
a26	B	B	(T+L)	Tt	0.0 – **13.5**	2/35	5.7
a27	(T+L+B)	(T+L+B)	Ac	Tt	0.0 – **13.7**	23/134	17.2
a28	Ac	Ac	(T+L+B)	Tt	0.0 – **4.7**	1/29	3.4
(b) *E. immersa* group (7 cases out of 26)							
b1	F	F	C	Im	0.0 – **3.5**	1/3	33.3
b2	Im	Im	F	Ip	0.4 – **8.8**	1/8	12.5
b3	Im	Im	Ip	F	0.0 – **3.5**	1/5	20.0
b4	(F+Ip)	(F+Ip)	(C+P)	Im	0.0 – **3.8**	1/19	5.3
b5	(C+P)	(C+P)	(F+Ip)	Im	2.3 – **5.4**	3/4	75.0
b6	(F+Ip)	(F+Ip)	Im	P	0.0 – **6.0**	6/29	20.7
b7	(F+Ip)	(F+Ip)	Im	C	0.0 – **6.7**	3/29	10.3

[1]Taxon names are abbreviated: In *E. longicornis* group, Ac: *E. alector*, Ap: *E. alpina*, B: *E. basalis*, L: *E. longicornis*, Lt: *E. loktini*, M: *E. minuta*, Sp11: *Empria* sp.11, Sp14: *Empria* sp.14, T: *E. triden*, Tt: *E. tridentis*. In *E. immersa* group, C: *E. camtschatica*, F: *E. fletcheri*, Im: *E. immersa*, Ip: *E. improba*, P: *E. plana*. Tests are referred to by number in the text. Insignificant cases were not shown.

[2]Bold indicates significance at α=0.01.

[3]Significant tests over possible sampled individuals.

[4]The percentage was calculated for the number of significant replicates shown (nSig) out of all possible four-sample replicates (n) in each test.

In contrast to nuclear data, mitochondrial COI does not support monophyly of any species (except possibly *E. montana* and sp14: Supplementary Data S10) and in some cases the non-monophyly is strongly supported (Fig. 2a). Besides the non-monophyly of species, the general topology of COI tree is very different from nuclear ML tree (Fig. 2a).

3.3. Empria immersa group

Morphologically defined species boundaries in *immersa* group (Prous et al., 2014) are not as well supported as in *longicornis* group. Only *E. immersa* based on ddRAD data and combined analyses of NaK and POL2 genes (but not in analysis based only on POL2), and *E. improba* based on limited amount of ddRAD data are found to be monophyletic (Figs 2b, 3b, Supplementary Data S12). Although two or three (depending on the dataset) specimens of European *E. fletcheri* (from Scotland, Sweden, and Estonia) unambiguously group together in all analyses (Figs 2b, 3b, Supplementary Data S12), they do not appear to be closely related to the single analysed North-American counterpart (Figs 2b, 3b). Within and between species divergences based on ddRAD data (*de novo* assembly) in *immersa* group partly overlap. Within species divergences (0.49–1.15%) are somewhat larger compared to *E. longicornis* group, while between species divergences are somewhat smaller (0.88–1.42%) (Table 5).

Similarly to *longicornis* group, there are some differences between NaK and POL2 phylogenies, one of which is rather well supported. *Empria immersa* is moderately supported as monophyletic according to NaK (Fig. 4a), but not according to POL2 (Fig. 4b), in which case two specimens of *E. immersa* are not separated from *E. camtschatica*, *E. improba*, and *E. plana*. Based on these two genes (altogether 4061 bp), net synonymous divergences between three species for which more than one individual was sampled were between 1.0–2.0%, therefore falling within the grey zone of speciation according to Roux et al. (2016). When only *E. immersa* and European *E. fletcheri* are considered (because North-American *E. fletcheri* did not group with European ones and *E. plana* was not monophyletic), net synonymous divergences between these species are 2.9%, falling outside the grey zone (Roux et al., 2016).

Admixture analysis with STRUCTURE at *K*=5 (the number of species based on morphology) does not support current taxonomy very well either, as only *E. immersa* and the European specimens of *E. fletcheri* are consistently supported as distinct populations from the others (Fig. 2b, Supplementary Data S11). Curiously, *E. camtschatica* and *E. improba* are supported as part of almost the same population, even though they are far apart in the ddRAD tree (Fig. 2a). Morphologically these two species could be the same, but STRUCTURE analyses with a different taxon sampling suggests that *E. camtschatica* and *E. improba* are largely separate populations (Supplementary Data S11). Interestingly, at *K*=3, STRUCTURE suggests that there are three clearly separated populations: European *E. fletcheri*, *E. immersa*, and the other species together (Fig. 5, Supplementary Data S11). North-American *E. fletcheri* is a mixture of *E. camtschatica*, *E. improba, E. plana,* and European *E. fletcheri* according to STRUCTURE analyses at *K*=2 to *K*=5 (Fig. 5).

The results of four-taxon D-statistic tests suggest some cases of possible introgression between different species (Table 6).

As in case of *longicornis* group, nuclear and mitochondrial trees of *immersa* group are very different from each other and monophyly of species is not supported (Fig. 2b).

4. Discussion

4.1. Cross-contamination or hybridisation?

Large amount of data generated with high-throughput sequencing methods precludes manual checking of every alignment. The main problems for these datasets are introduction of non-homologous alignment regions and contaminations, which would be easy to notice when dealing only with few genes by checking every alignment and gene tree. Because the species in our dataset are all closely related, the exclusion of non-homologous alignments is relatively easy by increasing clustering similarity threshold (up to 90% or 95% in our case) together with an addition of stringent filtering steps, which excludes all or most problematic alignments. However, in studies that pool specimens for sequencing and use single barcode or barcode combinations (but fewer unique barcodes than specimens) to link the reads to specimens after sequencing, it becomes especially difficult to detect cross-contamination when study organisms are closely related, because it might not be obvious if identical loci between specimens are due to biological or technical reasons. Nevertheless, the two species-groups of *Empria* studied here are morphologically and genetically (based on both mitochondrial and nuclear DNA) well separated (Prous, 2012) and hybridisations between them are unlikely. Therefore, by examining patterns of identical loci between the groups, it is possible to get an estimation of the level of cross-contamination in our dataset. In the dataset excluding divergent loci (19 413 loci, Supplementary Data S11), about 6% of the sequences involve identical pairs between *immersa* and *longicornis* groups (in order not to exclude any specimens, *E. tridentis* was treated as a member of *longicornis* group in these pairwise comparisons). This percentage is certainly over-estimation regarding cross-contamination as many of the loci (which are short, about 180 bp) might be too conserved to reveal differences between the groups. Better indication would be examination of the cases where one specimen is identical to any other in the wrong group while different from specimens in its own group (if present). In this case 1% of all sequences are identical to specimen(s) in the wrong group. Assuming the same cross-contamination rate within *immersa* and *longicornis* groups themselves suggests 2.4% of the sequences of the whole dataset to be affected (58% of pairwise comparisons are within *immersa* and *longicornis* groups). It is difficult to say if this is still over-estimation or instead under-estimation. Based on a more stringent criterion, e.g. considering loci present for four or more specimens from both groups (i.e. at least 8 specimens) gives cross-contamination rate of 0.6% for the whole dataset. Studies that specifically examined cross-contamination have found that barcode jumps can cause 0.3–2.5% of the sequence reads to be assigned to a wrong individual (Kircher et al., 2012; Schnell et al., 2015). Cross-contamination level of 1–2% could be considered acceptable if it affected every specimen in equal proportions, but might still lead to questionable conclusions if some specimens were affected much more than others (Valk et al., 2018). In our dataset, *E. japonica* USNM003 was a clear outlier in regard to possible cross-contamination between *immersa* and *longicornis* groups (Fig. 1a). Remarkably, when examining specific individuals that exclusively contribute identical loci to *E. japonica* USNM003, *E. immersa* DEI-GISHym80071 is the most common (85 loci out of 1015, 8.4%), while other specimens of *E. immersa* group contribute practically nothing (two other specimens contributed exclusively both only one locus) (Fig. 1b). It is highly unlikely that one specimen of *E. immersa* from Sweden and a one specimen of *E. japonica* from Hokkaido (Japan) share genes because of introgression, while the same is not seen between other specimens of the same species. If introgression was likely between *immersa* and *longicornis* groups, one would expect to see comparable levels of gene sharing in other specimens and preferably between specimens in geographic proximity (most studied specimens are from Europe). Similarly for the other *E. japonica* specimen (USNM038) from Hokkaido that we had to exclude because of possible cross-contamination (although involving specimens from the same species group), the largest

contributor of identical sequences (12.3%) was specific *E. minuta* specimen (MH10-01) from Estonia, while the other *E. minuta* specimens contributed practically nothing (Fig. 1c). The second largest contributor of identical sequences (5.1%) to USNM038 was *E. loktini* (Fig. 1c), which does live in sympatry with *E. japonica*. Although species might hybridise in *E. longicornis* group (at least in the past as suggested by mitochondrial phylogeny), this high proportion of identical sequences in USNM038 specifically from *E. minuta* and *E. loktini* seems unlikely from morphological perspective (*E. japonica* can unambiguously be distinguished from those two species, but not so well from *E. longicornis* and *E. tridens*) and generally suspicious compared to most other specimens (in most cases each heterospecific individual contributed less than 2.5% of identical sequences). Additionally, PCR and Sanger sequencing of two loci that were suspected to be cross-contamination in USNM038 contradicted the ddRAD data: sequences of two or three *E. japonica* specimens were identical to each other while different from all the other sequenced specimens (Supplementary Data S7). Although our dataset overall might not be affected by higher level of cross-contamination than usual (e.g. Schnell et al., 2015), the relatively high level of unequal recovery of loci (difference more than 10 times) among the specimens might explain why some of them were proportionally more affected than others (Valk et al., 2018). Among the specimens retained for the analyses, both *E. japonica* specimens were at the lower end of the number of loci recovered. If more loci had been recovered from both *E. japonica* specimens, these might have diluted the cross-contamination and we might not have realised that possibility. It is likely that some (perhaps even most) other specimens in our dataset have also been affected by cross-contamination (including among conspecific individuals, which we could not detect) to some degree, which weakens our biological conclusions for the studied species groups. Nevertheless, except in case of *E. japonica*, the results based ddRAD data seem plausible in light of morphological studies (Prous, 2012; Prous et al., 2014, 2011b) and Sanger sequencing (Fig. 4), but should be re-examined in future studies that better control for cross-contamination. Although more expensive, we suggest that whenever possible, additional replications should be done with different combinations of pooled specimens, pooling only distantly related species, sequencing every specimen separately, or adding specimen specific barcodes to both ends of the DNA fragments (not just different combinations of limited number of barcodes).

Even if 1–2% is considered an acceptable level of erroneous sequences (because of non-homology and/or contaminations) in phylogenomic datasets, this can still significantly affect downstream analyses. It is likely that even smaller proportion of errors could be detrimental to reconstructing rapid speciation events if the small amount signal is swamped be larger amount of error. On the other hand, resolving rapid speciation events would be among the questions to which large datasets could give the largest contribution (uncontroversial clades can be reliably reconstructed already based on small number of genes) and therefore data quality is essential before deciding among alternative phylogenetic hypotheses. Unfortunately, the bioinformatic tools are not yet reliable enough to completely remove manual interventions in phylogenomic datasets (Philippe et al., 2017; Simion et al., 2017).

4.2. Causes of mitonuclear discordance

In both studied species groups, mitochondrial phylogeny is very different from nuclear phylogeny (Fig. 2). Particularly striking is the non-monophyly of all or most species according to mitochondrial DNA, while there is little incongruence between nuclear and morphological evidence (Figs 2–4; Prous, 2012; Prous et al., 2011b). Strong mitonuclear discordance has been observed in other animal groups and usually interpreted as evidence of mitochondrial introgression (e.g. Bronstein et al., 2016; Papakostas et al., 2016; Tang et al., 2012), which does seem to be the most likely explanation (Bonnet et al., 2017; Sloan et al., 2017), although it may also result from

incomplete lineage sorting (Funk and Omland, 2003). Recently, Patten et al. (2015) found based on theoretical modelling that haplodiploid species may be especially prone to biased mitochondrial introgression, which could explain widespread mitonuclear discordance in several other species rich sawfly groups besides *Empria*, like *Neodiprion* (Linnen and Farrell, 2008, 2007) and *Pristiphora* (Prous et al., 2017). Nevertheless, haplodiploidy is probably not the only reason to promote widespread mitonuclear discordance, because in many other (most?) Hymenoptera, mitochondrial barcoding seems to work relatively well for species identification (Derocles et al., 2012; Klopfstein, 2014; Schmidt et al., 2015). One other factor that might influence rate of mitochondrial introgression is its mutation rate, lower rates making introgression more probable than higher rates, latter of which should more likely lead to compensatory co-evolution and mitonuclear incompatibilities (see Table 3 in Sloan et al., 2017). As mitochondrial genomes of basal hymenopterans do evolve significantly slower compared to Apocrita (particularly Xyeloidea, Pamphilioidea, and Tenthredionoidea; Niu et al., 2019; Tang et al., 2019), the combination of haplodiploidy and slow rate of mitochondrial evolution might better explain widespread mitonuclear discordance in some (many?) species rich groups of sawflies rather than just haplodiploidy. There is evidence that in parasitic lineages mitochondrial evolution tends to be much faster than non-parasitic lineages (Pentinsaari et al., 2016), explaining perhaps faster evolution of mtDNA in Apocrita which are ancestrally parasitic (and most species still are). It could be then that in most Hymenoptera (Apocrita), COI barcoding might be reliable for species identification despite of haplodiploidy.

4.3. Taxonomy of E. longicornis group

Since the revision of the species group (Prous et al., 2011b), two additional putative species have been found, and a third already described species (*E. montana*) is here for the first time recognised as member of *longicornis* group (Supplementary Data S9 and S10), bringing the total number of species to 12. The male specimen USNM2051678-040 from Hokkaido is so far the only known representative of a putative species “sp11” (sp.1 in Prous et al., 2011a). Because there has been very little sampling of sawflies in arctic habitats above treeline in Japan (and more generally outside Europe), the sp11 might normally be restricted to arctic habitats like *E. alpina* (sister species of sp11 according to some ddRAD trees: Fig. 2), although the single known specimen was collected in a Malaise trap well below treeline (at 1000 m, about 15 km East of Mount Asahi, the highest point on Hokkaido). We have studied several specimens of the second putative species, sp14 (male MH11-01 and female DEI-GISHym15231 reported here) collected in the Pyrenees and the Alps, in most cases below treeline, but at higher altitudes than 1500 m. Morphologically, the only rather clear indication that sp14 might be a different species from *E. alpina*, is the different structure of female ovipositor. Male penis valves do not seem to be different in *E. alpina* and sp14, but there is variation in the length of antennae. Confusingly, though, *E. alpina* in the Alps have distinctly longer antenna (both male and female) from the specimens in the northern Fennoscandia, the latter of which have antenna more similar to sp14 in the Alps. Although several additional female and possibly male specimens of sp14 are available, we refrain from describing new species, because more studies are required to more reliably resolve taxonomy of *E. alpina* and sp14, and to associate males and females. Prous et al. (2011b) noted that there might be an additional species amongst *E. tridens*, based on differences in larval colour pattern and diverging ITS sequences, but the data was too limited to decide this (no differences in adult morphology were detected). One of the specimens analysed here is the larva with diverging ITS sequence and a different colour pattern (TUZ615027, 06-05a in Prous et al., 2011b), but our ddRAD data and Sanger sequenced genes (Figs 2–4) do not clearly indicate that it should be treated as a different species. When excluding *E. alpina*, for which we lack sufficient amount of fresh material, *E. tridens* is known to be geographically the most widely distributed (from Europe to Hokkaido) among the remaining species (Prous et al., 2011a),

which might explain the higher genetic diversity of this taxon, rather than indicating presence of an additional species. For other species with more than one individual sampled (*E. alector, E. basalis, E. longicornis, E. minuta*) our results (Figs 2–4) agree perfectly with current taxonomy (Prous et al., 2011b) and do not suggest the presences of additional species. In case of *E. japonica*, Sanger data unambiguously supports validity of this species (Fig. 4) and it is found to be monophyletic also based on ddRAD data when *immersa* group (which might be source of cross-contamination in one *E. japonica* specimen) is excluded (Supplementary Data S12). Validity of the species is also supported by net synonymous divergences among species based on three protein coding genes (NaK, POL2, and ZC3H14), which in most cases (2.3–9.4%) fall outside the grey zone of speciation according to Roux et al. (2016). Only divergence (1.5%) falling within the grey zone is between *E. basalis* and *E. tridens* (according to Roux et al., 2016 the grey zone of speciation falls within 0.5%–2.0% of net synonymous divergence between species). Limitation of our dataset regarding species delimitation could be lack of sampling of specimens of same species from wider area than Europe, although at least some of them are known from West or Central Europe to East Asia (Prous et al., 2011b; Taeger et al., 2018). *Empria alector, E. basalis, E. longicornis,* and *E. minuta* were well supported as monophyletic (Figs 2–4), but this needs to be tested by sampling additional specimens from West and East Siberia.

4.4. Taxonomy of E. immersa group

Based on adult morphology there should be at least two species within *E. immersa* group, *E. fletcheri* (feeding on *Betula*) and the others (feeding on *Salix*). The saw (ovipositor) of *E. fletcheri* is clearly different from *Salix* feeding species. There is quite clear difference also in the structure of tarsal claws, *E. fletcheri* has small subapical tooth, while in the others it is distinctly longer (except in one possibly additional species not sampled here, *E. asiatica* that has a saw indistinguishable from *E. camtschatica* and *E. improba*). All of the *Salix* feeding species are very similar in adult morphology and might as well belong to same species. However, among the *Salix* feeders, genetic data suggests separation of *E. immersa* from the others (Figs 2–5), which might be supported by differences in colouration of larvae (based on unpublished *ex-ovo* rearings of *E. immersa* and *E. camtschatica*) and some morphological differences in the adults (Prous et al., 2014). Admixture analysis with Structure at K=3 (Fig. 5) suggest that *Empria camtschatica*, *E. plana*, and *E. improba* might belong together, which does not seem unlikely based on morphology (in this case the species name to be applied would be *E. improba* (Cresson, 1880), as the oldest), although more sampling throughout Asia and North-America for genetic studies would be preferably to decide among competing scenarios. Another issue requiring more attention is the apparently clear genetic separation of European and North-American *E. fletcheri*, which from a morphological perspective clearly belong together. Considering that habitats of *E. fletcheri* (bogs in boreal forests and tundra) in Eurasia and North-America were at least partly connected about 10 000 years ago, this species might well be Holarctic in distribution (in Eurasia the eastern-most specimens confirmed so far are from Irkutsk region). Unfortunately, our data does not currently allow disentangling effects of wide geographic separation and biological barriers to gene-flow in *immersa* and *longicornis* groups. In case of *longicornis* group, where taxonomy of most species is better resolved than in *immersa* group, none of the species analysed here include individuals collected within an area larger than Europe, although at least some of the species reach East Asia (Prous et al., 2011b; Taeger et al., 2018). Because species within *longicornis* and *immersa* groups are closely related (within and between-species genetic distances are quite similar, Table 5) conspecific samples analysed from much larger area than Europe might significantly complicate species delimitation based on genetic data. To test this, additional sampling from Central and Eastern parts of Asia should be analysed. In case of *E. fletcheri*, detection of two distinct genetic lineages living in sympatry in East-Asia or North-America would be a strong indication for

additional species, but our data is currently insufficient do decide this (for example *E. plana* from Sweden and Hokkaido are also genetically far apart: Figs 2–4).

Acknowledgements

We thank Laura Törmälä for her efficient work in the biology laboratory at University of Oulu. We also wish to acknowledge CSC – IT Centre for Science, Finland for computational resources. Matthias Hoffman (ZALF, Müncheberg) and Riina Klais (Tartu) helped with an R script. Funding: This work was supported by Finnish Academy grant #277984 to MM.

Competing interests statement

The authors have no competing interests to declare.

Appendix A. Supplementary material

Supplementary data to this article can be found online at https://doi.org/10.1016/…

References

Alex Smith, M., Fernández-Triana, J.L., Eveleigh, E., Gómez, J., Guclu, C., Hallwachs, W., Hebert, P.D.N., Hrcek, J., Huber, J.T., Janzen, D., Mason, P.G., Miller, S., Quicke, D.L.J., Rodriguez, J.J., Rougerie, R., Shaw, M.R., Várkonyi, G., Ward, D.F., Whitfield, J.B., Zaldívar-Riverón, A., 2013. DNA barcoding and the taxonomy of Microgastrinae wasps (Hymenoptera, Braconidae): impacts after 8 years and nearly 20 000 sequences. Mol. Ecol. Resour. 13, 168–176. https://doi.org/10.1111/1755-0998.12038

Bonnet, T., Leblois, R., Rousset, F., Crochet, P.A., 2017. A reassessment of explanations for discordant introgressions of mitochondrial and nuclear genomes. Evolution (N. Y). 71, 2140–2158. https://doi.org/10.1111/evo.13296

Bronstein, O., Kroh, A., Haring, E., 2016. Do genes lie? Mitochondrial capture masks the Red Sea collector urchin's true identity (Echinodermata: Echinoidea: Tripneustes). Mol. Phylogenet. Evol. 104, 1–13. https://doi.org/10.1016/j.ympev.2016.07.028

Chhatre, V.E., Emerson, K.J., 2017. StrAuto: automation and parallelization of STRUCTURE analysis. BMC Bioinformatics 18, 192. https://doi.org/10.1186/s12859-017-1593-0

Cruaud, P., Rasplus, J.-Y., Rodriguez, L.J., Cruaud, A., 2017. High-throughput sequencing of multiple amplicons for barcoding and integrative taxonomy. Sci. Rep. 7, 41948. https://doi.org/10.1038/srep41948

Derocles, S. a P., LE Ralec, A., Plantegenest, M., Chaubet, B., Cruaud, C., Cruaud, A., Rasplus, J.-Y., 2012. Identification of molecular markers for DNA barcoding in the Aphidiinae (Hym. Braconidae). Mol. Ecol. Resour. 12, 197–208. https://doi.org/10.1111/j.1755-0998.2011.03083.x

Durand, E.Y., Patterson, N., Reich, D., Slatkin, M., 2011. Testing for Ancient Admixture between Closely Related Populations. Mol. Biol. Evol. 28, 2239–2252. https://doi.org/10.1093/molbev/msr048

Eaton, D.A.R., 2014. PyRAD: assembly of de novo RADseq loci for phylogenetic analyses. Bioinformatics 30, 1844–1849. https://doi.org/10.1093/bioinformatics/btu121

Eaton, D.A.R., Overcast, I., 2016. ipyrad: interactive assembly and analysis of RADseq data sets. Available from: http://ipyrad.readthedocs.io/ [WWW Document].

Evanno, G., Regnaut, S., Goudet, J., 2005. Detecting the number of clusters of individuals using the software structure: a simulation study. Mol. Ecol. 14, 2611–2620.

https://doi.org/10.1111/j.1365-294X.2005.02553.x

Funk, D.J., Omland, K.E., 2003. Species-Level Paraphyly and Polyphyly: Frequency, Causes, and Consequences, with Insights from Animal Mitochondrial DNA. Annu. Rev. Ecol. Evol. Syst. 34, 397–423. https://doi.org/10.1146/annurev.ecolsys.34.011802.132421

Hebert, P.D.N., Braukmann, T.W.A., Prosser, S.W.J., Ratnasingham, S., DeWaard, J.R., Ivanova, N. V., Janzen, D.H., Hallwachs, W., Naik, S., Sones, J.E., Zakharov, E. V., 2018. A Sequel to Sanger: amplicon sequencing that scales. BMC Genomics 19, 219. https://doi.org/10.1186/s12864-018-4611-3

Hebert, P.D.N., Cywinska, A., Ball, S.L., DeWaard, J.R., 2003. Biological identifications through DNA barcodes. Proc. R. Soc. London. Ser. B Biol. Sci. 270, 313–321. https://doi.org/10.1098/rspb.2002.2218

Hebert, P.D.N., Ratnasingham, S., Zakharov, E. V, Telfer, A.C., Levesque-Beaudin, V., Milton, M.A., Pedersen, S., Jannetta, P., DeWaard, J.R., 2016. Counting animal species with DNA barcodes: Canadian insects. Philos. Trans. R. Soc. B Biol. Sci. 371, 20150333. https://doi.org/10.1098/rstb.2015.0333

Ivanov, V., Lee, K.M., Mutanen, M., 2018. Mitonuclear discordance in wolf spiders: Genomic evidence for species integrity and introgression. Mol. Ecol. 27, 1681–1695. https://doi.org/10.1111/mec.14564

Jakobsson, M., Rosenberg, N.A., 2007. CLUMPP: a cluster matching and permutation program for dealing with label switching and multimodality in analysis of population structure. Bioinformatics 23, 1801–1806. https://doi.org/10.1093/bioinformatics/btm233

Kaltenpoth, M., Showers Corneli, P., Dunn, D.M., Weiss, R.B., Strohm, E., Seger, J., 2012. Accelerated evolution of mitochondrial but not nuclear genomes of hymenoptera: new evidence from crabronid wasps. PLoS One 7, e32826. https://doi.org/10.1371/journal.pone.0032826

Kircher, M., Sawyer, S., Meyer, M., 2012. Double indexing overcomes inaccuracies in multiplex sequencing on the Illumina platform. Nucleic Acids Res. 40, 1–8. https://doi.org/10.1093/nar/gkr771

Klopfstein, S., 2014. Revision of the Western Palaearctic Diplazontinae (Hymenoptera, Ichneumonidae). Zootaxa 3801, 1. https://doi.org/10.11646/zootaxa.3801.1.1

Kumar, S., Stecher, G., Tamura, K., 2016. MEGA7: Molecular Evolutionary Genetics Analysis Version 7.0 for Bigger Datasets. Mol. Biol. Evol. 33, 1870–1874. https://doi.org/10.1093/molbev/msw054

Lee, K.M., 2018. The demultiplexed fastq NCBI Sequence Read Archive (SAR) [WWW Document]. URL http://www.ncbi.nlm.nih.gov/sra/PRJNA505249

Lee, K.M., Kivelä, S.M., Ivanov, V., Hausmann, A., Kaila, L., Wahlberg, N., Mutanen, M., 2018. Information Dropout Patterns in Restriction Site Associated DNA Phylogenomics and a Comparison with Multilocus Sanger Data in a Species-Rich Moth Genus. Syst. Biol. 67, 925–939. https://doi.org/10.1093/sysbio/syy029

Leppänen, S. a., Altenhofer, E., Liston, A.D., Nyman, T., 2012. Phylogenetics and evolution of host-plant use in leaf-mining sawflies (Hymenoptera: Tenthredinidae: Heterarthrinae). Mol. Phylogenet. Evol. 64, 331–341. https://doi.org/10.1016/j.ympev.2012.04.005

Li, H., 2013. Aligning sequence reads, clone sequences and assembly contigs with BWA-MEM. arXiv 1303.3997.

Linnen, C.R., Farrell, B.D., 2008. Phylogenetic analysis of nuclear and mitochondrial genes reveals evolutionary relationships and mitochondrial introgression in the sertifer species group of the genus Neodiprion (Hymenoptera: Diprionidae). Mol. Phylogenet. Evol. 48, 240–57. https://doi.org/10.1016/j.ympev.2008.03.021

Linnen, C.R., Farrell, B.D., 2007. Mitonuclear discordance is caused by rampant mitochondrial introgression in Neodiprion (Hymenoptera: Diprionidae) sawflies. Evolution (N. Y). 61, 1417–

38. https://doi.org/10.1111/j.1558-5646.2007.00114.x

Ma, Y., Zheng, B., Zhu, J., van Achterberg, C., Tang, P., Chen, X., 2019. The first two mitochondrial genomes of wood wasps (Hymenoptera: Symphyta): Novel gene rearrangements and higher-level phylogeny of the basal hymenopterans. Int. J. Biol. Macromol. 123, 1189–1196. https://doi.org/10.1016/j.ijbiomac.2018.11.017

Maddison, W.P., Maddison, D.R., 2017. Mesquite: a modular system for evolutionary analysis. Version 3.2.

Malm, T., Nyman, T., 2015. Phylogeny of the symphytan grade of Hymenoptera: New pieces into the old jigsaw(fly) puzzle. Cladistics 31, 1–17. https://doi.org/10.1111/cla.12069

Meier, R., Wong, W., Srivathsan, A., Foo, M., 2016. $1 DNA barcodes for reconstructing complex phenomes and finding rare species in specimen-rich samples. Cladistics 32, 100–110. https://doi.org/10.1111/cla.12115

Misof, B., Liu, S., Meusemann, K., Peters, R.S., Donath, A., Mayer, C., Frandsen, P.B., Ware, J., Flouri, T., Beutel, R.G., Niehuis, O., Petersen, M., Izquierdo-Carrasco, F., Wappler, T., Rust, J., Aberer, a. J., Aspock, U., Aspock, H., Bartel, D., Blanke, A., Berger, S., Bohm, A., Buckley, T.R., Calcott, B., Chen, J., Friedrich, F., Fukui, M., Fujita, M., Greve, C., Grobe, P., Gu, S., Huang, Y., Jermiin, L.S., Kawahara, a. Y., Krogmann, L., Kubiak, M., Lanfear, R., Letsch, H., Li, Y., Li, Z., Li, J., Lu, H., Machida, R., Mashimo, Y., Kapli, P., McKenna, D.D., Meng, G., Nakagaki, Y., Navarrete-Heredia, J.L., Ott, M., Ou, Y., Pass, G., Podsiadlowski, L., Pohl, H., von Reumont, B.M., Schutte, K., Sekiya, K., Shimizu, S., Slipinski, A., Stamatakis, A., Song, W., Su, X., Szucsich, N.U., Tan, M., Tan, X., Tang, M., Tang, J., Timelthaler, G., Tomizuka, S., Trautwein, M., Tong, X., Uchifune, T., Walzl, M.G., Wiegmann, B.M., Wilbrandt, J., Wipfler, B., Wong, T.K.F., Wu, Q., Wu, G., Xie, Y., Yang, S., Yang, Q., Yeates, D.K., Yoshizawa, K., Zhang, Q., Zhang, R., Zhang, W., Zhang, Y., Zhao, J., Zhou, C., Zhou, L., Ziesmann, T., Zou, S., Li, Y., Xu, X., Zhang, Y., Yang, H., Wang, J., Wang, J., Kjer, K.M., Zhou, X., 2014. Phylogenomics resolves the timing and pattern of insect evolution. Science (80-.). 346, 763–767. https://doi.org/10.1126/science.1257570

Mutanen, M., Kivelä, S.M., Vos, R.A., Doorenweerd, C., Ratnasingham, S., Hausmann, A., Huemer, P., Dincă, V., van Nieukerken, E.J., Lopez-Vaamonde, C., Vila, R., Aarvik, L., Decaëns, T., Efetov, K.A., Hebert, P.D.N., Johnsen, A., Karsholt, O., Pentinsaari, M., Rougerie, R., Segerer, A., Tarmann, G., Zahiri, R., Godfray, H.C.J., 2016. Species-Level Para- and Polyphyly in DNA Barcode Gene Trees: Strong Operational Bias in European Lepidoptera. Syst. Biol. 65, 1024–1040. https://doi.org/10.1093/sysbio/syw044

Niu, G., Korkmaz, E.M., Doğan, Ö., Zhang, Y., Aydemir, M.N., Budak, M., Du, S., Başıbüyük, H.H., Wei, M., 2019. The first mitogenomes of the superfamily Pamphilioidea (Hymenoptera: Symphyta): Mitogenome architecture and phylogenetic inference. Int. J. Biol. Macromol. 124, 185–199. https://doi.org/10.1016/j.ijbiomac.2018.11.129

Normark, B.B., Jordal, B.H., Farrell, B.D., 1999. Origin of a haplodiploid beetle lineage. Proc. R. Soc. B Biol. Sci. 266, 2253–2259. https://doi.org/10.1098/rspb.1999.0916

Nyman, T., Zinovjev, A.G., Vikberg, V., Farrell, B.D., 2006. Molecular phylogeny of the sawfly subfamily Nematinae (Hymenoptera: Tenthredinidae). Syst. Entomol. 31, 569–583. https://doi.org/10.1111/j.1365-3113.2006.00336.x

Papakostas, S., Michaloudi, E., Proios, K., Brehm, M., Verhage, L., Rota, J., Peña, C., Stamou, G., Pritchard, V.L., Fontaneto, D., Declerck, S.A.J., 2016. Integrative Taxonomy Recognizes Evolutionary Units Despite Widespread Mitonuclear Discordance: Evidence from a Rotifer Cryptic Species Complex. Syst. Biol. 65, 508–524. https://doi.org/10.1093/sysbio/syw016

Paradis, E., Schliep, K., 2018. ape 5.0: an environment for modern phylogenetics and evolutionary analyses in R. Bioinformatics 1–3. https://doi.org/10.1093/bioinformatics/bty633

Patten, M.M., Carioscia, S.A., Linnen, C.R., 2015. Biased introgression of mitochondrial and nuclear genes: a comparison of diploid and haplodiploid systems. Mol. Ecol. 24, 5200–5210.

https://doi.org/10.1111/mec.13318
Pentinsaari, M., Salmela, H., Mutanen, M., Roslin, T., 2016. Molecular evolution of a widely-adopted taxonomic marker (COI) across the animal tree of life. Sci. Rep. 6, 35275. https://doi.org/10.1038/srep35275
Pentinsaari, M., Vos, R., Mutanen, M., 2017. Algorithmic single-locus species delimitation: effects of sampling effort, variation and nonmonophyly in four methods and 1870 species of beetles. Mol. Ecol. Resour. 17, 393–404. https://doi.org/10.1111/1755-0998.12557
Peters, R.S., Krogmann, L., Mayer, C., Donath, A., Gunkel, S., Meusemann, K., Kozlov, A., Podsiadlowski, L., Petersen, M., Lanfear, R., Diez, P.A., Heraty, J., Kjer, K.M., Klopfstein, S., Meier, R., Polidori, C., Schmitt, T., Liu, S., Zhou, X., Wappler, T., Rust, J., Misof, B., Niehuis, O., 2017. Evolutionary History of the Hymenoptera. Curr. Biol. 27, 1013–1018. https://doi.org/10.1016/j.cub.2017.01.027
Peterson, B.K., Weber, J.N., Kay, E.H., Fisher, H.S., Hoekstra, H.E., 2012. Double Digest RADseq: An Inexpensive Method for De Novo SNP Discovery and Genotyping in Model and Non-Model Species. PLoS One 7, e37135. https://doi.org/10.1371/journal.pone.0037135
Philippe, H., Delsuc, F., Brinkmann, H., Lartillot, N., 2005. Phylogenomics. Annu. Rev. Ecol. Evol. Syst. 36, 541–562. https://doi.org/10.1146/annurev.ecolsys.35.112202.130205
Philippe, H., Vienne, D.M. de, Ranwez, V., Roure, B., Baurain, D., Delsuc, F., 2017. Pitfalls in supermatrix phylogenomics. Eur. J. Taxon. 283, 1–25. https://doi.org/10.5852/ejt.2017.283
Pritchard, J.K., Stephens, M., Donnelly, P., 2000. Inference of population structure using multilocus genotype data. Genetics 155, 945–59.
Prous, M., 2012. Taxonomy and phylogeny of the sawfly genus Empria (Hymenoptera, Tenthredinidae). Dissertationes biologicae universitatis tartuensis. Tartu Ülikooli Kirjastus.
Prous, M., Blank, S.M., Heibo, E., Lønnve, O.J., Vårdal, H., Liston, A., 2014. Sawflies (Hymenoptera, Symphyta) newly recorded from Sweden. Entomol. Tidskr. 135, 135–146.
Prous, M., Heidemaa, M., Shinohara, A., Soon, V., 2011a. Review of the sawfly genus Empria (Hymenoptera, Tenthredinidae) in Japan. Zookeys 150, 347–380. https://doi.org/10.3897/zookeys.150.1968
Prous, M., Heidemaa, M., Soon, V., 2011b. Empria longicornis species group: taxonomic revision with notes on phylogeny and ecology (Hymenoptera, Tenthredinidae). Zootaxa 2756, 1–39.
Prous, M., Kramp, K., Vikberg, V., Liston, A., 2017. North-Western Palaearctic species of Pristiphora (Hymenoptera, Tenthredinidae). J. Hymenopt. Res. 59, 1–190. https://doi.org/10.3897/jhr.59.12656
Prous, M., Vikberg, V., Liston, A., Kramp, K., 2016. North-Western Palaearctic species of the Pristiphora ruficornis group (Hymenoptera, Tenthredinidae). J. Hymenopt. Res. 51, 1–54. https://doi.org/10.3897/jhr.51.9162
R Core Team, 2017. R: A language and environment for statistical computing.
Rambaut, A., 2015. FigTree, v1.4.2: Tree Figure Drawing Tool. Molecular evolution, phylogenetics and epidemiology. Available from: http://tree.bio.ed.ac.uk/software/figtree/.
Rosenberg, N.A., 2004. distruct: a program for the graphical display of population structure. Mol. Ecol. Notes 4, 137–138. https://doi.org/10.1046/j.1471-8286.2003.00566.x
Roux, C., Fraïsse, C., Romiguier, J., Anciaux, Y., Galtier, N., Bierne, N., 2016. Shedding Light on the Grey Zone of Speciation along a Continuum of Genomic Divergence. PLOS Biol. 14, e2000234. https://doi.org/10.1371/journal.pbio.2000234
Schmidt, S., Schmid-Egger, C., Morinière, J., Haszprunar, G., Hebert, P.D.N., 2015. DNA barcoding largely supports 250 years of classical taxonomy: identifications for Central European bees (Hymenoptera, Apoidea partim). Mol. Ecol. Resour. 15, 985–1000. https://doi.org/10.1111/1755-0998.12363
Schmidt, S., Taeger, A., Morinière, J., Liston, A., Blank, S.M., Kramp, K., Kraus, M., Schmidt, O., Heibo, E., Prous, M., Nyman, T., Malm, T., Stahlhut, J., 2017. Identification of sawflies and

horntails (Hymenoptera, 'Symphyta') through DNA barcodes: successes and caveats. Mol. Ecol. Resour. 17, 670–685. https://doi.org/10.1111/1755-0998.12614

Schnell, I.B., Bohmann, K., Gilbert, M.T.P., 2015. Tag jumps illuminated - reducing sequence-to-sample misidentifications in metabarcoding studies. Mol. Ecol. Resour. 15, 1289–1303. https://doi.org/10.1111/1755-0998.12402

Simion, P., Philippe, H., Baurain, D., Jager, M., Richter, D.J., Di Franco, A., Roure, B., Satoh, N., Quéinnec, É., Ereskovsky, A., Lapébie, P., Corre, E., Delsuc, F., King, N., Wörheide, G., Manuel, M., 2017. A Large and Consistent Phylogenomic Dataset Supports Sponges as the Sister Group to All Other Animals. Curr. Biol. 27, 958–967. https://doi.org/10.1016/j.cub.2017.02.031

Sloan, D.B., Havird, J.C., Sharbrough, J., 2017. The on-again, off-again relationship between mitochondrial genomes and species boundaries. Mol. Ecol. 2212–2236. https://doi.org/10.1111/mec.13959

Stamatakis, A., 2014. RAxML version 8: a tool for phylogenetic analysis and post-analysis of large phylogenies. Bioinformatics 30, 1312–1313. https://doi.org/10.1093/bioinformatics/btu033

Swofford, D.L., 2003. PAUP*: phylogenetic analysis using parsimony, version 4.0 b10. Sinauer Associates, Sunderland, MA.

Taeger, A., Liston, A.D., Prous, M., Groll, E.K., Gehroldt, T., M., B.S., 2018. ECatSym – Electronic World Catalog of Symphyta (Insecta, Hymenoptera). Program version 5.0 (19 Dec 2018), data version 40 (23 Sep 2018) [WWW Document]. URL https://sdei.de/ecatsym/

Tamura, K., Stecher, G., Peterson, D., Filipski, A., Kumar, S., 2013. MEGA6: Molecular Evolutionary Genetics Analysis version 6.0. Mol. Biol. Evol. 30, 2725–2729. https://doi.org/10.1093/molbev/mst197

Tang, P., Zhu, J., Zheng, B., Wei, S., Sharkey, M., Chen, X., Vogler, A.P., 2019. Mitochondrial phylogenomics of the Hymenoptera. Mol. Phylogenet. Evol. 131, 8–18. https://doi.org/10.1016/j.ympev.2018.10.040

Tang, Q.-Y., Liu, S.-Q., Yu, D., Liu, H.-Z., Danley, P.D., 2012. Mitochondrial capture and incomplete lineage sorting in the diversification of balitorine loaches (Cypriniformes, Balitoridae) revealed by mitochondrial and nuclear genes. Zool. Scr. 41, 233–247. https://doi.org/10.1111/j.1463-6409.2011.00530.x

Tarver, J.E., dos Reis, M., Mirarab, S., Moran, R.J., Parker, S., O'Reilly, J.E., King, B.L., O'Connell, M.J., Asher, R.J., Warnow, T., Peterson, K.J., Donoghue, P.C.J., Pisani, D., 2016. The Interrelationships of Placental Mammals and the Limits of Phylogenetic Inference. Genome Biol. Evol. 8, 330–344. https://doi.org/10.1093/gbe/evv261

Valk, T. van der, Vezzi, F., Ormestad, M., Dalen, L., Guschanski, K., 2018. Index hopping on the Illumina HiseqX platform and its consequences for ancient DNA studies. bioRxiv 179028. https://doi.org/10.1101/179028

Zahiri, R., Lafontaine, J.D., Schmidt, B.C., DeWaard, J.R., Zakharov, E. V., Hebert, P.D.N., 2017. Probing planetary biodiversity with DNA barcodes: The Noctuoidea of North America. PLoS One 12, e0178548. https://doi.org/10.1371/journal.pone.0178548

[Figures and figure captions]

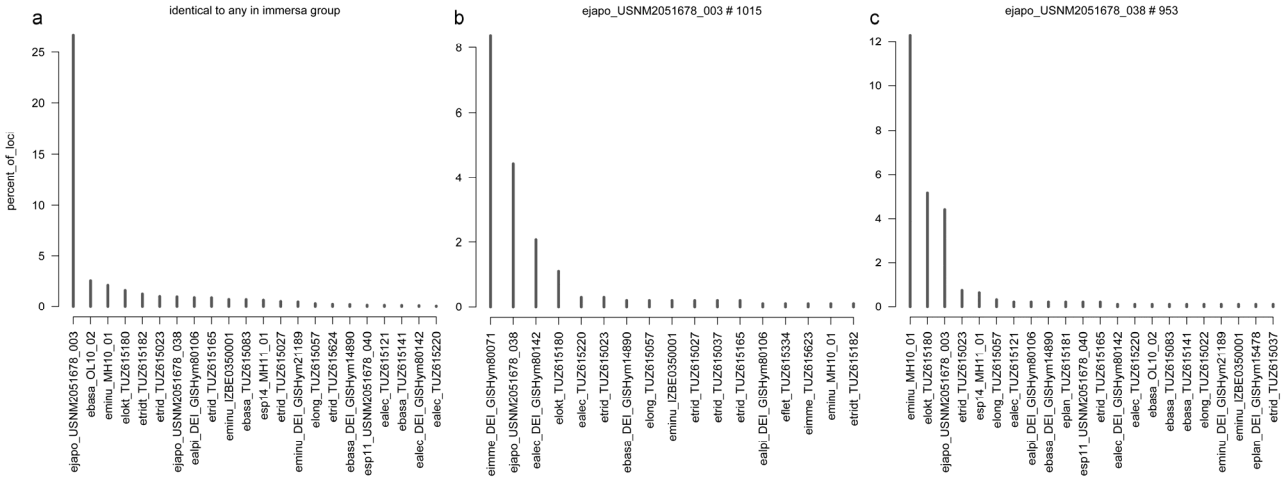

Fig. 1. Examples of results of cross-contamination check by counting identical loci among *Empria* specimens (dataset with 19 413 loci, Supplementary Data S4). For results of all samples see Supplementary Data S5. (a) Percent of loci in every *longicornis* group specimen (X-axis) (including *E. tridentis*) that are identical to any specimen in *immersa* group, while different from other specimens in *longicornis* group (if present). (b, c) Percent of loci in *E. japonica* USNM2051678_003 (b) and USNM2051678_038 (c) that are identical to a particular specimen (listed along X-axis) while different from the others in the dataset.

(a) *E. longicornis* group

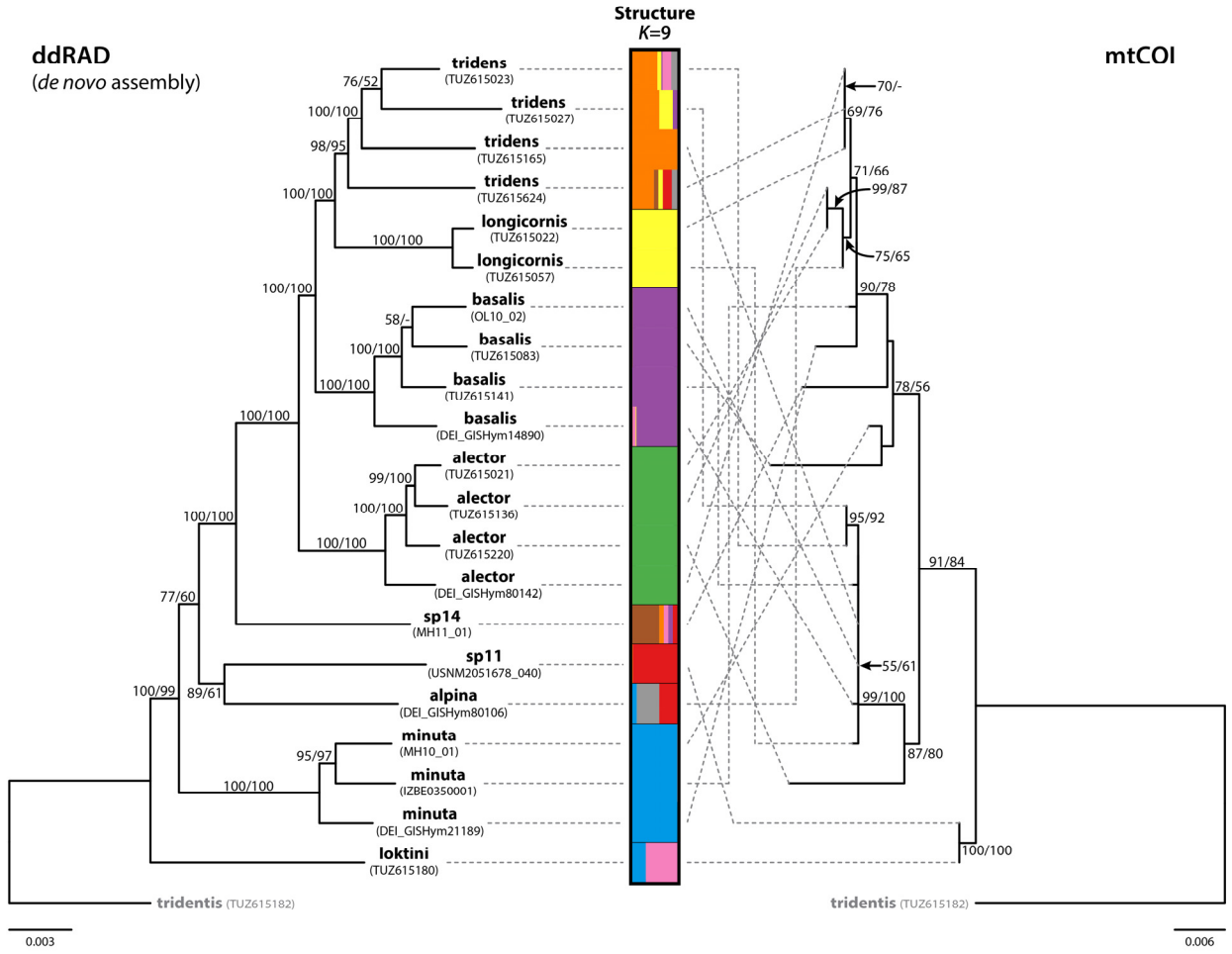

(b) *E. immersa* group

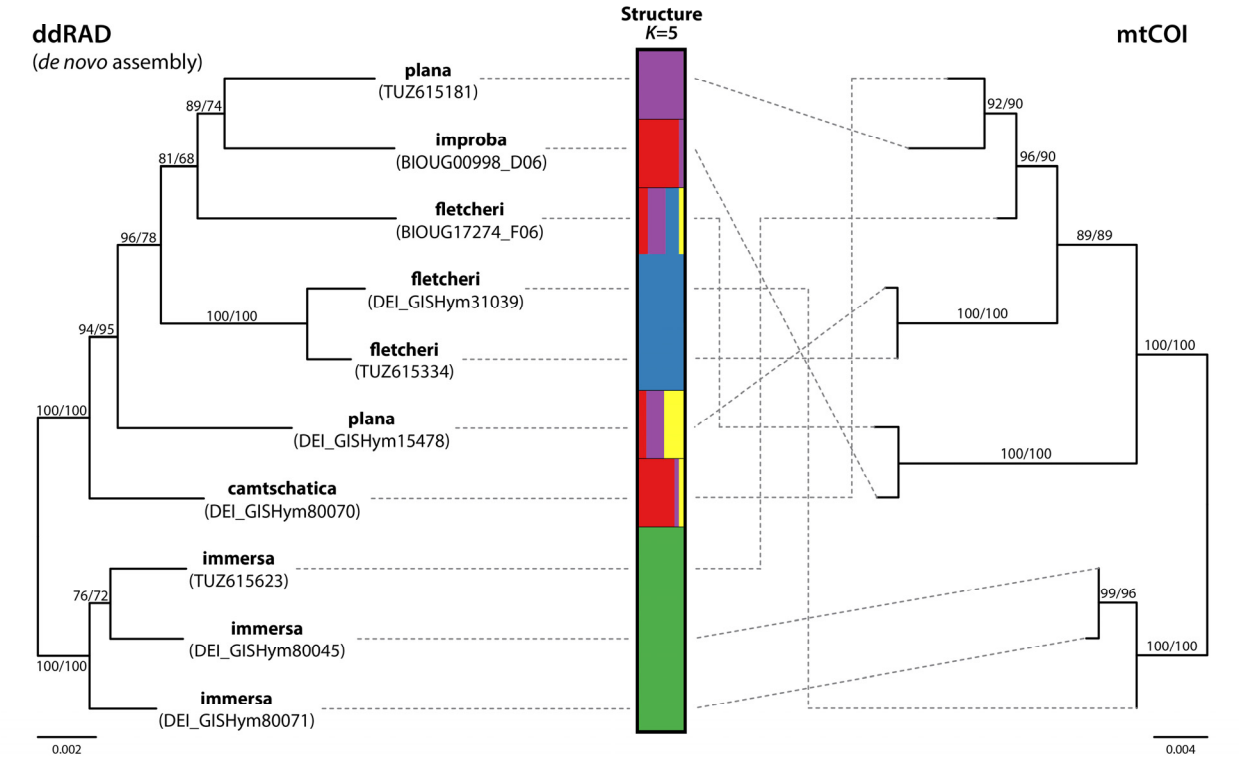

Fig. 2. Maximum likelihood trees of two *Empria* species groups and population admixture analyses based on ddRAD *de novo* assemblies in comparison with mitochondrial COI maximum likelihood tree (1536 bp). (a) *E. longicornis* group (ddRAD dataset with 20 871 loci). (b) *E. immersa* group (ddRAD dataset with 9 362 loci). Bootstrap support values (%) below or above branches resulting from maximum likelihood (ML) and maximum parsimony (MP) analyses are shown as ML/MP.

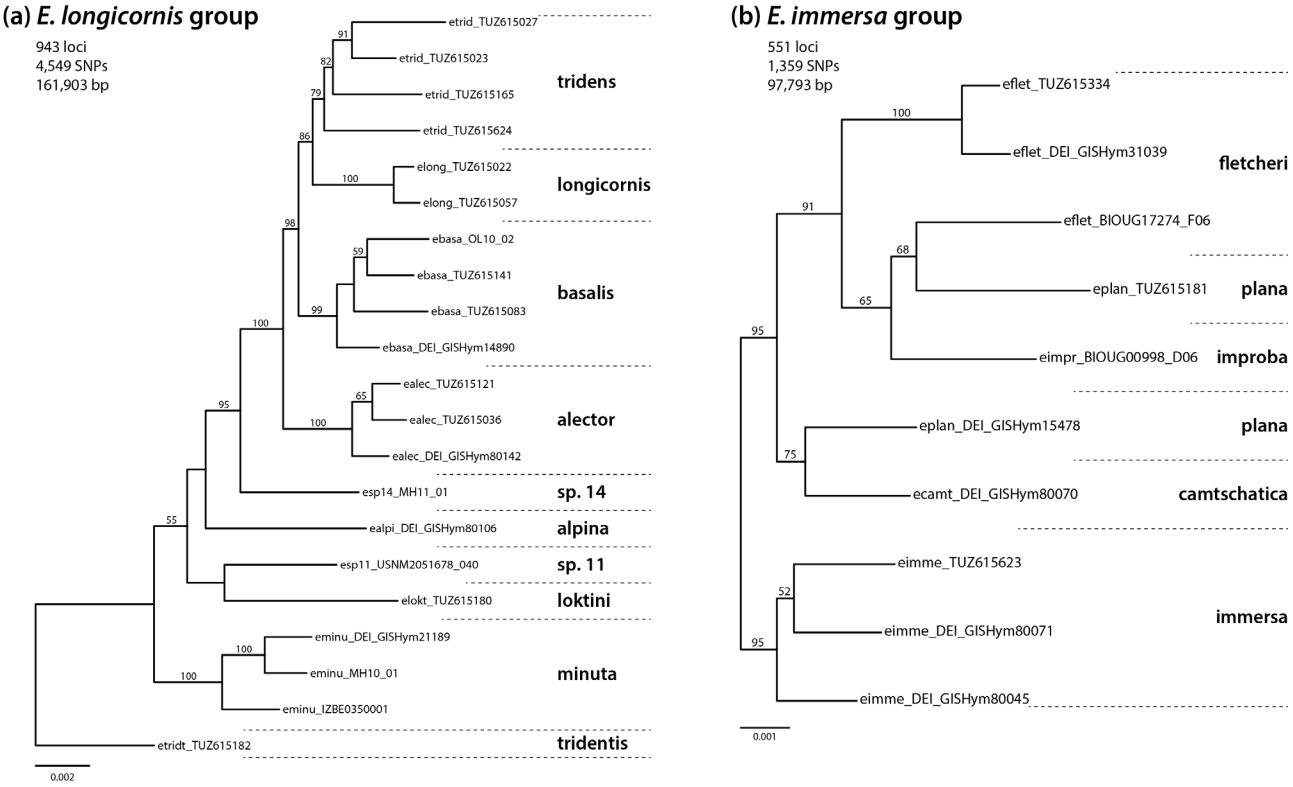

Fig. 3. Maximum likelihood trees of two *Empria* species groups based on ddRAD reference assembly. (a) *E. longicornis* group. (b) *E. immersa* group.

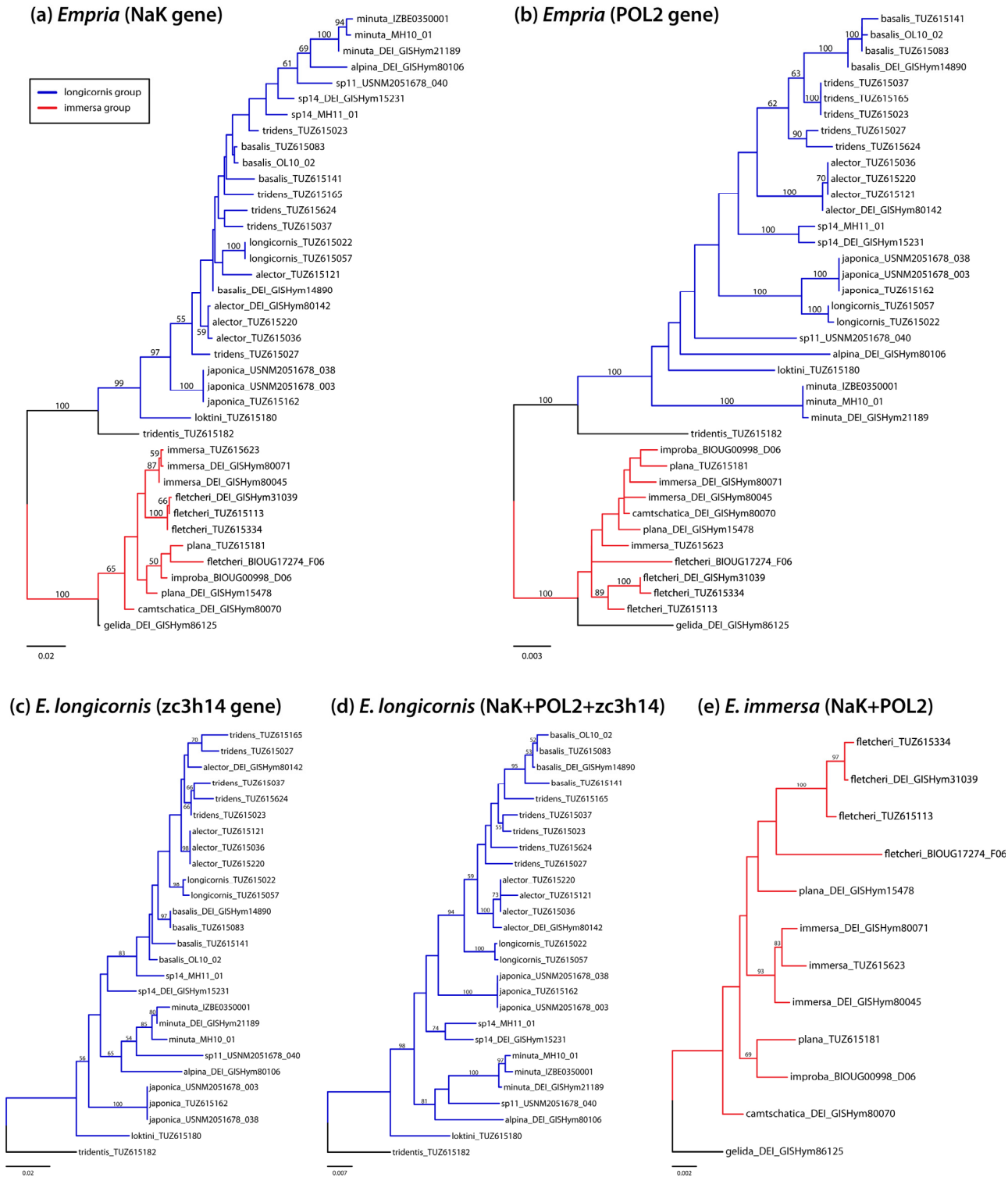

Fig. 4. Maximum likelihood trees based on three nuclear protein coding genes obtained by Sanger sequencing. (a) NaK (1654 bp). (b) POL2 (2494 bp). (c) ZC3H14 (alignment 1654 bp). (d) Concatenated NaK, POL2, and ZC3H14 (alignment 5802 bp) for *longicornis* group. (e) Concatenated NaK and POL2 (4148 bp) for *immersa* group.

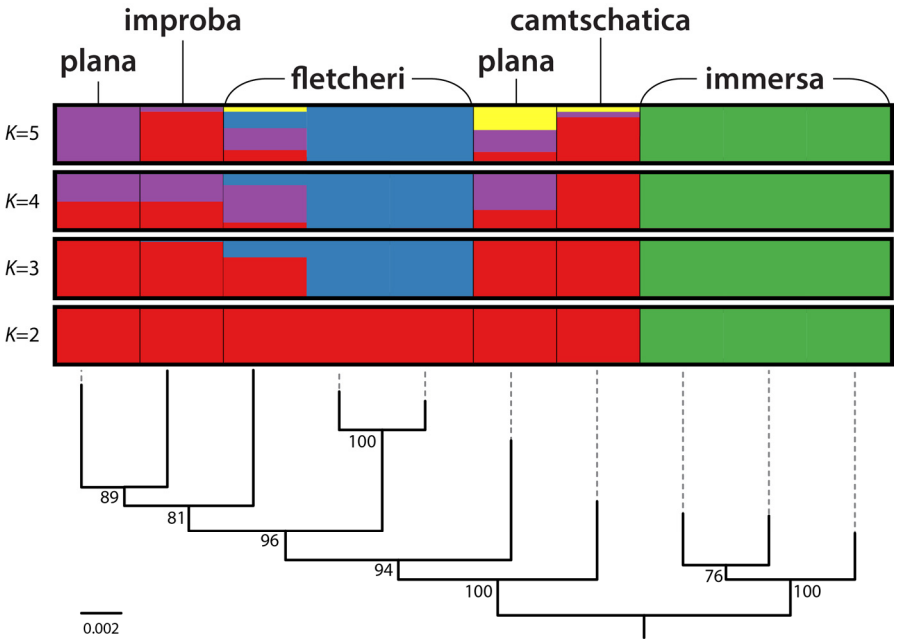

Fig. 5. Population admixture analysis of *Empria immersa* group with Structure at *K*=3 to *K*=5 (*de novo* assembly). Maximum likelihood tree from Fig. 2 is shown below the results of Structure analyses.

Supplementary Data S1–S12

Detection of cross-contamination and strong mitonuclear discordance in two species groups of sawfly genus *Empria* (Hymenoptera, Tenthredinidae)

Marko Prousa, Kyung Min Lee, Marko Mutanen

Supplementary Data S1
ddRAD ML tree_Empria

c80m4_emp_35samp data matrix
29,859 loci
674,527 SNPs
5,945,539 bp

* excluded samples (15):
ealpi_DEI-GISHym15214, ealpi_DEI-GISHym80011, ebasa_TUZ615625, ecamt_DEI-GISHym20706, eflet_BIOUG00998-E05, eflet_TUZ615113, eimpr_BIOUG00998-B05, eimpr_BIOUG00998-D05, ejapo_TUZ615162, elong_DEI-GISHym14886, emont_DEI-GISHym80040, eplan_BIOUG00998-C05, esp14_DEI-GISHym15231, etrid_DEI-GISHym20872, etridt_USNM2057434_19

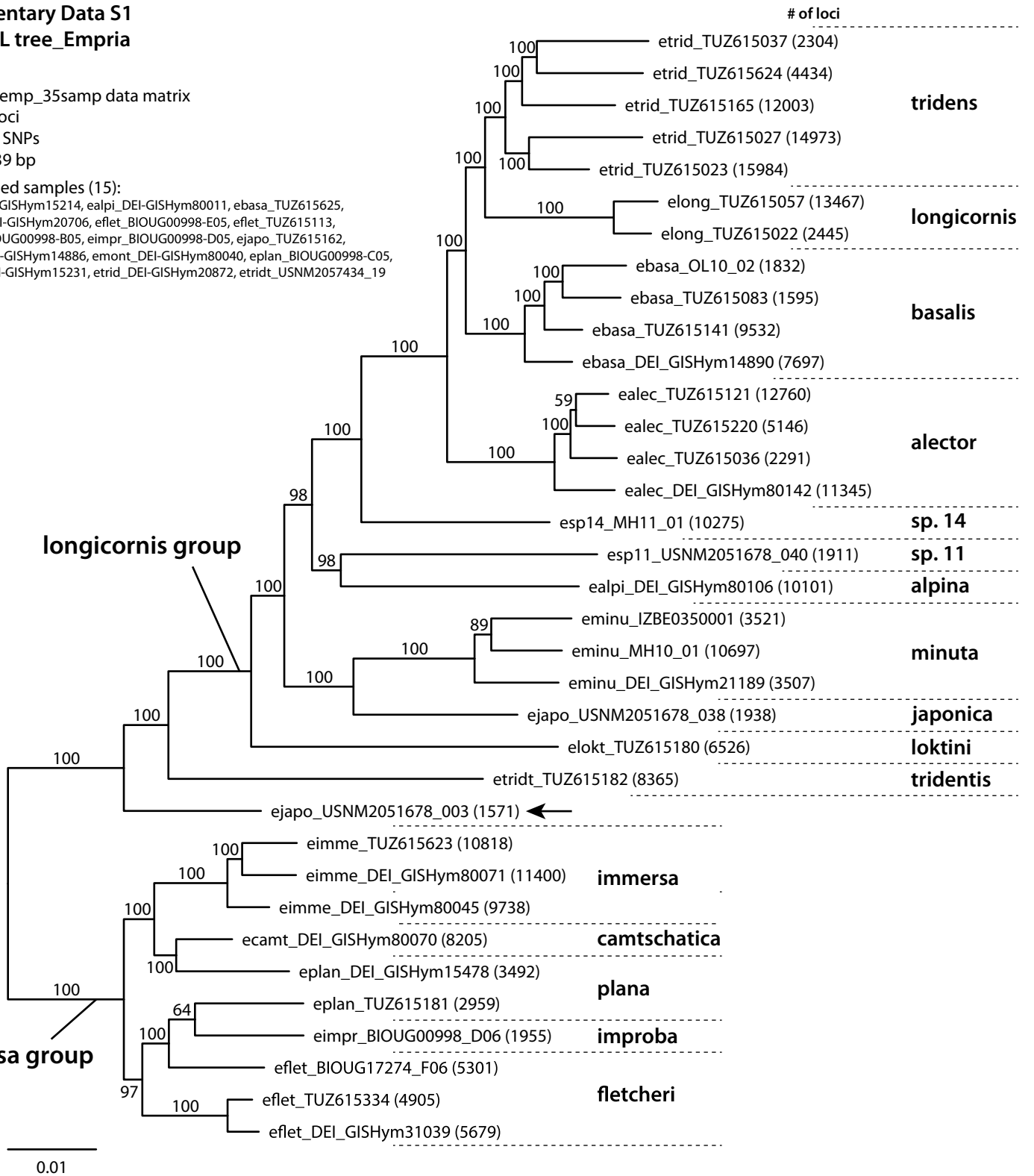

Supplementary Data S2

a

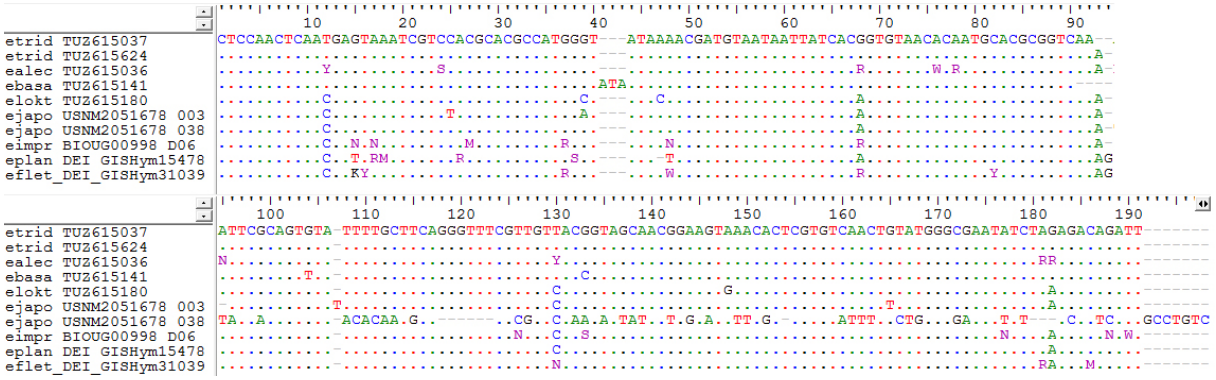

b

Two examples of problematic loci (possibly due to mis-association of paired-end reads) from the initial dataset with 29 859 loci (*de novo* assembly at clustering threshold of 80% similarity; Supplementary Data S1). In the first example (a) *Empria japonica* USNM2051678_038 is unalignable compared to others in the second half of the locus. In the second example (b) most specimens are very different from each other in the second half of the locus.

Supplementary Data S3

An example of locus from the initial dataset with 29 859 loci (*de novo* assembly at clustering threshold of 80% similarity; Supplementary Data S1) where *Empria japonica* USNM2051678_003 is identical (except for one indel) to *E. immersa* DEI-GISHym80071 while clearly different from other specimens, especially from specimens of *longicornis* group. The one additional "C" in the middle of USNM2051678_003 compared to DEI-GISHym80071 could be due to differences in lengths of quality trimmed paired-end reads.

Supplementary Data S4
ddRAD ML tree_Empria

c80m4_emp_35samp data matrix
19,413 loci
223,828 SNPs
3,517,320 bp

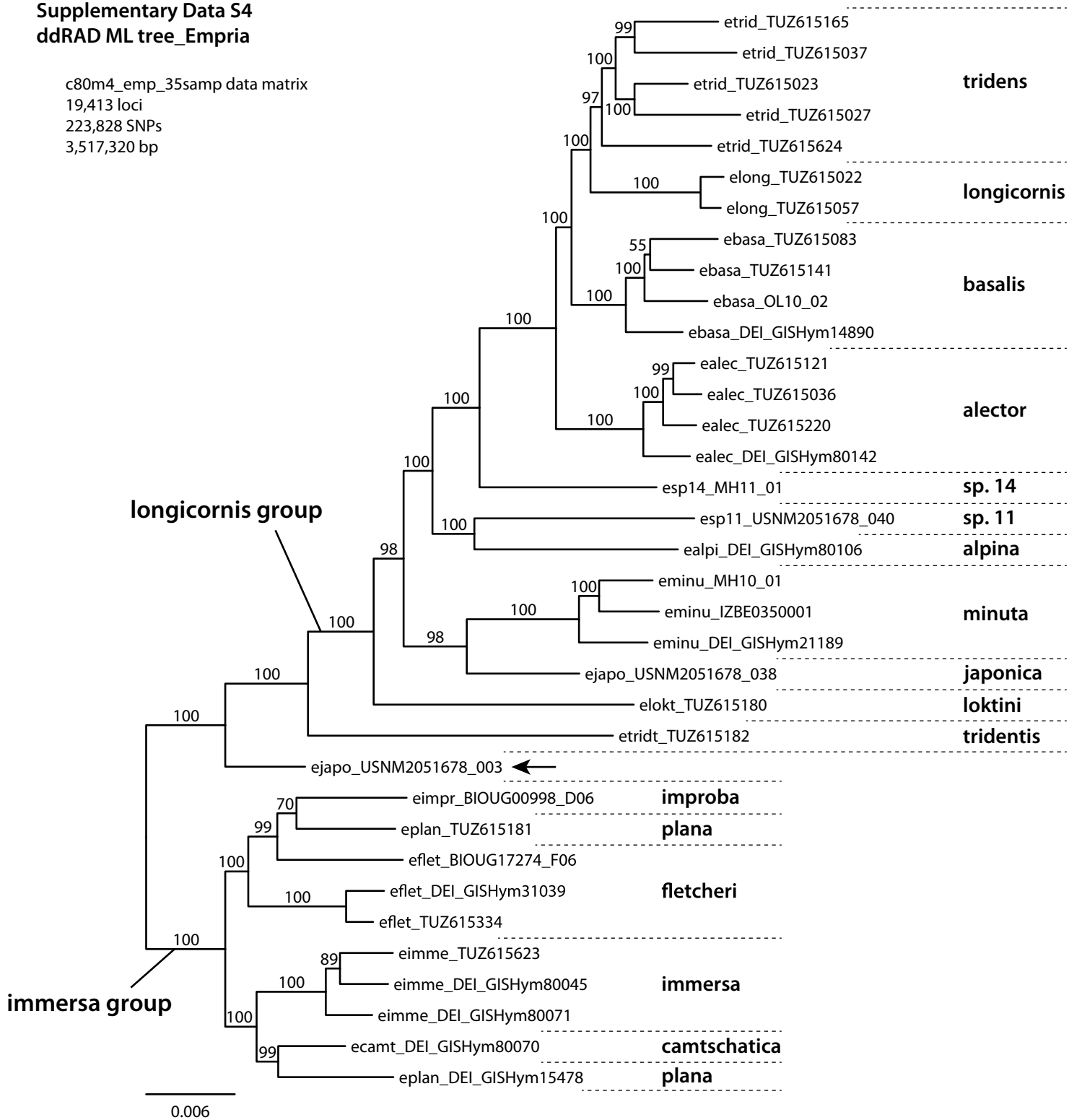

Supplementary Data S5

20 pp.

Next 20 pages show results of loci counts that are identical between *Empria longicornis* and *E. immersa* groups and among all specimens (*de novo* assembly, 19 413 loci; Supplementary Data S4). First two graphs show percent of loci in every *longicornis* (including *E. tridentis*) and *immersa* group specimen (X-axis) that are identical to any specimen in *immersa* or *longicorns* group, respectively, while different from other specimens in its own group (if present). The following graphs on 18 pages show for every specimen the percent of loci and normalised percent of loci that are identical to a particular specimen (X-axis) while different from all others in the dataset. Normalised numbers of loci for specimens were calculated as half of the maximum number of loci divided by the number of loci of that specimen. # - number of loci present for that specimen.

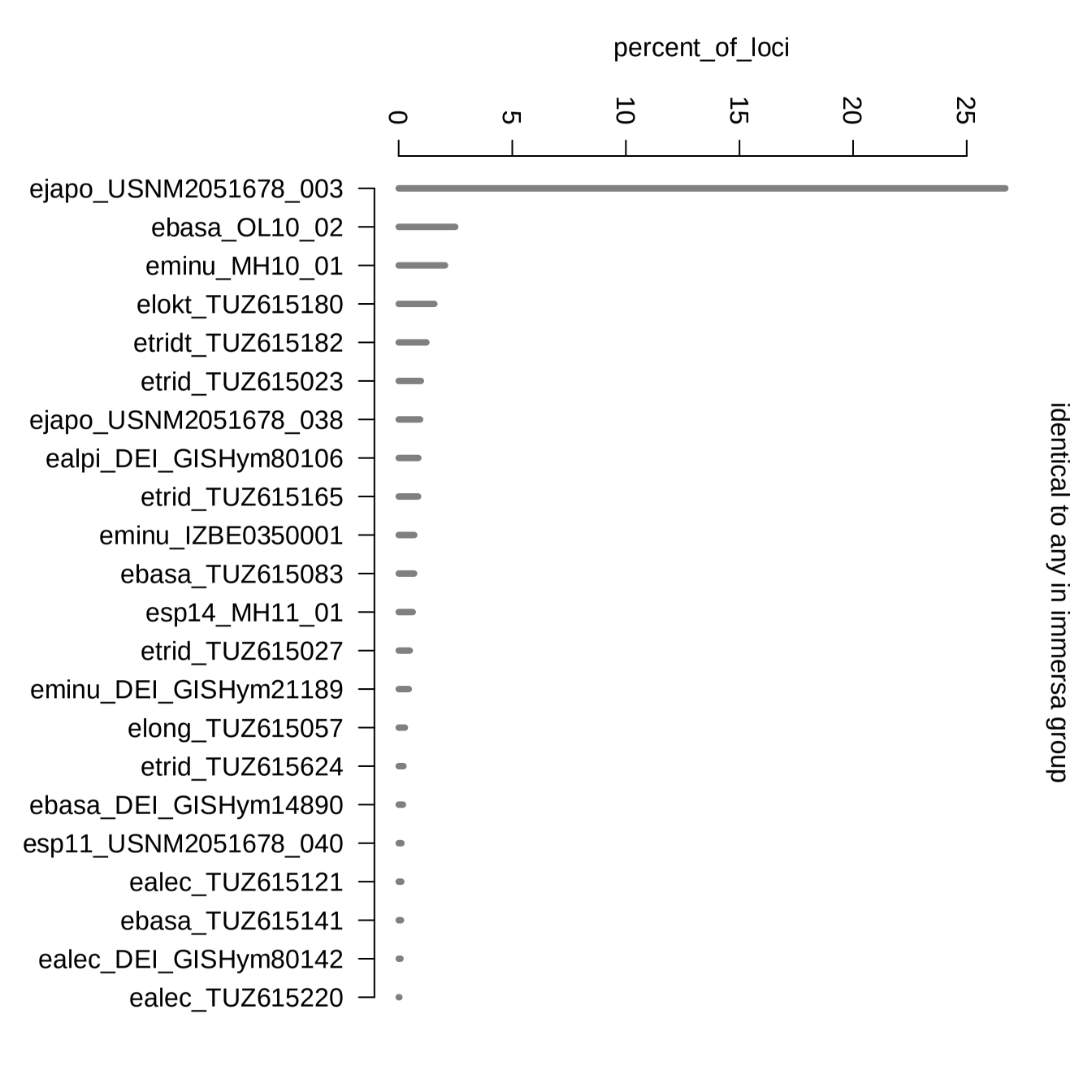
percent_of_loci
0
5
10
15
20
25
ejapo_USNM2051678_003
ebasa_OL10_02
eminu_MH10_01
elokt_TUZ615180
etridt_TUZ615182
etrid_TUZ615023
ejapo_USNM2051678_038
ealpi_DEI_GISHym80106
etrid_TUZ615165
eminu_IZBE0350001
ebasa_TUZ615083
esp14_MH11_01
etrid_TUZ615027
eminu_DEI_GISHym21189
elong_TUZ615057
etrid_TUZ615624
ebasa_DEI_GISHym14890
esp11_USNM2051678_040
ealec_TUZ615121
ebasa_TUZ615141
ealec_DEI_GISHym80142
ealec_TUZ615220
identical to any in immersa group

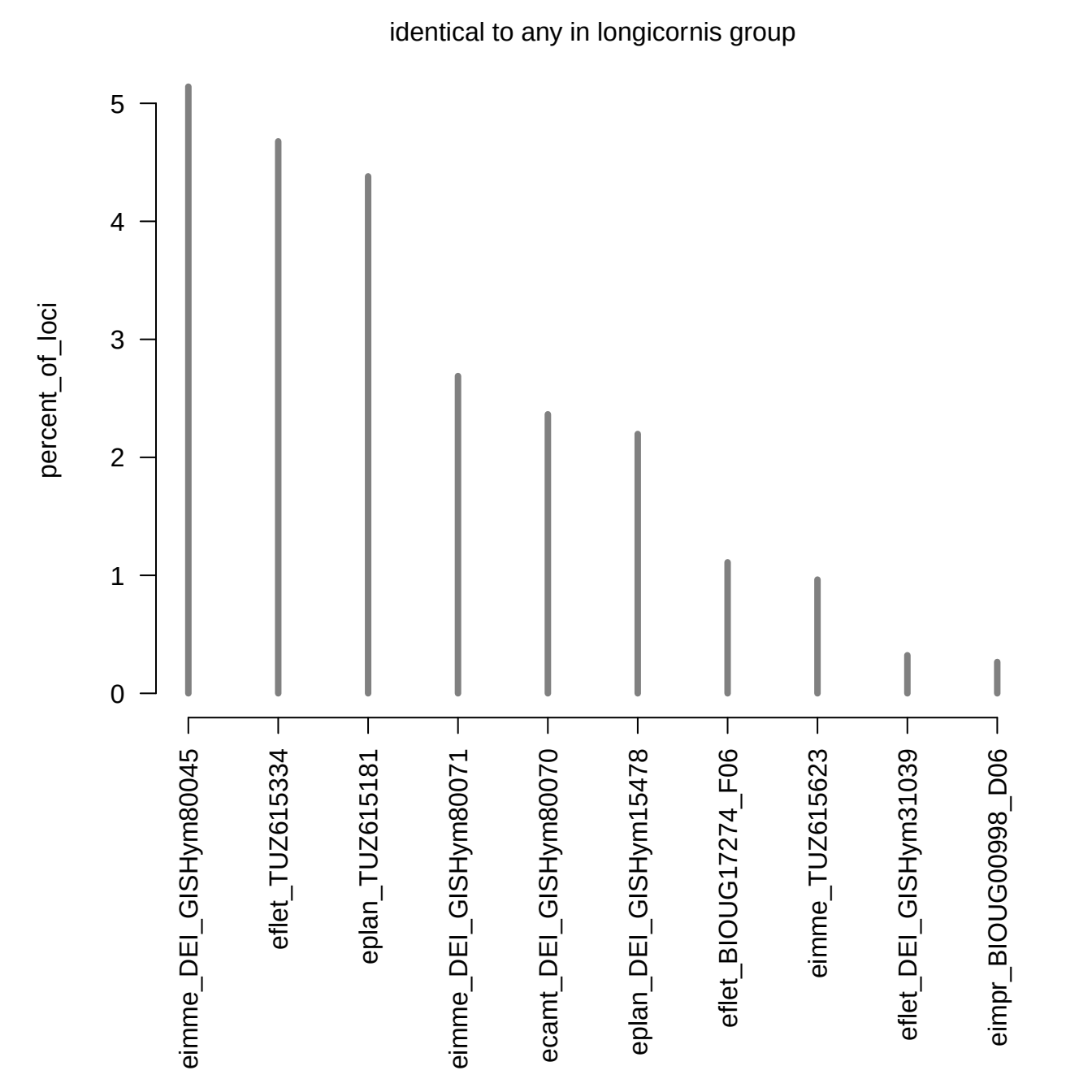
identical to any in longicornis group
percent_of_loci
0
1
2
3
4
5
eimme_DEI_GISHym80045
eflet_TUZ615334
eplan_TUZ615181
eimme_DEI_GISHym80071
ecamt_DEI_GISHym80070
eplan_DEI_GISHym15478
eflet_BIOUG17274_F06
eimme_TUZ615623
eflet_DEI_GISHym31039
eimpr_BIOUG00998_D06

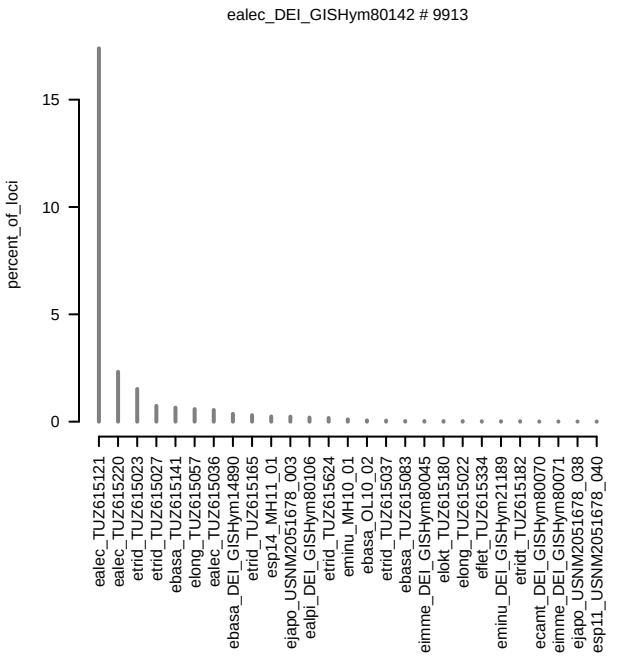
ealec_DEI_GISHym80142 # 9913
percent_of_loci
0
5
10
15
ealec_TUZ615121
ealec_TUZ615220
etrid_TUZ615023
etrid_TUZ615027
ebasa_TUZ615141
elong_TUZ615057
ealec_TUZ615036
ebasa_DEI_GISHym14890
etrid_TUZ615165
esp14_MH11_01
ejapo_USNM2051678_003
ealpi_DEI_GISHym80106
etrid_TUZ615624
eminu_MH10_01
ebasa_OL10_02
etrid_TUZ615037
ebasa_TUZ615083
eimme_DEI_GISHym80045
elokt_TUZ615180
elong_TUZ615022
eflet_TUZ615334
eminu_DEI_GISHym21189
etridt_TUZ615182
ecamt_DEI_GISHym80070
eimme_DEI_GISHym80071
ejapo_USNM2051678_038
esp11_USNM2051678_040

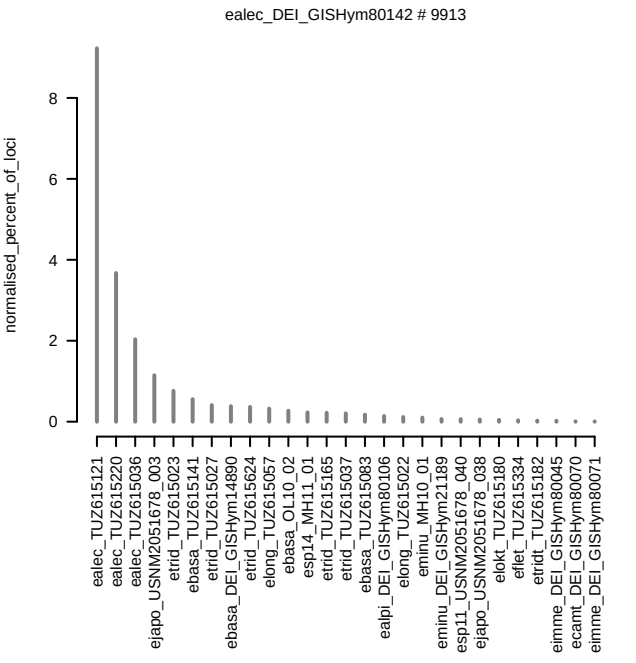
ealec_DEI_GISHym80142 # 9913
normalised_percent_of_loci
0
2
4
6
8
ealec_TUZ615121
ealec_TUZ615220
ealec_TUZ615036
ejapo_USNM2051678_003
etrid_TUZ615023
ebasa_TUZ615141
etrid_TUZ615027
ebasa_DEI_GISHym14890
etrid_TUZ615624
elong_TUZ615057
ebasa_OL10_02
esp14_MH11_01
etrid_TUZ615165
etrid_TUZ615037
ebasa_TUZ615083
ealpi_DEI_GISHym80106
elong_TUZ615022
eminu_MH10_01
eminu_DEI_GISHym21189
esp11_USNM2051678_040
ejapo_USNM2051678_038
elokt_TUZ615180
eflet_TUZ615334
etridt_TUZ615182
eimme_DEI_GISHym80045
ecamt_DEI_GISHym80070
eimme_DEI_GISHym80071

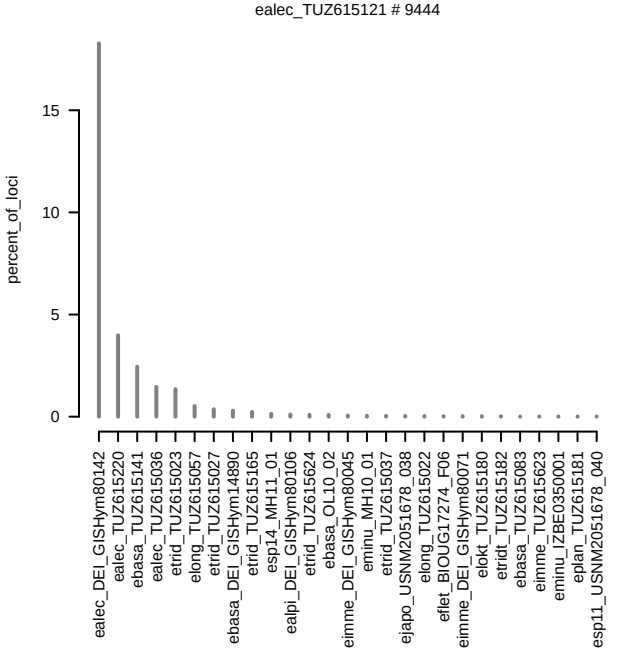
ealec_TUZ615121 # 9444
percent_of_loci
0
5
10
15
ealec_DEI_GISHym80142
ealec_TUZ615220
ebasa_TUZ615141
ealec_TUZ615036
etrid_TUZ615023
elong_TUZ615057
etrid_TUZ615027
ebasa_DEI_GISHym14890
etrid_TUZ615165
esp14_MH11_01
ealpi_DEI_GISHym80106
etrid_TUZ615624
ebasa_OL10_02
eimme_DEI_GISHym80045
eminu_MH10_01
etrid_TUZ615037
ejapo_USNM2051678_038
elong_TUZ615022
eflet_BIOUG17274_F06
eimme_DEI_GISHym80071
elokt_TUZ615180
etridt_TUZ615182
ebasa_TUZ615083
eimme_TUZ615623
eminu_IZBE0350001
eplan_TUZ615181
esp11_USNM2051678_040

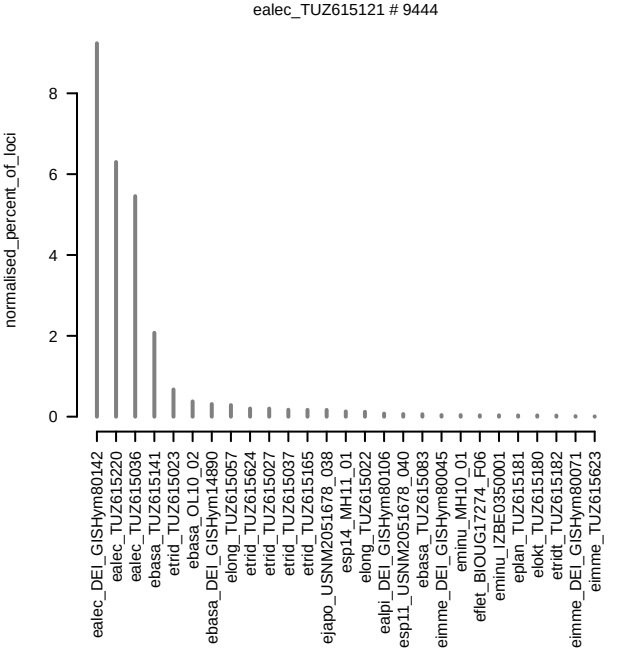
ealec_TUZ615121 # 9444
normalised_percent_of_loci
0
2
4
6
8
ealec_DEI_GISHym80142
ealec_TUZ615220
ealec_TUZ615036
ebasa_TUZ615141
etrid_TUZ615023
ebasa_OL10_02
ebasa_DEI_GISHym14890
elong_TUZ615057
etrid_TUZ615624
etrid_TUZ615027
etrid_TUZ615037
etrid_TUZ615165
ejapo_USNM2051678_038
esp14_MH11_01
elong_TUZ615022
ealpi_DEI_GISHym80106
esp11_USNM2051678_040
ebasa_TUZ615083
eimme_DEI_GISHym80045
eminu_MH10_01
eflet_BIOUG17274_F06
eminu_IZBE0350001
eplan_TUZ615181
elokt_TUZ615180
etridt_TUZ615182
eimme_DEI_GISHym80071
eimme_TUZ615623

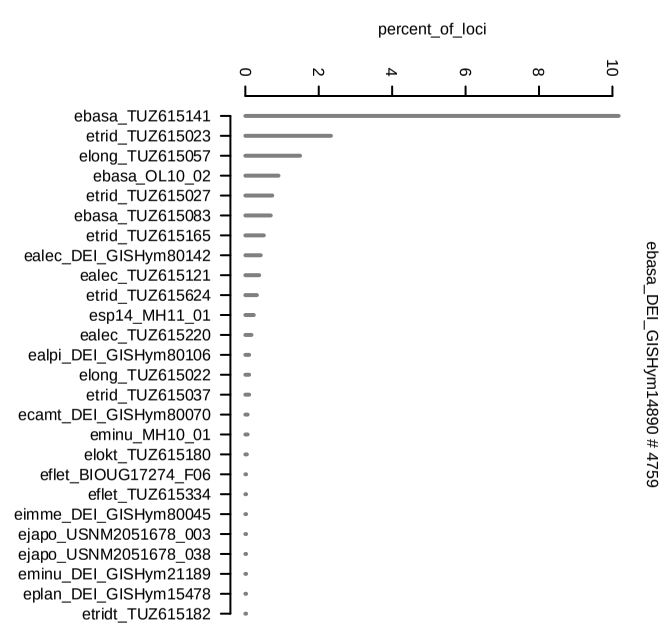
percent_of_loci
0
2
4
6
8
10
ebasa_TUZ615141
etrid_TUZ615023
elong_TUZ615057
ebasa_OL10_02
etrid_TUZ615027
ebasa_TUZ615083
etrid_TUZ615165
ealec_DEI_GISHym80142
ealec_TUZ615121
etrid_TUZ615624
esp14_MH11_01
ealec_TUZ615220
ealpi_DEI_GISHym80106
elong_TUZ615022
etrid_TUZ615037
ecamt_DEI_GISHym80070
eminu_MH10_01
elokt_TUZ615180
eflet_BIOUG17274_F06
eflet_TUZ615334
eimme_DEI_GISHym80045
ejapo_USNM2051678_003
ejapo_USNM2051678_038
eminu_DEI_GISHym21189
eplan_DEI_GISHym15478
etridt_TUZ615182
ebasa_DEI_GISHym14890 # 4759

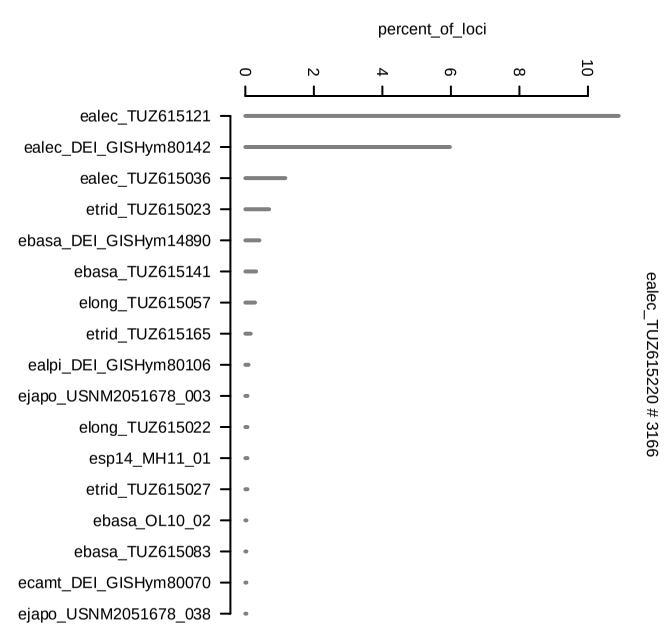
percent_of_loci
0
2
4
6
8
10
ealec_TUZ615121
ealec_DEI_GISHym80142
ealec_TUZ615036
etrid_TUZ615023
ebasa_DEI_GISHym14890
ebasa_TUZ615141
elong_TUZ615057
etrid_TUZ615165
ealpi_DEI_GISHym80106
ejapo_USNM2051678_003
elong_TUZ615022
esp14_MH11_01
etrid_TUZ615027
ebasa_OL10_02
ebasa_TUZ615083
ecamt_DEI_GISHym80070
ejapo_USNM2051678_038
ealec_TUZ615220 # 3166

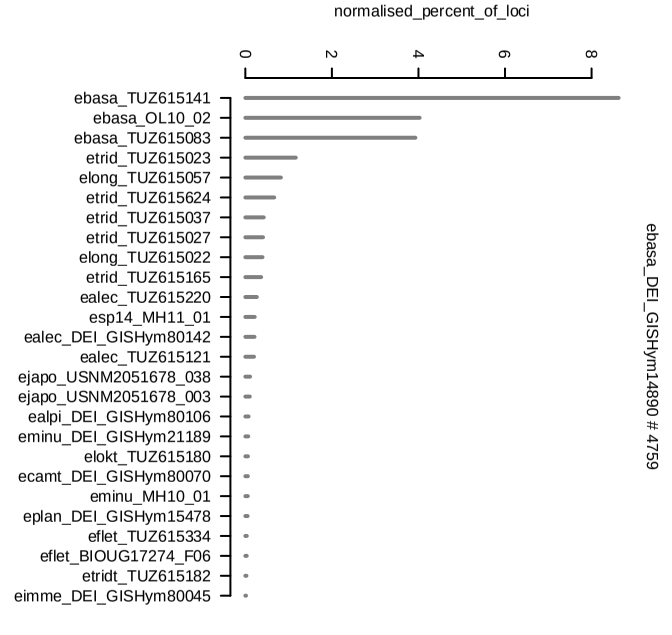
normalised_percent_of_loci
0
2
4
6
8
ebasa_TUZ615141
ebasa_OL10_02
ebasa_TUZ615083
etrid_TUZ615023
elong_TUZ615057
etrid_TUZ615624
etrid_TUZ615037
etrid_TUZ615027
elong_TUZ615022
etrid_TUZ615165
ealec_TUZ615220
esp14_MH11_01
ealec_DEI_GISHym80142
ealec_TUZ615121
ejapo_USNM2051678_038
ejapo_USNM2051678_003
ealpi_DEI_GISHym80106
eminu_DEI_GISHym21189
elokt_TUZ615180
ecamt_DEI_GISHym80070
eminu_MH10_01
eplan_DEI_GISHym15478
eflet_TUZ615334
eflet_BIOUG17274_F06
etridt_TUZ615182
eimme_DEI_GISHym80045
ebasa_DEI_GISHym14890 # 4759

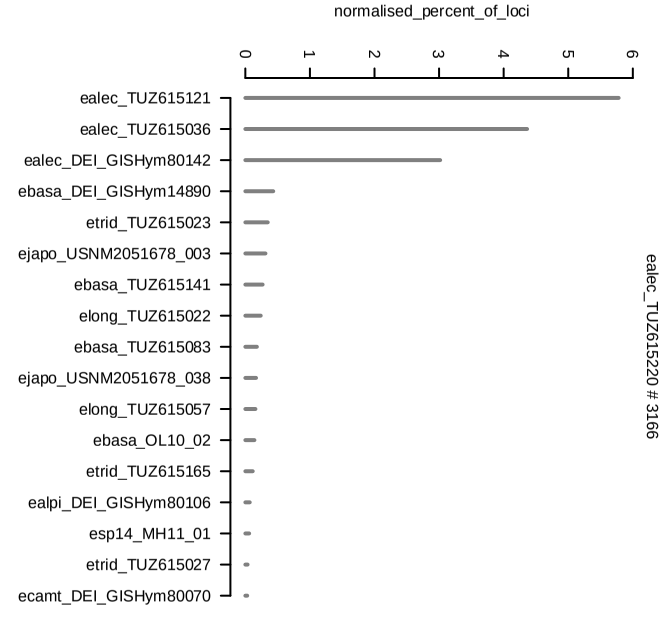
normalised_percent_of_loci
0
1
2
3
4
5
6
ealec_TUZ615121
ealec_TUZ615036
ealec_DEI_GISHym80142
ebasa_DEI_GISHym14890
etrid_TUZ615023
ejapo_USNM2051678_003
ebasa_TUZ615141
elong_TUZ615022
ebasa_TUZ615083
ejapo_USNM2051678_038
elong_TUZ615057
ebasa_OL10_02
etrid_TUZ615165
ealpi_DEI_GISHym80106
esp14_MH11_01
etrid_TUZ615027
ecamt_DEI_GISHym80070
ealec_TUZ615220 # 3166

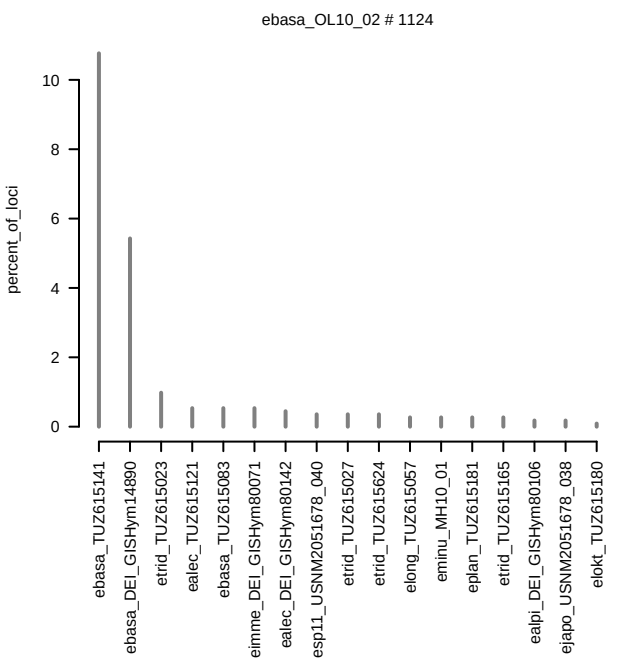
ebasa_OL10_02 # 1124
percent_of_loci
0
2
4
6
8
10
ebasa_TUZ615141
ebasa_DEI_GISHym14890
etrid_TUZ615023
ealec_TUZ615121
ebasa_TUZ615083
eimme_DEI_GISHym80071
ealec_DEI_GISHym80142
esp11_USNM2051678_040
etrid_TUZ615027
etrid_TUZ615624
elong_TUZ615057
eminu_MH10_01
eplan_TUZ615181
etrid_TUZ615165
ealpi_DEI_GISHym80106
ejapo_USNM2051678_038
elokt_TUZ615180

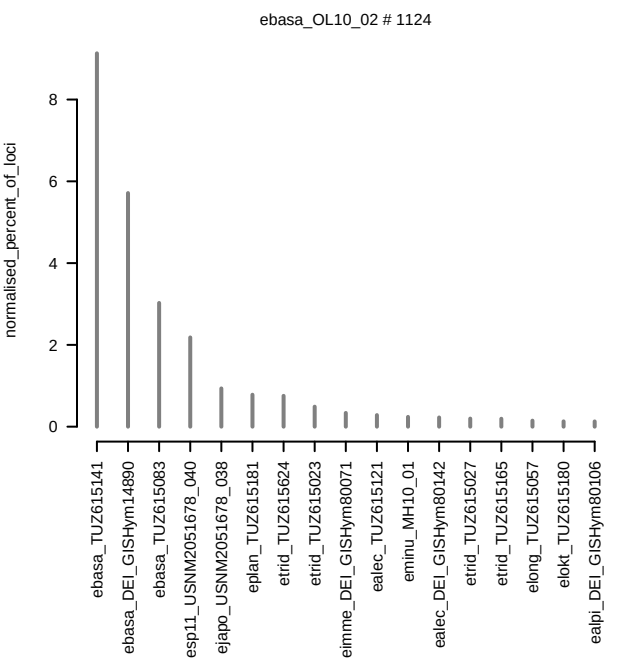
ebasa_OL10_02 # 1124
normalised_percent_of_loci
0
2
4
6
8
ebasa_TUZ615141
ebasa_DEI_GISHym14890
ebasa_TUZ615083
esp11_USNM2051678_040
ejapo_USNM2051678_038
eplan_TUZ615181
etrid_TUZ615624
etrid_TUZ615023
eimme_DEI_GISHym80071
ealec_TUZ615121
eminu_MH10_01
ealec_DEI_GISHym80142
etrid_TUZ615027
etrid_TUZ615165
elong_TUZ615057
elokt_TUZ615180
ealpi_DEI_GISHym80106

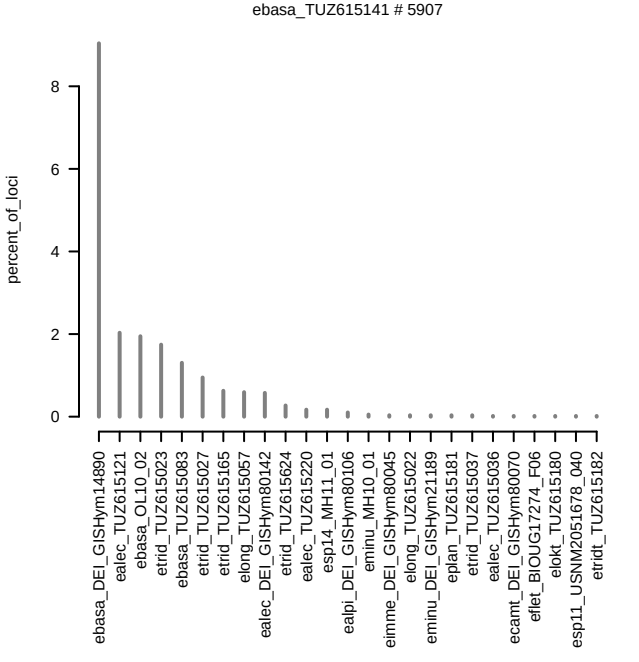
ebasa_TUZ615141 # 5907
percent_of_loci
0
2
4
6
8
ebasa_DEI_GISHym14890
ealec_TUZ615121
ebasa_OL10_02
etrid_TUZ615023
ebasa_TUZ615083
etrid_TUZ615027
etrid_TUZ615165
elong_TUZ615057
ealec_DEI_GISHym80142
etrid_TUZ615624
ealec_TUZ615220
esp14_MH11_01
ealpi_DEI_GISHym80106
eminu_MH10_01
eimme_DEI_GISHym80045
elong_TUZ615022
eminu_DEI_GISHym21189
eplan_TUZ615181
etrid_TUZ615037
ealec_TUZ615036
ecamt_DEI_GISHym80070
eflet_BIOUG17274_F06
elokt_TUZ615180
esp11_USNM2051678_040
etridt_TUZ615182

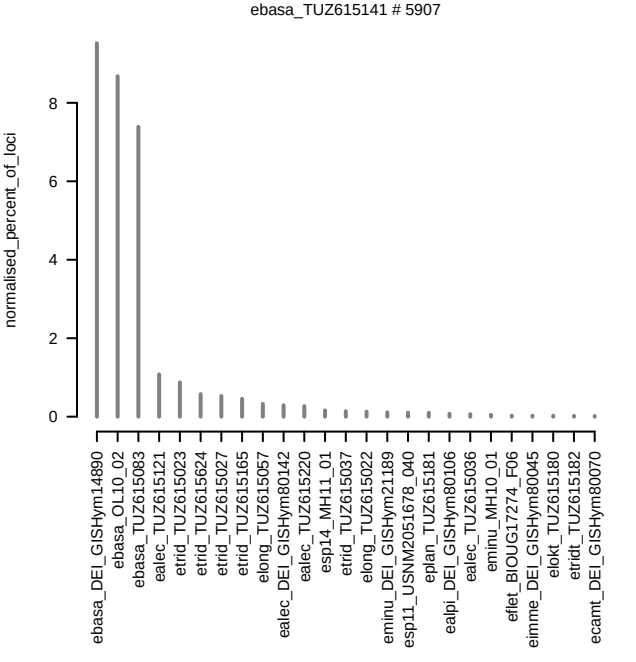
ebasa_TUZ615141 # 5907
normalised_percent_of_loci
0
2
4
6
8
ebasa_DEI_GISHym14890
ebasa_OL10_02
ebasa_TUZ615083
ealec_TUZ615121
etrid_TUZ615023
etrid_TUZ615624
etrid_TUZ615027
etrid_TUZ615165
elong_TUZ615057
ealec_DEI_GISHym80142
ealec_TUZ615220
esp14_MH11_01
etrid_TUZ615037
elong_TUZ615022
eminu_DEI_GISHym21189
esp11_USNM2051678_040
eplan_TUZ615181
ealpi_DEI_GISHym80106
ealec_TUZ615036
eminu_MH10_01
eflet_BIOUG17274_F06
eimme_DEI_GISHym80045
elokt_TUZ615180
etridt_TUZ615182
ecamt_DEI_GISHym80070

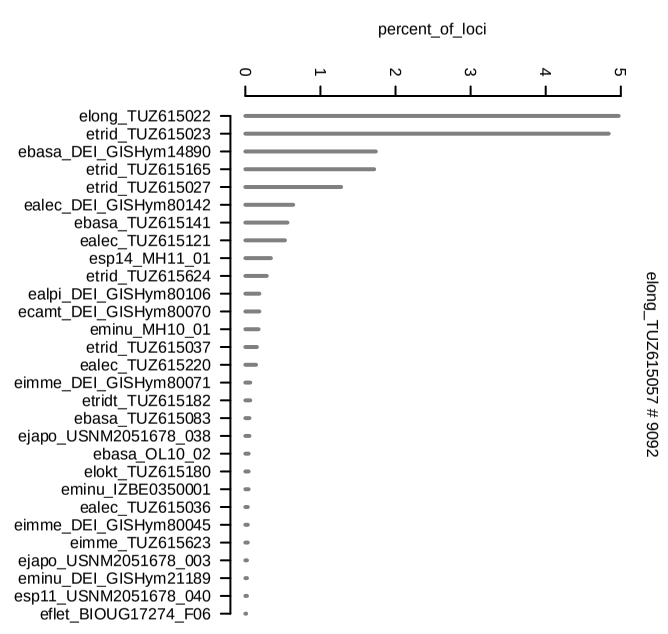
percent_of_loci
0
1
2
3
4
5
elong_TUZ615022
etrid_TUZ615023
ebasa_DEI_GISHym14890
etrid_TUZ615165
etrid_TUZ615027
ealec_DEI_GISHym80142
ebasa_TUZ615141
ealec_TUZ615121
esp14_MH11_01
etrid_TUZ615624
ealpi_DEI_GISHym80106
ecamt_DEI_GISHym80070
eminu_MH10_01
etrid_TUZ615037
ealec_TUZ615220
eimme_DEI_GISHym80071
etridt_TUZ615182
ebasa_TUZ615083
ejapo_USNM2051678_038
ebasa_OL10_02
elokt_TUZ615180
eminu_IZBE0350001
ealec_TUZ615036
eimme_DEI_GISHym80045
eimme_TUZ615623
ejapo_USNM2051678_003
eminu_DEI_GISHym21189
esp11_USNM2051678_040
eflet_BIOUG17274_F06
elong_TUZ615057 # 9092

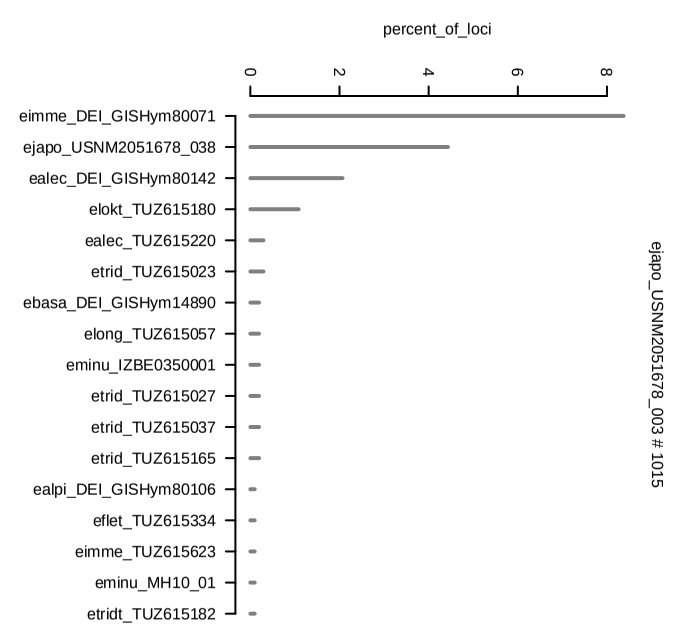
percent_of_loci
0
2
4
6
8
eimme_DEI_GISHym80071
ejapo_USNM2051678_038
ealec_DEI_GISHym80142
elokt_TUZ615180
ealec_TUZ615220
etrid_TUZ615023
ebasa_DEI_GISHym14890
elong_TUZ615057
eminu_IZBE0350001
etrid_TUZ615027
etrid_TUZ615037
etrid_TUZ615165
ealpi_DEI_GISHym80106
eflet_TUZ615334
eimme_TUZ615623
eminu_MH10_01
etridt_TUZ615182
ejapo_USNM2051678_003 # 1015

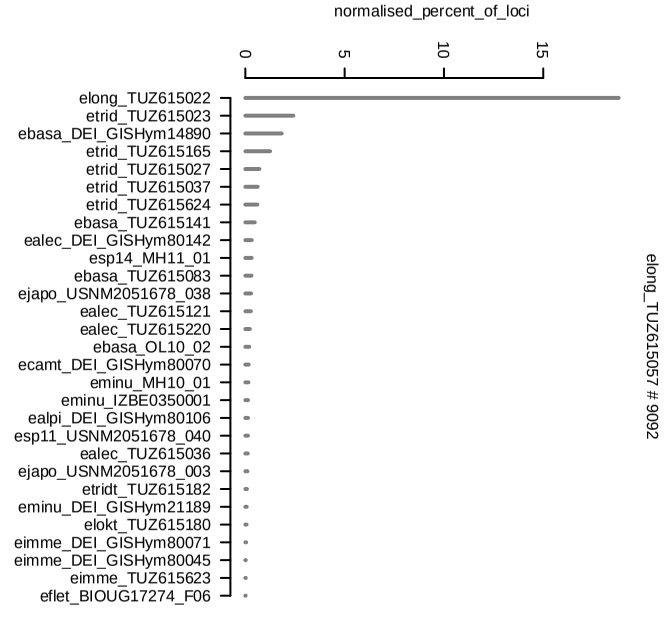
normalised_percent_of_loci
0
5
10
15
elong_TUZ615022
etrid_TUZ615023
ebasa_DEI_GISHym14890
etrid_TUZ615165
etrid_TUZ615027
etrid_TUZ615037
etrid_TUZ615624
ebasa_TUZ615141
ealec_DEI_GISHym80142
esp14_MH11_01
ebasa_TUZ615083
ejapo_USNM2051678_038
ealec_TUZ615121
ealec_TUZ615220
ebasa_OL10_02
ecamt_DEI_GISHym80070
eminu_MH10_01
eminu_IZBE0350001
ealpi_DEI_GISHym80106
esp11_USNM2051678_040
ealec_TUZ615036
ejapo_USNM2051678_003
etridt_TUZ615182
eminu_DEI_GISHym21189
elokt_TUZ615180
eimme_DEI_GISHym80071
eimme_DEI_GISHym80045
eimme_TUZ615623
eflet_BIOUG17274_F06
elong_TUZ615057 # 9092

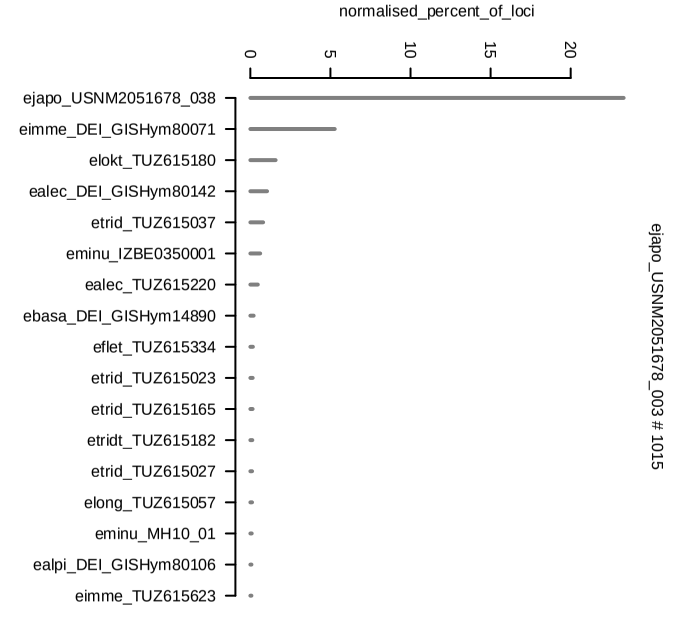
normalised_percent_of_loci
0
5
10
15
20
ejapo_USNM2051678_038
eimme_DEI_GISHym80071
elokt_TUZ615180
ealec_DEI_GISHym80142
etrid_TUZ615037
eminu_IZBE0350001
ealec_TUZ615220
ebasa_DEI_GISHym14890
eflet_TUZ615334
etrid_TUZ615023
etrid_TUZ615165
etridt_TUZ615182
etrid_TUZ615027
elong_TUZ615057
eminu_MH10_01
ealpi_DEI_GISHym80106
eimme_TUZ615623
ejapo_USNM2051678_003 # 1015

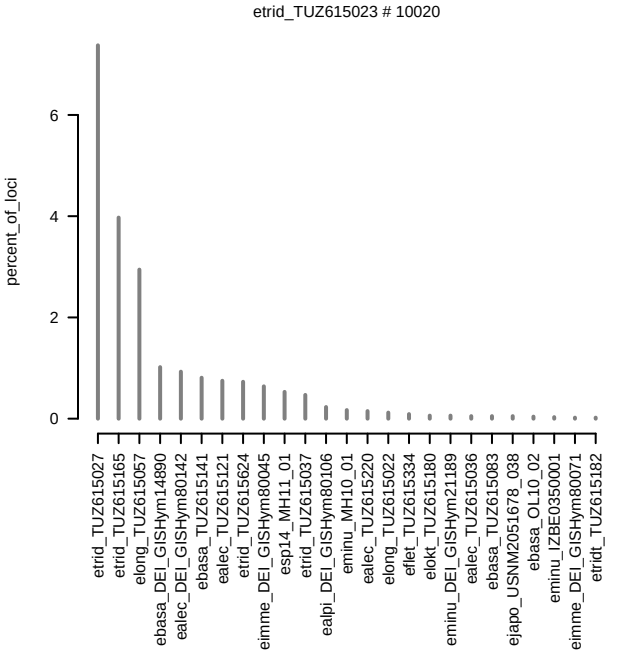
etrid_TUZ615023 # 10020
percent_of_loci
0
2
4
6
etrid_TUZ615027
etrid_TUZ615165
elong_TUZ615057
ebasa_DEI_GISHym14890
ealec_DEI_GISHym80142
ebasa_TUZ615141
ealec_TUZ615121
etrid_TUZ615624
eimme_DEI_GISHym80045
esp14_MH11_01
etrid_TUZ615037
ealpi_DEI_GISHym80106
eminu_MH10_01
ealec_TUZ615220
elong_TUZ615022
eflet_TUZ615334
elokt_TUZ615180
eminu_DEI_GISHym21189
ealec_TUZ615036
ebasa_TUZ615083
ejapo_USNM2051678_038
ebasa_OL10_02
eminu_IZBE0350001
eimme_DEI_GISHym80071
etridt_TUZ615182

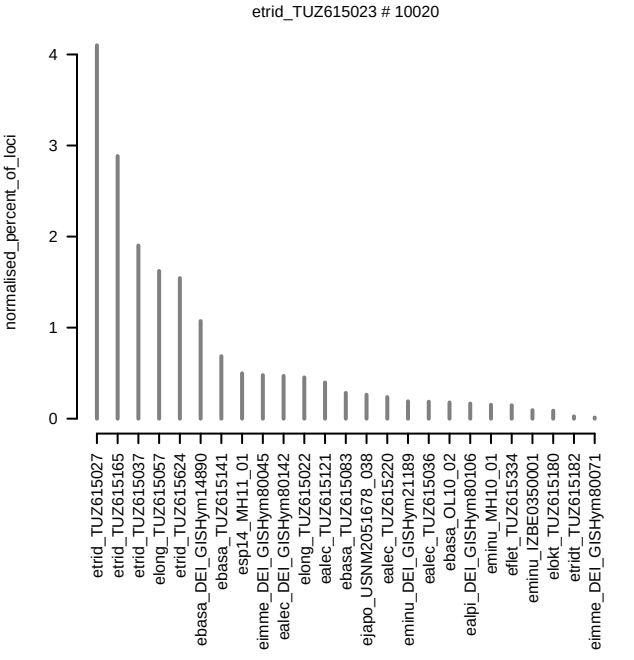
etrid_TUZ615023 # 10020
normalised_percent_of_loci
0
1
2
3
4
etrid_TUZ615027
etrid_TUZ615165
etrid_TUZ615037
elong_TUZ615057
etrid_TUZ615624
ebasa_DEI_GISHym14890
ebasa_TUZ615141
esp14_MH11_01
eimme_DEI_GISHym80045
ealec_DEI_GISHym80142
elong_TUZ615022
ealec_TUZ615121
ebasa_TUZ615083
ejapo_USNM2051678_038
ealec_TUZ615220
eminu_DEI_GISHym21189
ealec_TUZ615036
ebasa_OL10_02
ealpi_DEI_GISHym80106
eminu_MH10_01
eflet_TUZ615334
eminu_IZBE0350001
elokt_TUZ615180
etridt_TUZ615182
eimme_DEI_GISHym80071

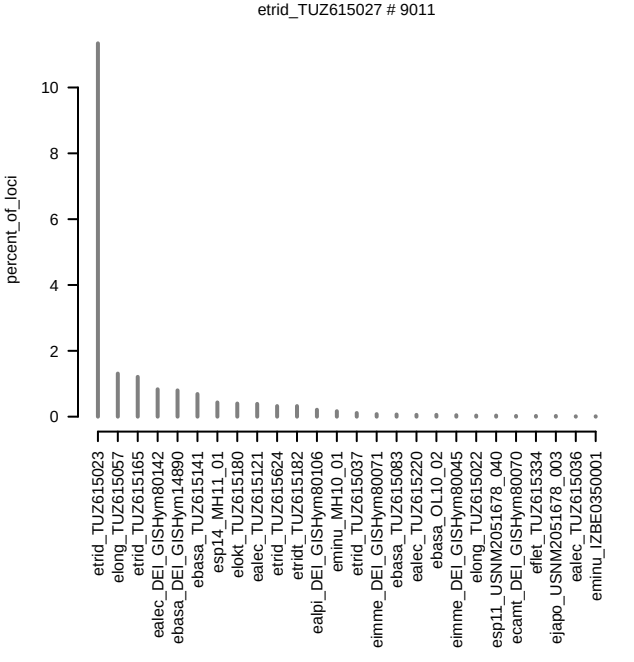
etrid_TUZ615027 # 9011
percent_of_loci
0
2
4
6
8
10
etrid_TUZ615023
elong_TUZ615057
etrid_TUZ615165
ealec_DEI_GISHym80142
ebasa_DEI_GISHym14890
ebasa_TUZ615141
esp14_MH11_01
elokt_TUZ615180
ealec_TUZ615121
etrid_TUZ615624
etridt_TUZ615182
ealpi_DEI_GISHym80106
eminu_MH10_01
etrid_TUZ615037
eimme_DEI_GISHym80071
ebasa_TUZ615083
ealec_TUZ615220
ebasa_OL10_02
eimme_DEI_GISHym80045
elong_TUZ615022
esp11_USNM2051678_040
ecamt_DEI_GISHym80070
eflet_TUZ615334
ejapo_USNM2051678_003
ealec_TUZ615036
eminu_IZBE0350001

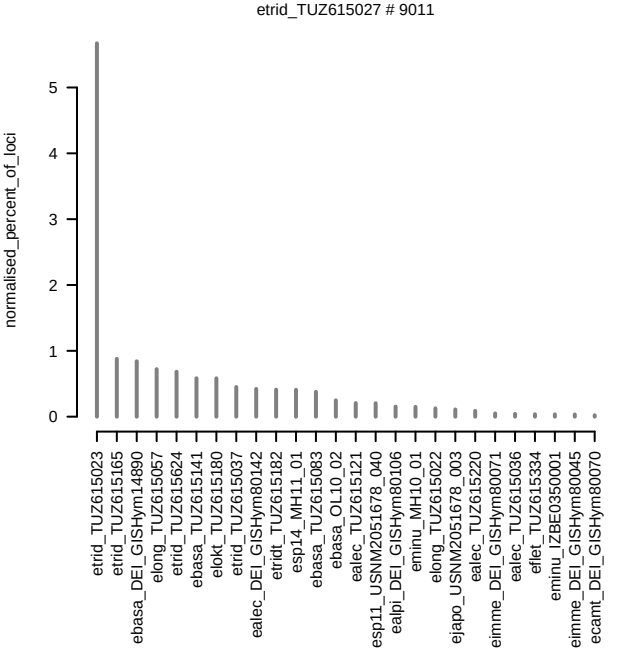
etrid_TUZ615027 # 9011
normalised_percent_of_loci
0
1
2
3
4
5
etrid_TUZ615023
etrid_TUZ615165
ebasa_DEI_GISHym14890
elong_TUZ615057
etrid_TUZ615624
ebasa_TUZ615141
elokt_TUZ615180
etrid_TUZ615037
ealec_DEI_GISHym80142
etridt_TUZ615182
esp14_MH11_01
ebasa_TUZ615083
ebasa_OL10_02
ealec_TUZ615121
esp11_USNM2051678_040
ealpi_DEI_GISHym80106
eminu_MH10_01
elong_TUZ615022
ejapo_USNM2051678_003
ealec_TUZ615220
eimme_DEI_GISHym80071
ealec_TUZ615036
eflet_TUZ615334
eminu_IZBE0350001
eimme_DEI_GISHym80045
ecamt_DEI_GISHym80070

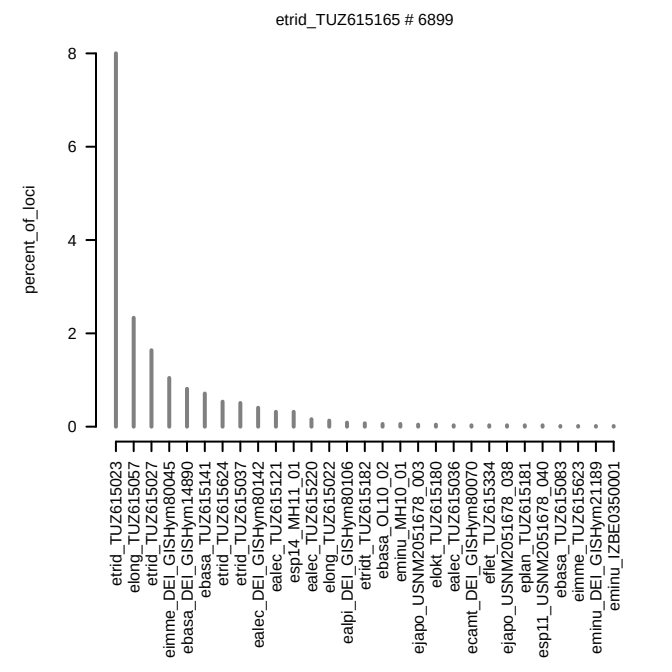
etrid_TUZ615165 # 6899
percent_of_loci
0
2
4
6
8
etrid_TUZ615023
elong_TUZ615057
etrid_TUZ615027
eimme_DEI_GISHym80045
ebasa_DEI_GISHym14890
ebasa_TUZ615141
etrid_TUZ615624
etrid_TUZ615037
ealec_DEI_GISHym80142
ealec_TUZ615121
esp14_MH11_01
ealec_TUZ615220
elong_TUZ615022
ealpi_DEI_GISHym80106
etridt_TUZ615182
ebasa_OL10_02
eminu_MH10_01
ejapo_USNM2051678_003
elokt_TUZ615180
ealec_TUZ615036
ecamt_DEI_GISHym80070
eflet_TUZ615334
ejapo_USNM2051678_038
eplan_TUZ615181
esp11_USNM2051678_040
ebasa_TUZ615083
eimme_TUZ615623
eminu_DEI_GISHym21189
eminu_IZBE0350001

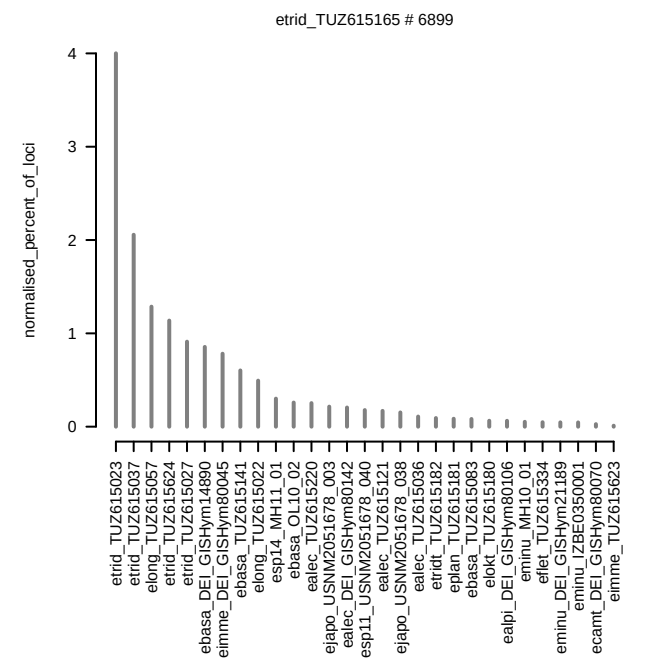
etrid_TUZ615165 # 6899
normalised_percent_of_loci
0
1
2
3
4
etrid_TUZ615023
etrid_TUZ615037
elong_TUZ615057
etrid_TUZ615624
etrid_TUZ615027
ebasa_DEI_GISHym14890
eimme_DEI_GISHym80045
ebasa_TUZ615141
elong_TUZ615022
esp14_MH11_01
ebasa_OL10_02
ealec_TUZ615220
ejapo_USNM2051678_003
ealec_DEI_GISHym80142
esp11_USNM2051678_040
ealec_TUZ615121
ejapo_USNM2051678_038
ealec_TUZ615036
etridt_TUZ615182
eplan_TUZ615181
ebasa_TUZ615083
elokt_TUZ615180
ealpi_DEI_GISHym80106
eminu_MH10_01
eflet_TUZ615334
eminu_DEI_GISHym21189
eminu_IZBE0350001
ecamt_DEI_GISHym80070
eimme_TUZ615623

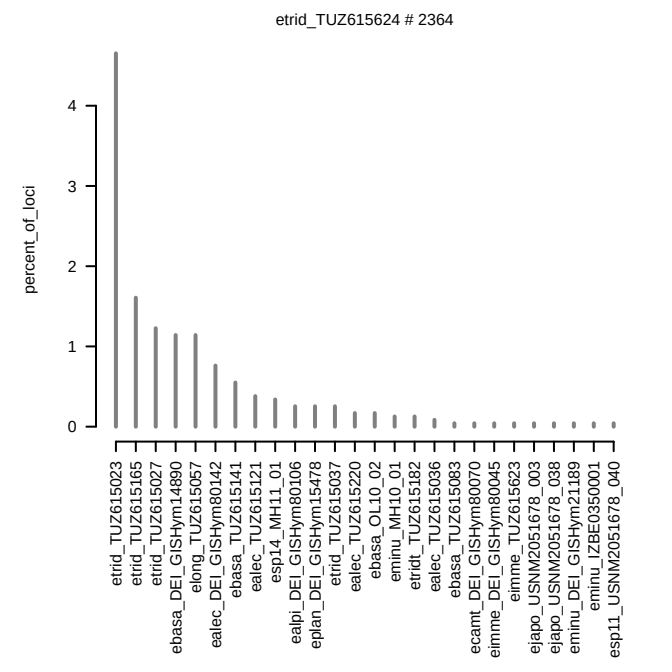
etrid_TUZ615624 # 2364
percent_of_loci
0
1
2
3
4
etrid_TUZ615023
etrid_TUZ615165
etrid_TUZ615027
ebasa_DEI_GISHym14890
elong_TUZ615057
ealec_DEI_GISHym80142
ebasa_TUZ615141
ealec_TUZ615121
esp14_MH11_01
ealpi_DEI_GISHym80106
eplan_DEI_GISHym15478
etrid_TUZ615037
ealec_TUZ615220
ebasa_OL10_02
eminu_MH10_01
etridt_TUZ615182
ealec_TUZ615036
ebasa_TUZ615083
ecamt_DEI_GISHym80070
eimme_DEI_GISHym80045
eimme_TUZ615623
ejapo_USNM2051678_003
ejapo_USNM2051678_038
eminu_DEI_GISHym21189
eminu_IZBE0350001
esp11_USNM2051678_040

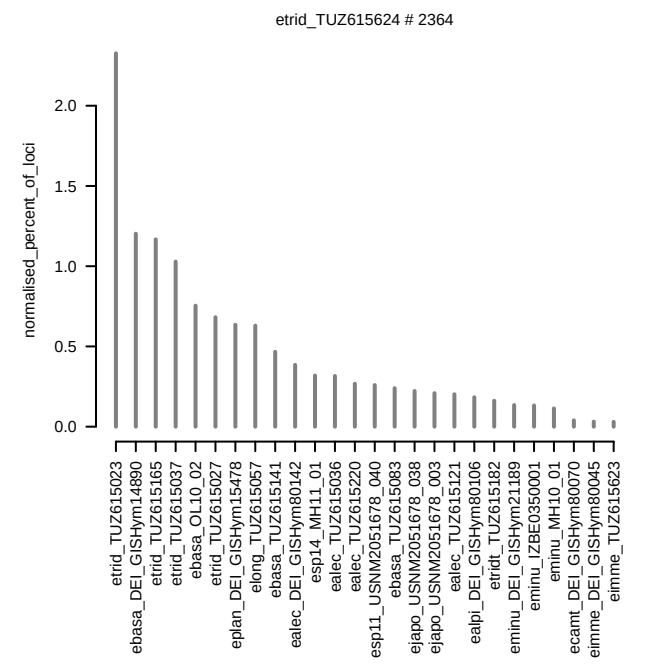
etrid_TUZ615624 # 2364
normalised_percent_of_loci
0.0
0.5
1.0
1.5
2.0
etrid_TUZ615023
ebasa_DEI_GISHym14890
etrid_TUZ615165
etrid_TUZ615037
ebasa_OL10_02
etrid_TUZ615027
eplan_DEI_GISHym15478
elong_TUZ615057
ebasa_TUZ615141
ealec_DEI_GISHym80142
esp14_MH11_01
ealec_TUZ615036
ealec_TUZ615220
esp11_USNM2051678_040
ebasa_TUZ615083
ejapo_USNM2051678_038
ejapo_USNM2051678_003
ealec_TUZ615121
ealpi_DEI_GISHym80106
etridt_TUZ615182
eminu_DEI_GISHym21189
eminu_IZBE0350001
eminu_MH10_01
ecamt_DEI_GISHym80070
eimme_DEI_GISHym80045
eimme_TUZ615623

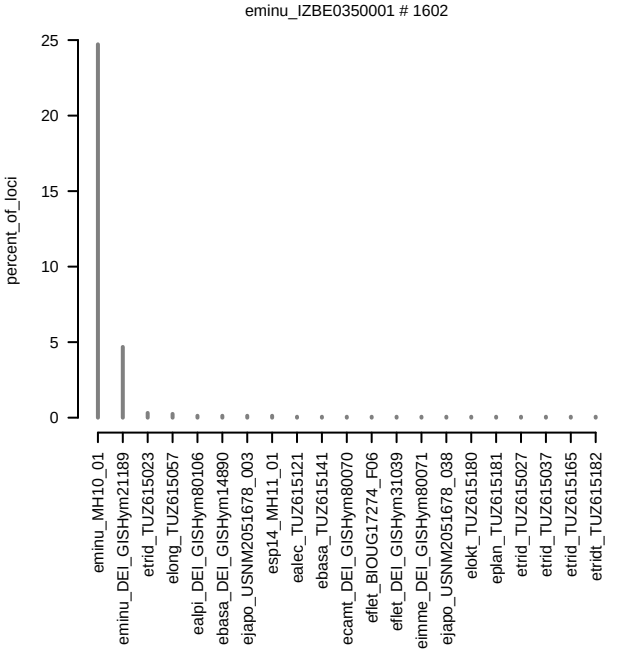
eminu_IZBE0350001 # 1602
percent_of_loci
0
5
10
15
20
25
eminu_MH10_01
eminu_DEI_GISHym21189
etrid_TUZ615023
elong_TUZ615057
ealpi_DEI_GISHym80106
ebasa_DEI_GISHym14890
ejapo_USNM2051678_003
esp14_MH11_01
ealec_TUZ615121
ebasa_TUZ615141
ecamt_DEI_GISHym80070
eflet_BIOUG17274_F06
eflet_DEI_GISHym31039
eimme_DEI_GISHym80071
ejapo_USNM2051678_038
elokt_TUZ615180
eplan_TUZ615181
etrid_TUZ615027
etrid_TUZ615037
etrid_TUZ615165
etridt_TUZ615182

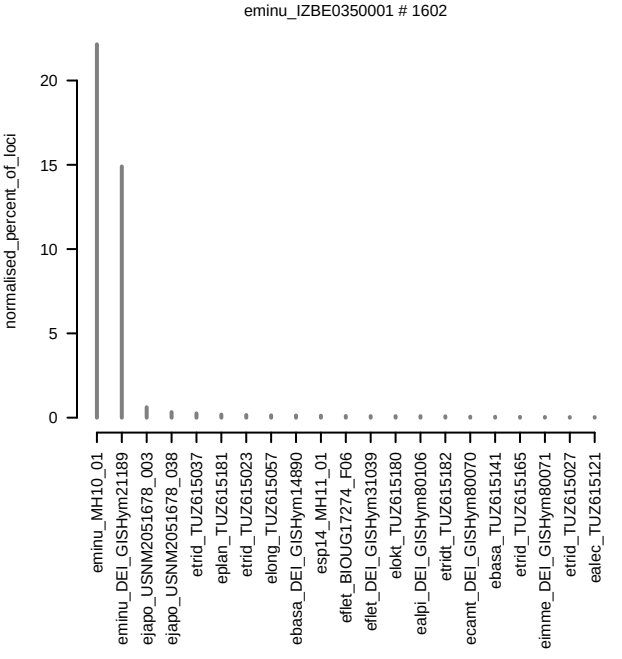
eminu_IZBE0350001 # 1602
normalised_percent_of_loci
0
5
10
15
20
eminu_MH10_01
eminu_DEI_GISHym21189
ejapo_USNM2051678_003
ejapo_USNM2051678_038
etrid_TUZ615037
eplan_TUZ615181
etrid_TUZ615023
elong_TUZ615057
ebasa_DEI_GISHym14890
esp14_MH11_01
eflet_BIOUG17274_F06
eflet_DEI_GISHym31039
elokt_TUZ615180
ealpi_DEI_GISHym80106
etridt_TUZ615182
ecamt_DEI_GISHym80070
ebasa_TUZ615141
etrid_TUZ615165
eimme_DEI_GISHym80071
etrid_TUZ615027
ealec_TUZ615121

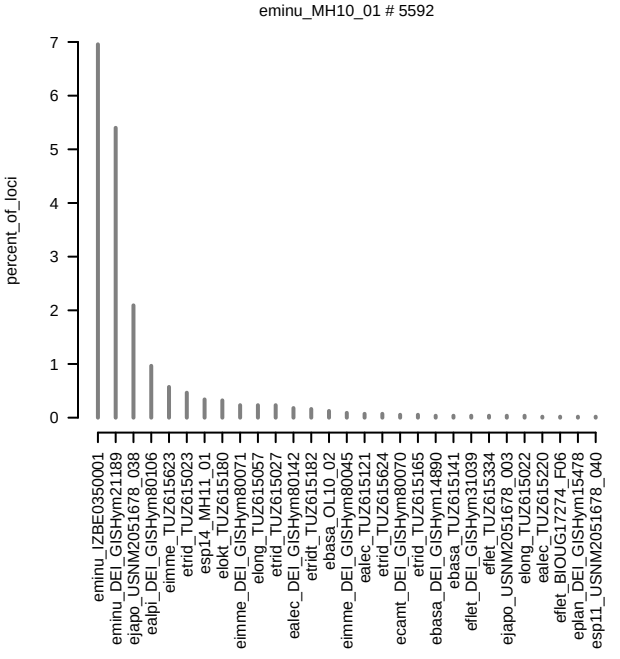
eminu_MH10_01 # 5592
percent_of_loci
0
1
2
3
4
5
6
7
eminu_IZBE0350001
eminu_DEI_GISHym21189
ejapo_USNM2051678_038
ealpi_DEI_GISHym80106
eimme_TUZ615623
etrid_TUZ615023
esp14_MH11_01
elokt_TUZ615180
eimme_DEI_GISHym80071
elong_TUZ615057
etrid_TUZ615027
ealec_DEI_GISHym80142
etridt_TUZ615182
ebasa_OL10_02
eimme_DEI_GISHym80045
ealec_TUZ615121
etrid_TUZ615624
ecamt_DEI_GISHym80070
etrid_TUZ615165
ebasa_DEI_GISHym14890
ebasa_TUZ615141
eflet_DEI_GISHym31039
eflet_TUZ615334
ejapo_USNM2051678_003
elong_TUZ615022
ealec_TUZ615220
eflet_BIOUG17274_F06
eplan_DEI_GISHym15478
esp11_USNM2051678_040

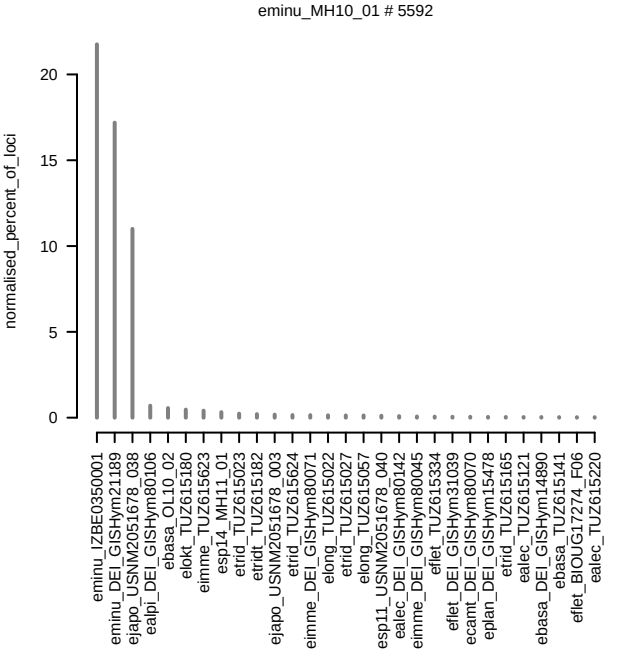
eminu_MH10_01 # 5592
normalised_percent_of_loci
0
5
10
15
20
eminu_IZBE0350001
eminu_DEI_GISHym21189
ejapo_USNM2051678_038
ealpi_DEI_GISHym80106
ebasa_OL10_02
elokt_TUZ615180
eimme_TUZ615623
esp14_MH11_01
etrid_TUZ615023
etridt_TUZ615182
ejapo_USNM2051678_003
etrid_TUZ615624
eimme_DEI_GISHym80071
elong_TUZ615022
etrid_TUZ615027
elong_TUZ615057
esp11_USNM2051678_040
ealec_DEI_GISHym80142
eimme_DEI_GISHym80045
eflet_TUZ615334
eflet_DEI_GISHym31039
ecamt_DEI_GISHym80070
eplan_DEI_GISHym15478
etrid_TUZ615165
ealec_TUZ615121
ebasa_DEI_GISHym14890
ebasa_TUZ615141
eflet_BIOUG17274_F06
ealec_TUZ615220

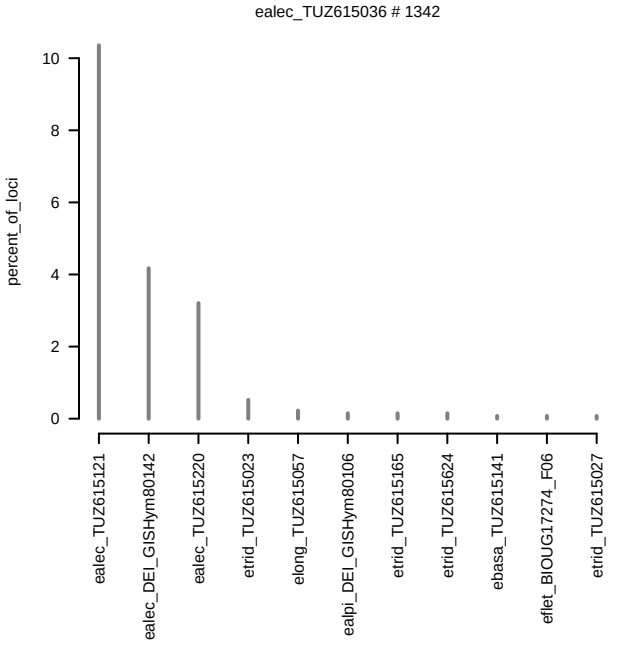
ealec_TUZ615036 # 1342
percent_of_loci
0
2
4
6
8
10
ealec_TUZ615121
ealec_DEI_GISHym80142
ealec_TUZ615220
etrid_TUZ615023
elong_TUZ615057
ealpi_DEI_GISHym80106
etrid_TUZ615165
etrid_TUZ615624
ebasa_TUZ615141
eflet_BIOUG17274_F06
etrid_TUZ615027

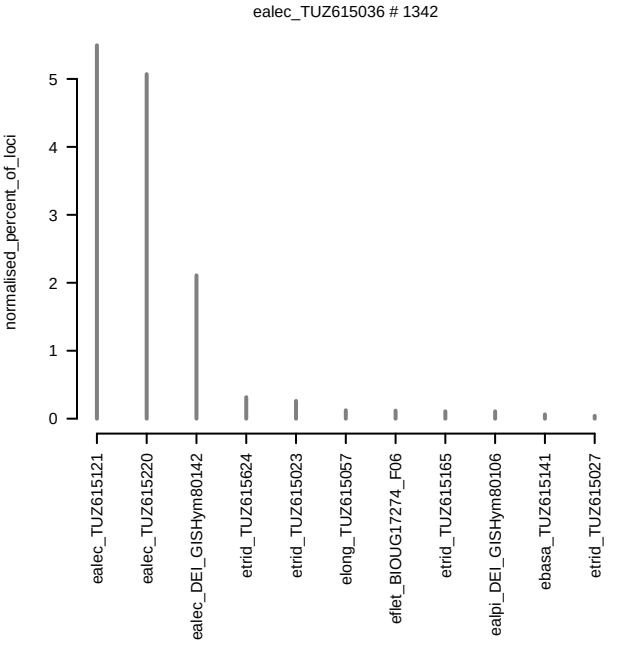
ealec_TUZ615036 # 1342
normalised_percent_of_loci
0
1
2
3
4
5
ealec_TUZ615121
ealec_TUZ615220
ealec_DEI_GISHym80142
etrid_TUZ615624
etrid_TUZ615023
elong_TUZ615057
eflet_BIOUG17274_F06
etrid_TUZ615165
ealpi_DEI_GISHym80106
ebasa_TUZ615141
etrid_TUZ615027

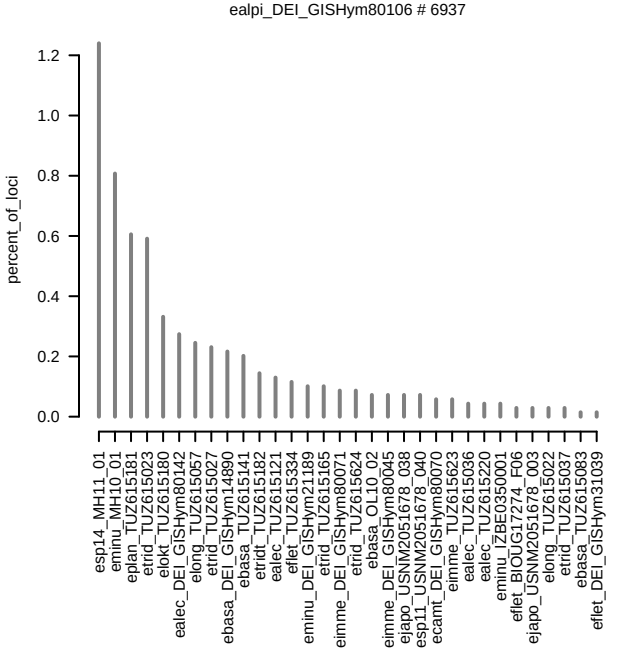
ealpi_DEI_GISHym80106 # 6937
percent_of_loci
0.0
0.2
0.4
0.6
0.8
1.0
1.2
esp14_MH11_01
eminu_MH10_01
eplan_TUZ615181
etrid_TUZ615023
elokt_TUZ615180
ealec_DEI_GISHym80142
elong_TUZ615057
etrid_TUZ615027
ebasa_DEI_GISHym14890
ebasa_TUZ615141
etridt_TUZ615182
ealec_TUZ615121
eflet_TUZ615334
eminu_DEI_GISHym21189
etrid_TUZ615165
eimme_DEI_GISHym80071
etrid_TUZ615624
ebasa_OL10_02
eimme_DEI_GISHym80045
ejapo_USNM2051678_038
esp11_USNM2051678_040
ecamt_DEI_GISHym80070
eimme_TUZ615623
ealec_TUZ615036
ealec_TUZ615220
eminu_IZBE0350001
eflet_BIOUG17274_F06
ejapo_USNM2051678_003
elong_TUZ615022
etrid_TUZ615037
ebasa_TUZ615083
eflet_DEI_GISHym31039

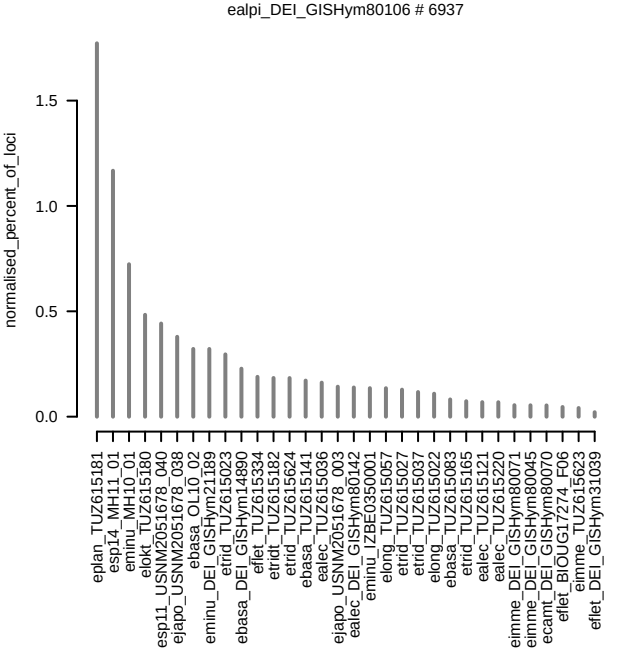
ealpi_DEI_GISHym80106 # 6937
normalised_percent_of_loci
0.0
0.5
1.0
1.5
eplan_TUZ615181
esp14_MH11_01
eminu_MH10_01
elokt_TUZ615180
esp11_USNM2051678_040
ejapo_USNM2051678_038
ebasa_OL10_02
eminu_DEI_GISHym21189
etrid_TUZ615023
ebasa_DEI_GISHym14890
eflet_TUZ615334
etridt_TUZ615182
ebasa_TUZ615141
ealec_TUZ615036
ejapo_USNM2051678_003
ealec_DEI_GISHym80142
eminu_IZBE0350001
elong_TUZ615057
etrid_TUZ615027
etrid_TUZ615037
elong_TUZ615022
ebasa_TUZ615083
etrid_TUZ615165
ealec_TUZ615121
ealec_TUZ615220
eimme_DEI_GISHym80071
eimme_DEI_GISHym80045
ecamt_DEI_GISHym80070
eflet_BIOUG17274_F06
eimme_TUZ615623
eflet_DEI_GISHym31039

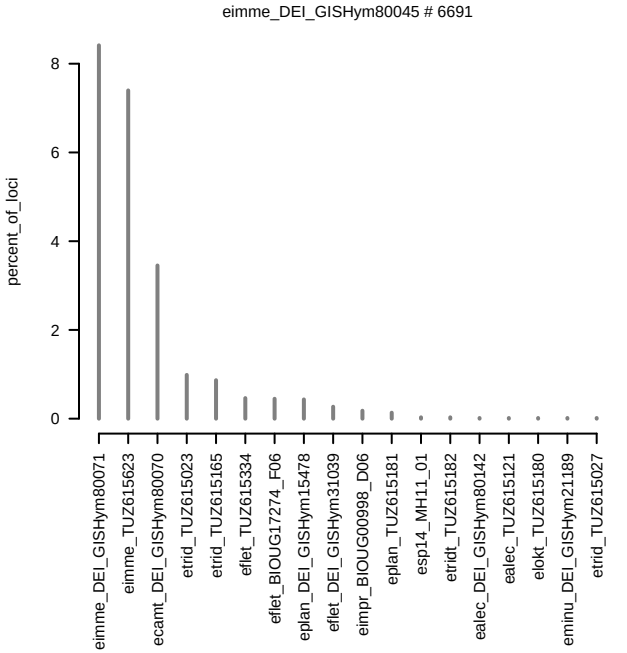
eimme_DEI_GISHym80045 # 6691
percent_of_loci
0
2
4
6
8
eimme_DEI_GISHym80071
eimme_TUZ615623
ecamt_DEI_GISHym80070
etrid_TUZ615023
etrid_TUZ615165
eflet_TUZ615334
eflet_BIOUG17274_F06
eplan_DEI_GISHym15478
eflet_DEI_GISHym31039
eimpr_BIOUG00998_D06
eplan_TUZ615181
esp14_MH11_01
etridt_TUZ615182
ealec_DEI_GISHym80142
ealec_TUZ615121
elokt_TUZ615180
eminu_DEI_GISHym21189
etrid_TUZ615027

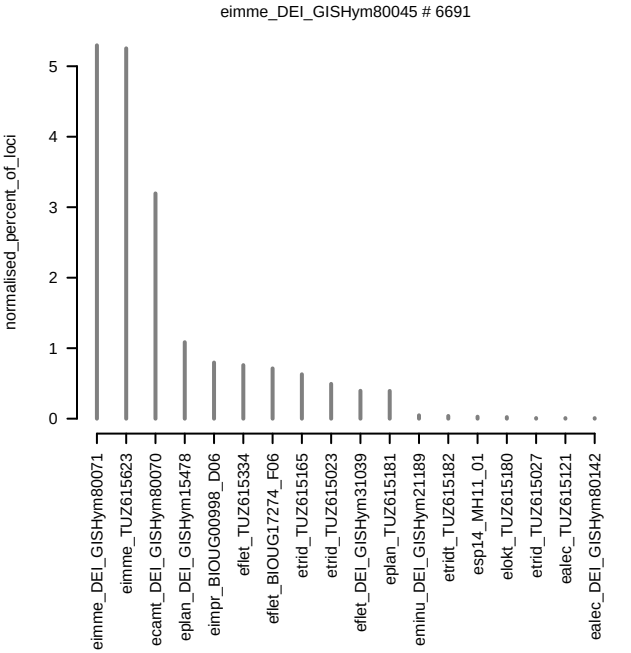
eimme_DEI_GISHym80045 # 6691
normalised_percent_of_loci
0
1
2
3
4
5
eimme_DEI_GISHym80071
eimme_TUZ615623
ecamt_DEI_GISHym80070
eplan_DEI_GISHym15478
eimpr_BIOUG00998_D06
eflet_TUZ615334
eflet_BIOUG17274_F06
etrid_TUZ615165
etrid_TUZ615023
eflet_DEI_GISHym31039
eplan_TUZ615181
eminu_DEI_GISHym21189
etridt_TUZ615182
esp14_MH11_01
elokt_TUZ615180
etrid_TUZ615027
ealec_TUZ615121
ealec_DEI_GISHym80142

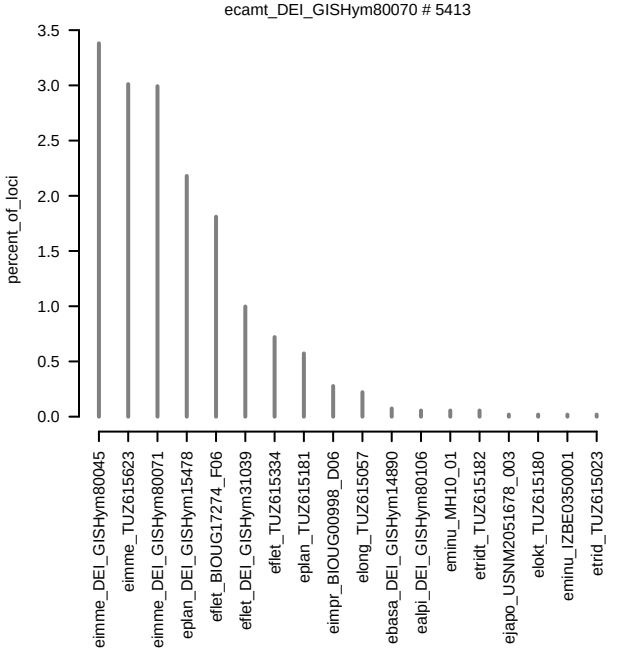
ecamt_DEI_GISHym80070 # 5413
percent_of_loci
0.0
0.5
1.0
1.5
2.0
2.5
3.0
3.5
eimme_DEI_GISHym80045
eimme_TUZ615623
eimme_DEI_GISHym80071
eplan_DEI_GISHym15478
eflet_BIOUG17274_F06
eflet_DEI_GISHym31039
eflet_TUZ615334
eplan_TUZ615181
eimpr_BIOUG00998_D06
elong_TUZ615057
ebasa_DEI_GISHym14890
ealpi_DEI_GISHym80106
eminu_MH10_01
etridt_TUZ615182
ejapo_USNM2051678_003
elokt_TUZ615180
eminu_IZBE0350001
etrid_TUZ615023

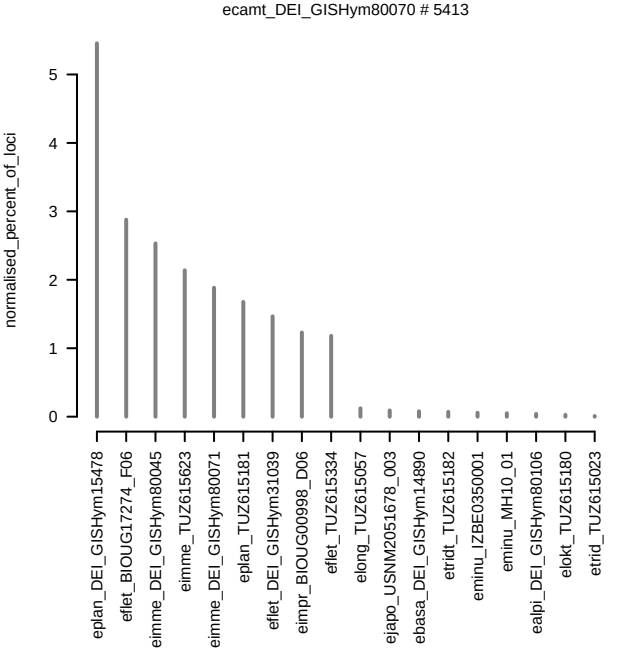
ecamt_DEI_GISHym80070 # 5413
normalised_percent_of_loci
0
1
2
3
4
5
eplan_DEI_GISHym15478
eflet_BIOUG17274_F06
eimme_DEI_GISHym80045
eimme_TUZ615623
eimme_DEI_GISHym80071
eplan_TUZ615181
eflet_DEI_GISHym31039
eimpr_BIOUG00998_D06
eflet_TUZ615334
elong_TUZ615057
ejapo_USNM2051678_003
ebasa_DEI_GISHym14890
etridt_TUZ615182
eminu_IZBE0350001
eminu_MH10_01
ealpi_DEI_GISHym80106
elokt_TUZ615180
etrid_TUZ615023

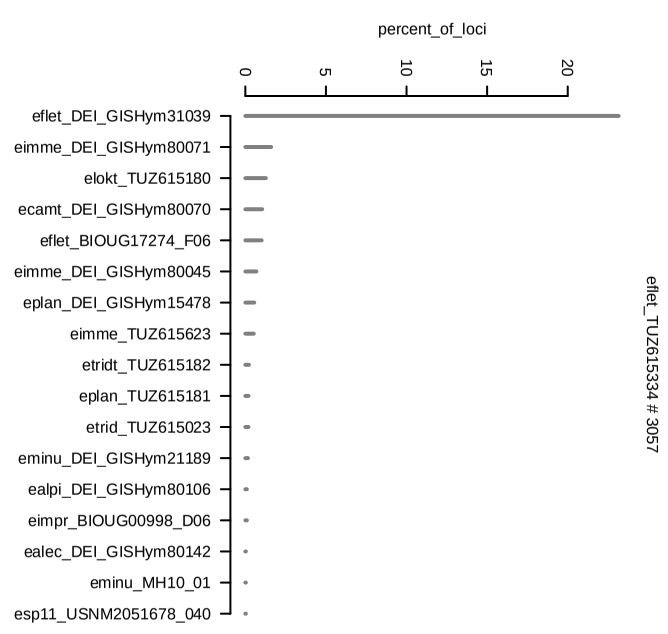
percent_of_loci
0
5
10
15
20
eflet_DEI_GISHym31039
eimme_DEI_GISHym80071
elokt_TUZ615180
ecamt_DEI_GISHym80070
eflet_BIOUG17274_F06
eimme_DEI_GISHym80045
eplan_DEI_GISHym15478
eimme_TUZ615623
etridt_TUZ615182
eplan_TUZ615181
etrid_TUZ615023
eminu_DEI_GISHym21189
ealpi_DEI_GISHym80106
eimpr_BIOUG00998_D06
ealec_DEI_GISHym80142
eminu_MH10_01
esp11_USNM2051678_040
eflet_TUZ615334 # 3057

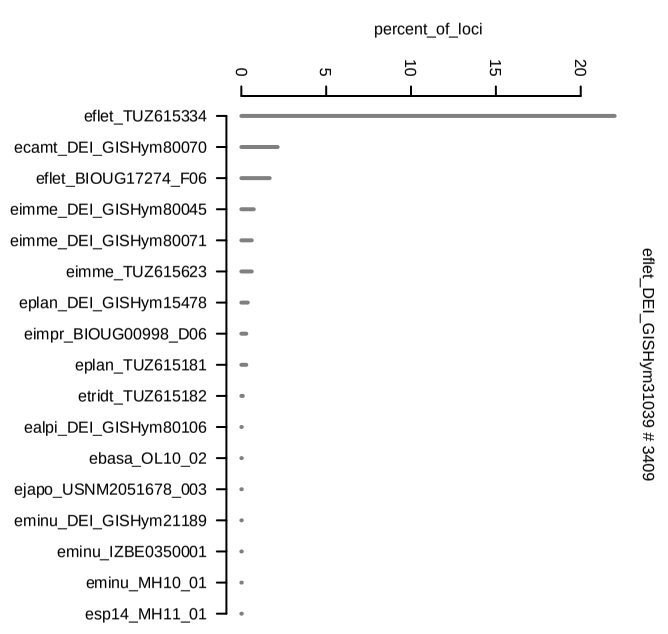
percent_of_loci
0
5
10
15
20
eflet_TUZ615334
ecamt_DEI_GISHym80070
eflet_BIOUG17274_F06
eimme_DEI_GISHym80045
eimme_DEI_GISHym80071
eimme_TUZ615623
eplan_DEI_GISHym15478
eimpr_BIOUG00998_D06
eplan_TUZ615181
etridt_TUZ615182
ealpi_DEI_GISHym80106
ebasa_OL10_02
ejapo_USNM2051678_003
eminu_DEI_GISHym21189
eminu_IZBE0350001
eminu_MH10_01
esp14_MH11_01
eflet_DEI_GISHym31039 # 3409

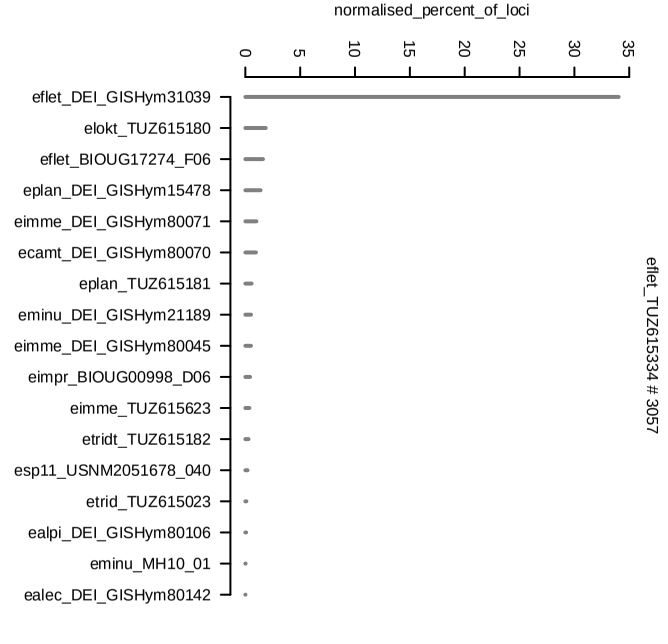
normalised_percent_of_loci
0
5
10
15
20
25
30
35
eflet_DEI_GISHym31039
elokt_TUZ615180
eflet_BIOUG17274_F06
eplan_DEI_GISHym15478
eimme_DEI_GISHym80071
ecamt_DEI_GISHym80070
eplan_TUZ615181
eminu_DEI_GISHym21189
eimme_DEI_GISHym80045
eimpr_BIOUG00998_D06
eimme_TUZ615623
etridt_TUZ615182
esp11_USNM2051678_040
etrid_TUZ615023
ealpi_DEI_GISHym80106
eminu_MH10_01
ealec_DEI_GISHym80142
eflet_TUZ615334 # 3057

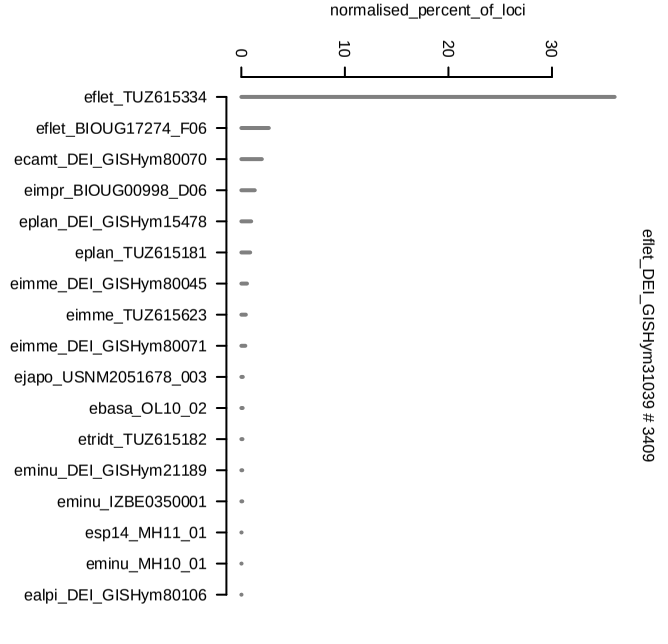
normalised_percent_of_loci
0
10
20
30
eflet_TUZ615334
eflet_BIOUG17274_F06
ecamt_DEI_GISHym80070
eimpr_BIOUG00998_D06
eplan_DEI_GISHym15478
eplan_TUZ615181
eimme_DEI_GISHym80045
eimme_TUZ615623
eimme_DEI_GISHym80071
ejapo_USNM2051678_003
ebasa_OL10_02
etridt_TUZ615182
eminu_DEI_GISHym21189
eminu_IZBE0350001
esp14_MH11_01
eminu_MH10_01
ealpi_DEI_GISHym80106
eflet_DEI_GISHym31039 # 3409

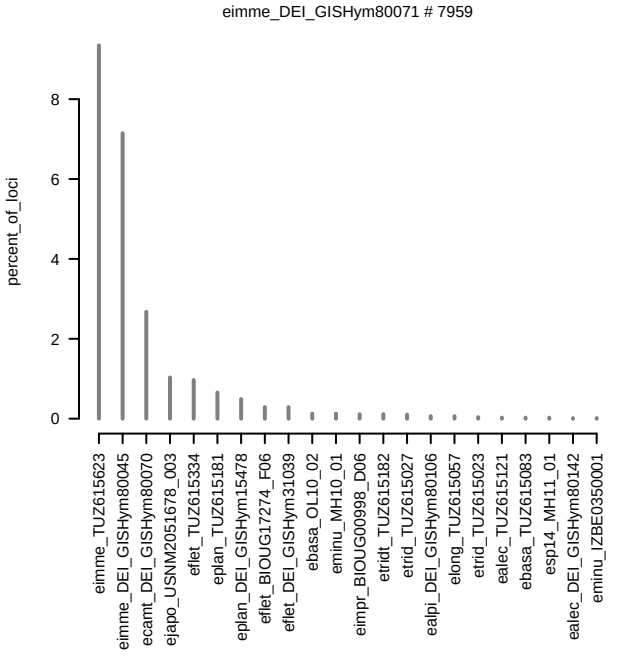
eimme_DEI_GISHym80071 # 7959
percent_of_loci
0
2
4
6
8
eimme_TUZ615623
eimme_DEI_GISHym80045
ecamt_DEI_GISHym80070
ejapo_USNM2051678_003
eflet_TUZ615334
eplan_TUZ615181
eplan_DEI_GISHym15478
eflet_BIOUG17274_F06
eflet_DEI_GISHym31039
ebasa_OL10_02
eminu_MH10_01
eimpr_BIOUG00998_D06
etridt_TUZ615182
etrid_TUZ615027
ealpi_DEI_GISHym80106
elong_TUZ615057
etrid_TUZ615023
ealec_TUZ615121
ebasa_TUZ615083
esp14_MH11_01
ealec_DEI_GISHym80142
eminu_IZBE0350001

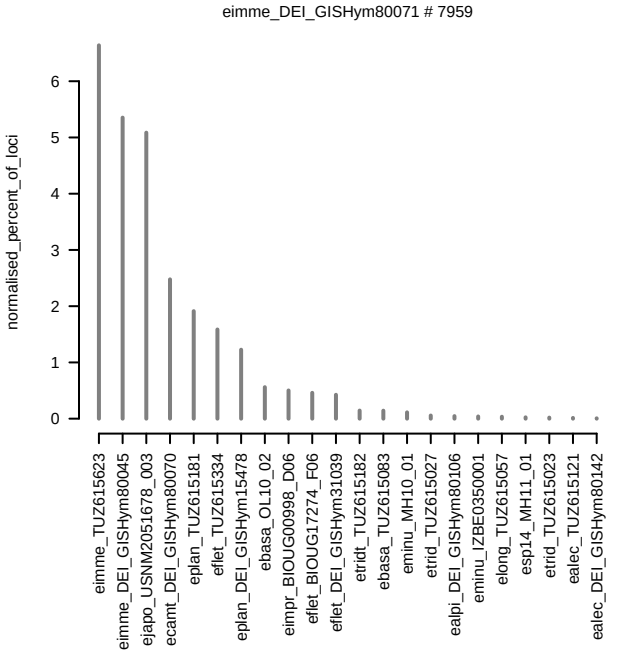
eimme_DEI_GISHym80071 # 7959
normalised_percent_of_loci
0
1
2
3
4
5
6
eimme_TUZ615623
eimme_DEI_GISHym80045
ejapo_USNM2051678_003
ecamt_DEI_GISHym80070
eplan_TUZ615181
eflet_TUZ615334
eplan_DEI_GISHym15478
ebasa_OL10_02
eimpr_BIOUG00998_D06
eflet_BIOUG17274_F06
eflet_DEI_GISHym31039
etridt_TUZ615182
ebasa_TUZ615083
eminu_MH10_01
etrid_TUZ615027
ealpi_DEI_GISHym80106
eminu_IZBE0350001
elong_TUZ615057
esp14_MH11_01
etrid_TUZ615023
ealec_TUZ615121
ealec_DEI_GISHym80142

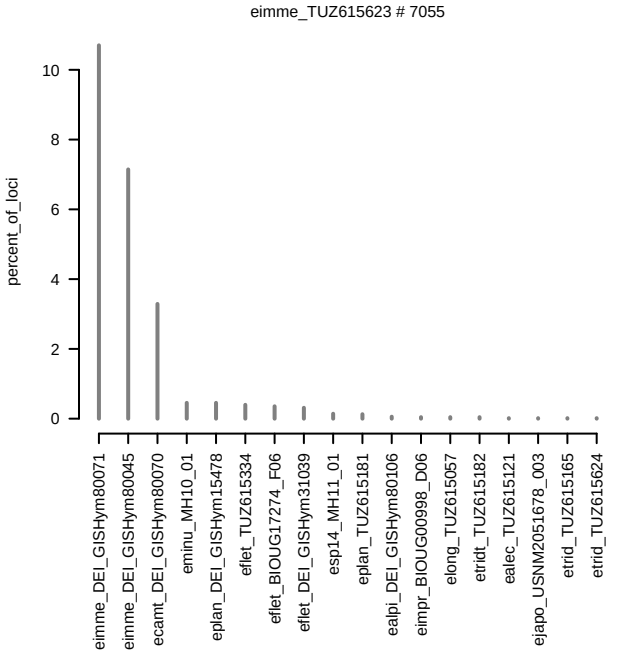
eimme_TUZ615623 # 7055
percent_of_loci
0
2
4
6
8
10
eimme_DEI_GISHym80071
eimme_DEI_GISHym80045
ecamt_DEI_GISHym80070
eminu_MH10_01
eplan_DEI_GISHym15478
eflet_TUZ615334
eflet_BIOUG17274_F06
eflet_DEI_GISHym31039
esp14_MH11_01
eplan_TUZ615181
ealpi_DEI_GISHym80106
eimpr_BIOUG00998_D06
elong_TUZ615057
etridt_TUZ615182
ealec_TUZ615121
ejapo_USNM2051678_003
etrid_TUZ615165
etrid_TUZ615624

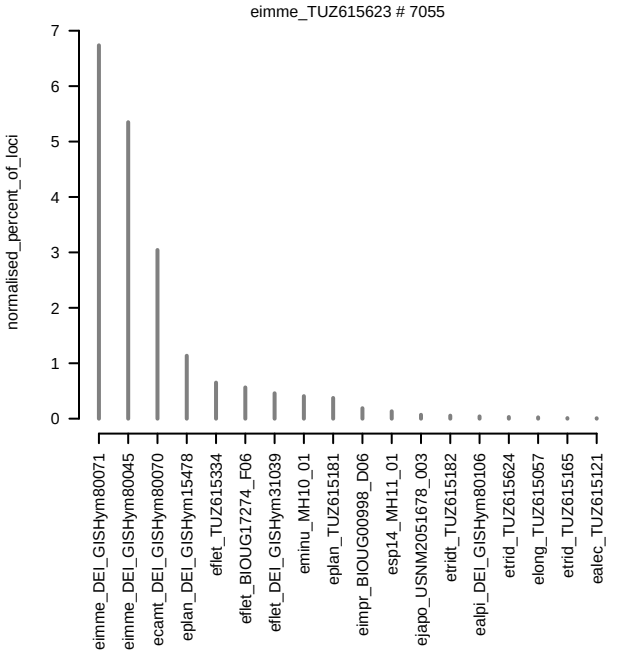
eimme_TUZ615623 # 7055
normalised_percent_of_loci
0
1
2
3
4
5
6
7
eimme_DEI_GISHym80071
eimme_DEI_GISHym80045
ecamt_DEI_GISHym80070
eplan_DEI_GISHym15478
eflet_TUZ615334
eflet_BIOUG17274_F06
eflet_DEI_GISHym31039
eminu_MH10_01
eplan_TUZ615181
eimpr_BIOUG00998_D06
esp14_MH11_01
ejapo_USNM2051678_003
etridt_TUZ615182
ealpi_DEI_GISHym80106
etrid_TUZ615624
elong_TUZ615057
etrid_TUZ615165
ealec_TUZ615121

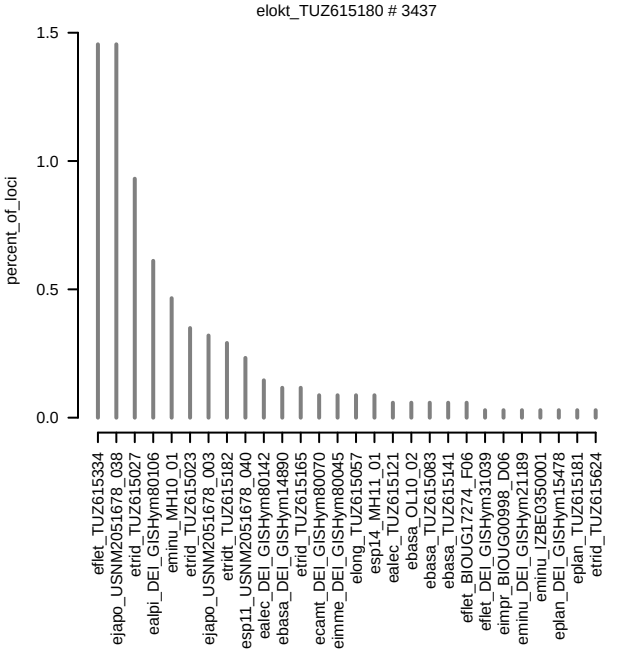
elokt_TUZ615180 # 3437
percent_of_loci
1.5
1.0
0.5
0.0
eflet_TUZ615334
ejapo_USNM2051678_038
etrid_TUZ615027
ealpi_DEI_GISHym80106
eminu_MH10_01
etrid_TUZ615023
ejapo_USNM2051678_003
etridt_TUZ615182
esp11_USNM2051678_040
ealec_DEI_GISHym80142
ebasa_DEI_GISHym14890
etrid_TUZ615165
ecamt_DEI_GISHym80070
eimme_DEI_GISHym80045
elong_TUZ615057
esp14_MH11_01
ealec_TUZ615121
ebasa_OL10_02
ebasa_TUZ615083
ebasa_TUZ615141
eflet_BIOUG17274_F06
eflet_DEI_GISHym31039
eimpr_BIOUG00998_D06
eminu_DEI_GISHym21189
eminu_IZBE0350001
eplan_DEI_GISHym15478
eplan_TUZ615181
etrid_TUZ615624

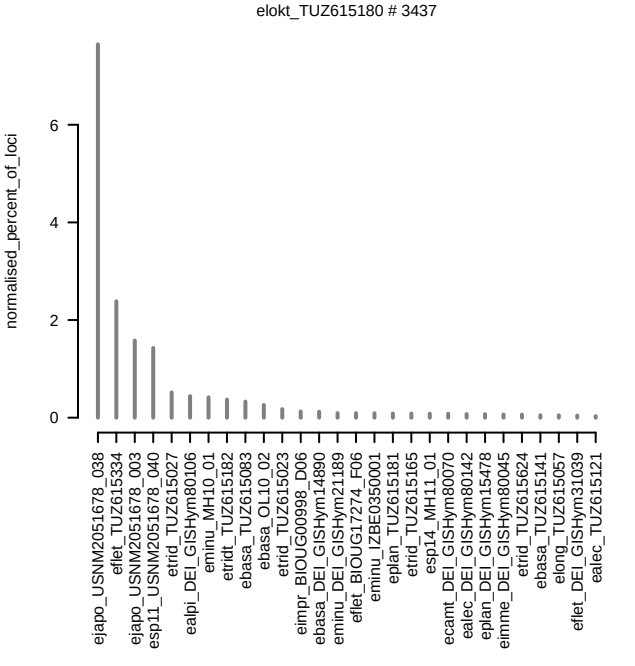
elokt_TUZ615180 # 3437
normalised_percent_of_loci
6
4
2
0
ejapo_USNM2051678_038
eflet_TUZ615334
ejapo_USNM2051678_003
esp11_USNM2051678_040
etrid_TUZ615027
ealpi_DEI_GISHym80106
eminu_MH10_01
etridt_TUZ615182
ebasa_TUZ615083
ebasa_OL10_02
etrid_TUZ615023
eimpr_BIOUG00998_D06
ebasa_DEI_GISHym14890
eminu_DEI_GISHym21189
eflet_BIOUG17274_F06
eminu_IZBE0350001
eplan_TUZ615181
etrid_TUZ615165
esp14_MH11_01
ecamt_DEI_GISHym80070
ealec_DEI_GISHym80142
eplan_DEI_GISHym15478
eimme_DEI_GISHym80045
etrid_TUZ615624
ebasa_TUZ615141
elong_TUZ615057
eflet_DEI_GISHym31039
ealec_TUZ615121

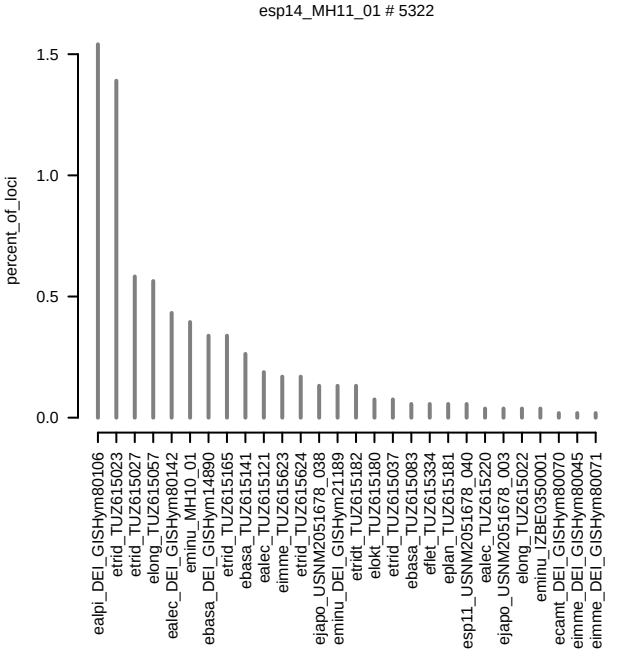
esp14_MH11_01 # 5322
percent_of_loci
1.5
1.0
0.5
0.0
ealpi_DEI_GISHym80106
etrid_TUZ615023
etrid_TUZ615027
elong_TUZ615057
ealec_DEI_GISHym80142
eminu_MH10_01
ebasa_DEI_GISHym14890
etrid_TUZ615165
ebasa_TUZ615141
ealec_TUZ615121
eimme_TUZ615623
etrid_TUZ615624
ejapo_USNM2051678_038
eminu_DEI_GISHym21189
etridt_TUZ615182
elokt_TUZ615180
etridt_TUZ615037
ebasa_TUZ615083
eflet_TUZ615334
eplan_TUZ615181
esp11_USNM2051678_040
ealec_TUZ615220
ejapo_USNM2051678_003
elong_TUZ615022
eminu_IZBE0350001
ecamt_DEI_GISHym80070
eimme_DEI_GISHym80045
eimme_DEI_GISHym80071

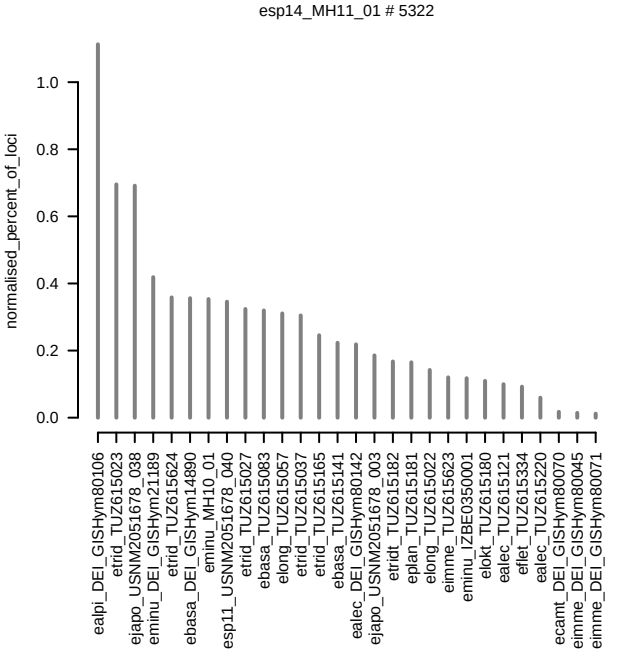
esp14_MH11_01 # 5322
normalised_percent_of_loci
1.0
0.8
0.6
0.4
0.2
0.0
ealpi_DEI_GISHym80106
etrid_TUZ615023
ejapo_USNM2051678_038
eminu_DEI_GISHym21189
etrid_TUZ615624
ebasa_DEI_GISHym14890
eminu_MH10_01
esp11_USNM2051678_040
etrid_TUZ615027
ebasa_TUZ615083
elong_TUZ615057
etrid_TUZ615037
etrid_TUZ615165
ebasa_TUZ615141
ealec_DEI_GISHym80142
ejapo_USNM2051678_003
etridt_TUZ615182
eplan_TUZ615181
elong_TUZ615022
eimme_TUZ615623
eminu_IZBE0350001
elokt_TUZ615180
ealec_TUZ615121
eflet_TUZ615334
ealec_TUZ615220
ecamt_DEI_GISHym80070
eimme_DEI_GISHym80045
eimme_DEI_GISHym80071

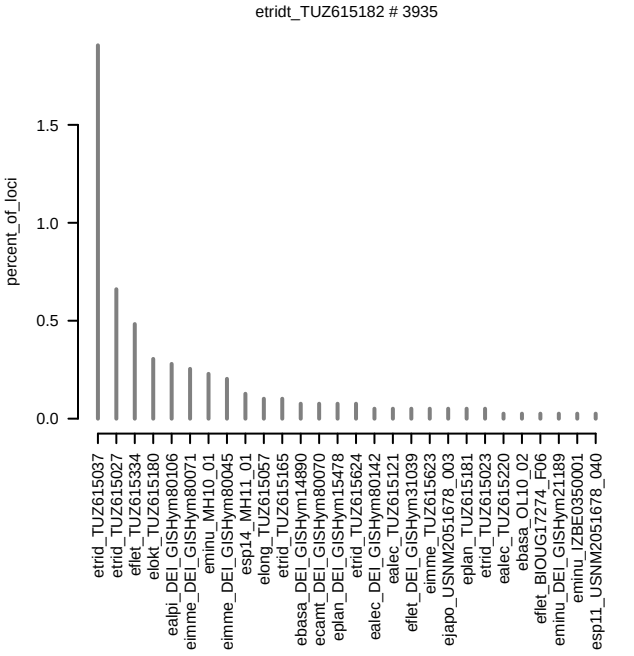
etridt_TUZ615182 # 3935
percent_of_loci
0.0
0.5
1.0
1.5
etrid_TUZ615037
etrid_TUZ615027
eflet_TUZ615334
elokt_TUZ615180
ealpi_DEI_GISHym80106
eimme_DEI_GISHym80071
eminu_MH10_01
eimme_DEI_GISHym80045
esp14_MH11_01
elong_TUZ615057
etrid_TUZ615165
ebasa_DEI_GISHym14890
ecamt_DEI_GISHym80070
eplan_DEI_GISHym15478
etrid_TUZ615624
ealec_DEI_GISHym80142
ealec_TUZ615121
eflet_DEI_GISHym31039
eimme_TUZ615623
ejapo_USNM2051678_003
eplan_TUZ615181
etrid_TUZ615023
ealec_TUZ615220
ebasa_OL10_02
eflet_BIOUG17274_F06
eminu_DEI_GISHym21189
eminu_IZBE0350001
esp11_USNM2051678_040

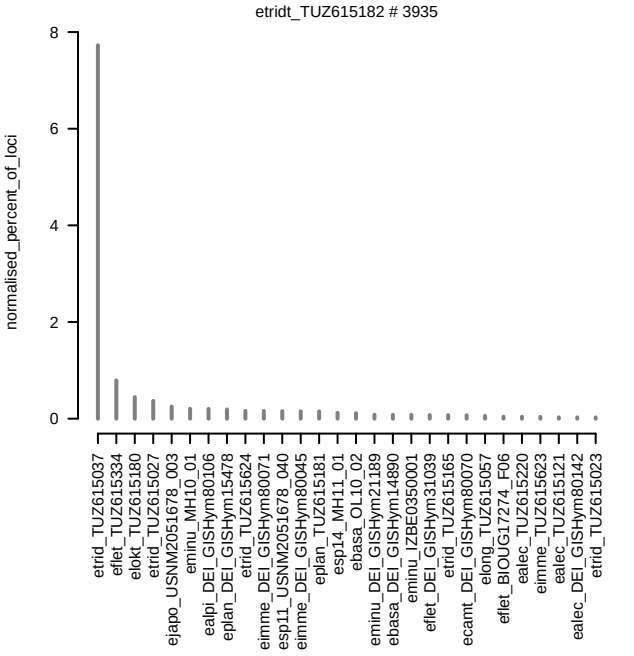
etridt_TUZ615182 # 3935
normalised_percent_of_loci
0
2
4
6
8
etrid_TUZ615037
eflet_TUZ615334
elokt_TUZ615180
etrid_TUZ615027
ejapo_USNM2051678_003
eminu_MH10_01
ealpi_DEI_GISHym80106
eplan_DEI_GISHym15478
etrid_TUZ615624
eimme_DEI_GISHym80071
esp11_USNM2051678_040
eimme_DEI_GISHym80045
eplan_TUZ615181
esp14_MH11_01
ebasa_OL10_02
eminu_DEI_GISHym21189
ebasa_DEI_GISHym14890
eminu_IZBE0350001
eflet_DEI_GISHym31039
etrid_TUZ615165
ecamt_DEI_GISHym80070
elong_TUZ615057
eflet_BIOUG17274_F06
ealec_TUZ615220
eimme_TUZ615623
ealec_TUZ615121
ealec_DEI_GISHym80142
etrid_TUZ615023

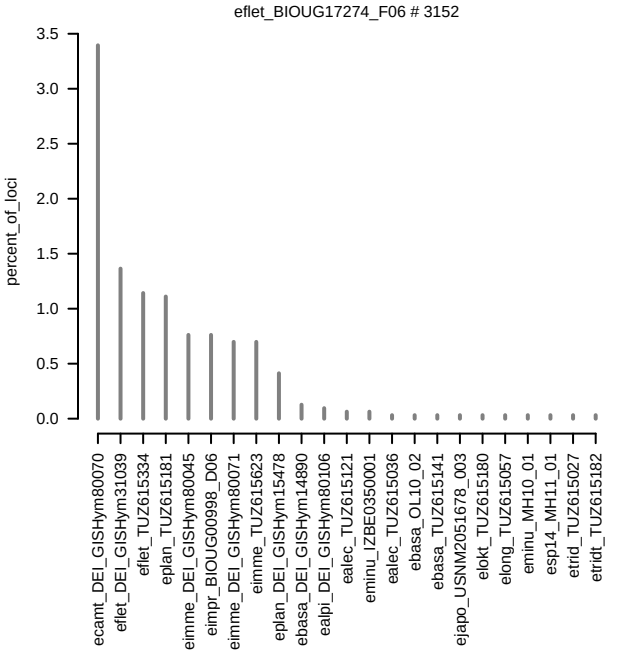
eflet_BIOUG17274_F06 # 3152
percent_of_loci
0.0
0.5
1.0
1.5
2.0
2.5
3.0
3.5
ecamt_DEI_GISHym80070
eflet_DEI_GISHym31039
eflet_TUZ615334
eplan_TUZ615181
eimme_DEI_GISHym80045
eimpr_BIOUG00998_D06
eimme_DEI_GISHym80071
eimme_TUZ615623
eplan_DEI_GISHym15478
ebasa_DEI_GISHym14890
ealpi_DEI_GISHym80106
ealec_TUZ615121
eminu_IZBE0350001
ealec_TUZ615036
ebasa_OL10_02
ebasa_TUZ615141
ejapo_USNM2051678_003
elokt_TUZ615180
elong_TUZ615057
eminu_MH10_01
esp14_MH11_01
etrid_TUZ615027
etridt_TUZ615182

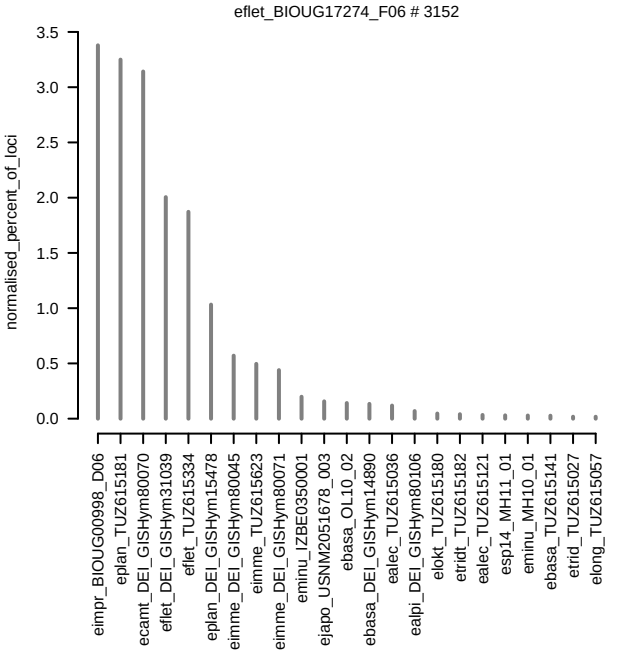
eflet_BIOUG17274_F06 # 3152
normalised_percent_of_loci
0.0
0.5
1.0
1.5
2.0
2.5
3.0
3.5
eimpr_BIOUG00998_D06
eplan_TUZ615181
ecamt_DEI_GISHym80070
eflet_DEI_GISHym31039
eflet_TUZ615334
eplan_DEI_GISHym15478
eimme_DEI_GISHym80045
eimme_TUZ615623
eimme_DEI_GISHym80071
eminu_IZBE0350001
ejapo_USNM2051678_003
ebasa_OL10_02
ebasa_DEI_GISHym14890
ealec_TUZ615036
ealpi_DEI_GISHym80106
elokt_TUZ615180
etridt_TUZ615182
ealec_TUZ615121
esp14_MH11_01
eminu_MH10_01
ebasa_TUZ615141
etrid_TUZ615027
elong_TUZ615057

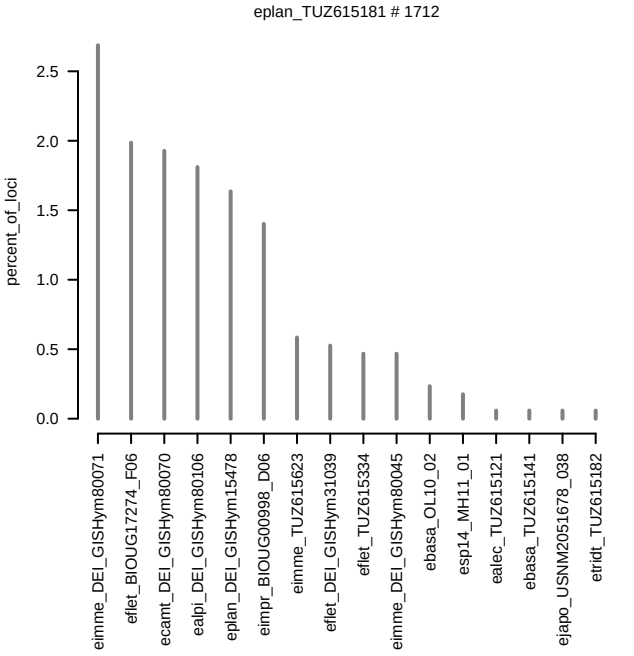
eplan_TUZ615181 # 1712
percent_of_loci
0.0
0.5
1.0
1.5
2.0
2.5
eimme_DEI_GISHym80071
eflet_BIOUG17274_F06
ecamt_DEI_GISHym80070
ealpi_DEI_GISHym80106
eplan_DEI_GISHym15478
eimpr_BIOUG00998_D06
eimme_TUZ615623
eflet_DEI_GISHym31039
eflet_TUZ615334
eimme_DEI_GISHym80045
ebasa_OL10_02
esp14_MH11_01
ealec_TUZ615121
ebasa_TUZ615141
ejapo_USNM2051678_038
etridt_TUZ615182

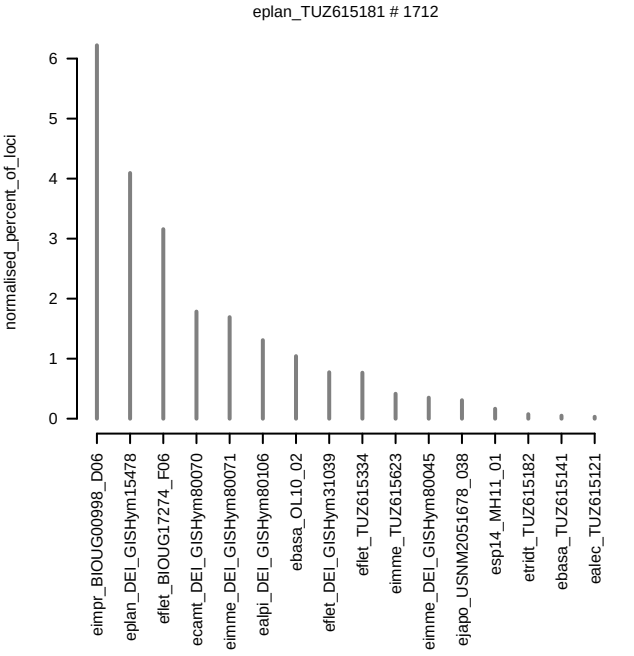
eplan_TUZ615181 # 1712
normalised_percent_of_loci
0
1
2
3
4
5
6
eimpr_BIOUG00998_D06
eplan_DEI_GISHym15478
eflet_BIOUG17274_F06
ecamt_DEI_GISHym80070
eimme_DEI_GISHym80071
ealpi_DEI_GISHym80106
ebasa_OL10_02
eflet_DEI_GISHym31039
eflet_TUZ615334
eimme_TUZ615623
eimme_DEI_GISHym80045
ejapo_USNM2051678_038
esp14_MH11_01
etridt_TUZ615182
ebasa_TUZ615141
ealec_TUZ615121

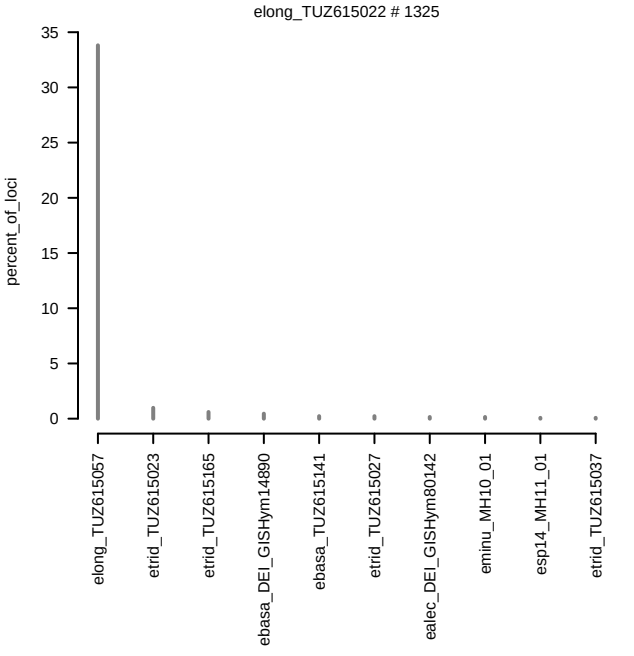
elong_TUZ615022 # 1325
percent_of_loci
0
5
10
15
20
25
30
35
elong_TUZ615057
etrid_TUZ615023
etrid_TUZ615165
ebasa_DEI_GISHym14890
ebasa_TUZ615141
etrid_TUZ615027
ealec_DEI_GISHym80142
eminu_MH10_01
esp14_MH11_01
etrid_TUZ615037

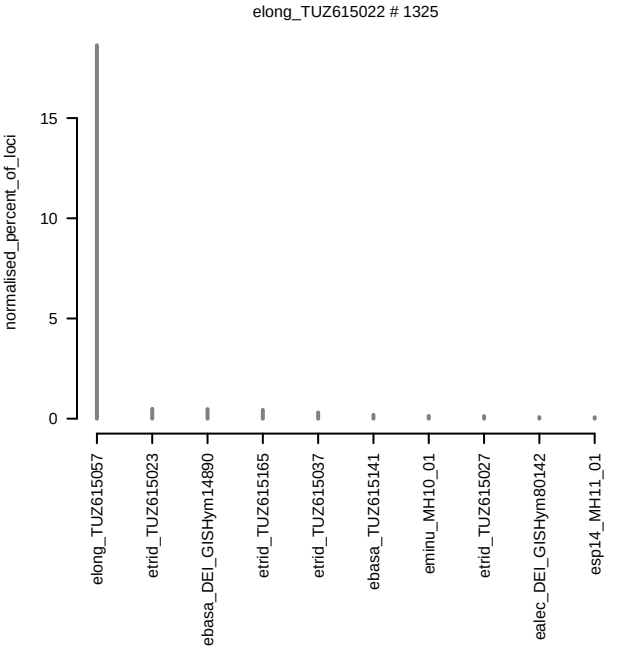
elong_TUZ615022 # 1325
normalised_percent_of_loci
0
5
10
15
elong_TUZ615057
etrid_TUZ615023
ebasa_DEI_GISHym14890
etrid_TUZ615165
etrid_TUZ615037
ebasa_TUZ615141
eminu_MH10_01
etrid_TUZ615027
ealec_DEI_GISHym80142
esp14_MH11_01

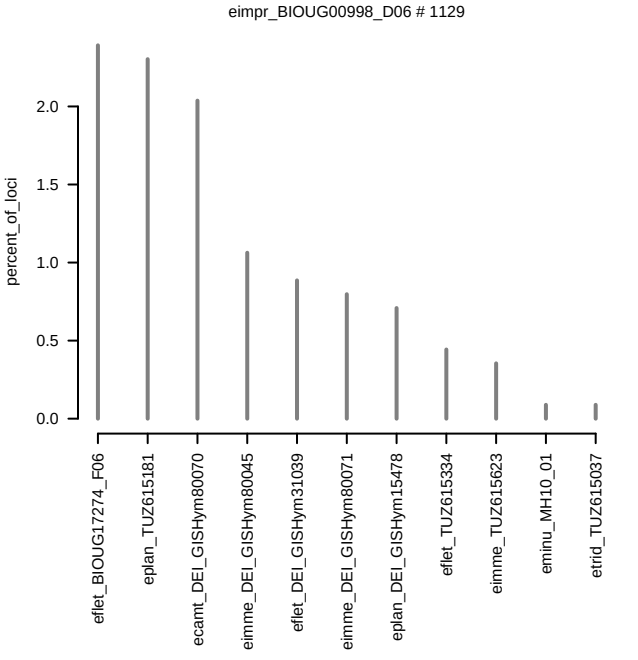
eimpr_BIOUG00998_D06 # 1129
percent_of_loci
0.0
0.5
1.0
1.5
2.0
eflet_BIOUG17274_F06
eplan_TUZ615181
ecamt_DEI_GISHym80070
eimme_DEI_GISHym80045
eflet_DEI_GISHym31039
eimme_DEI_GISHym80071
eplan_DEI_GISHym15478
eflet_TUZ615334
eimme_TUZ615623
eminu_MH10_01
etrid_TUZ615037

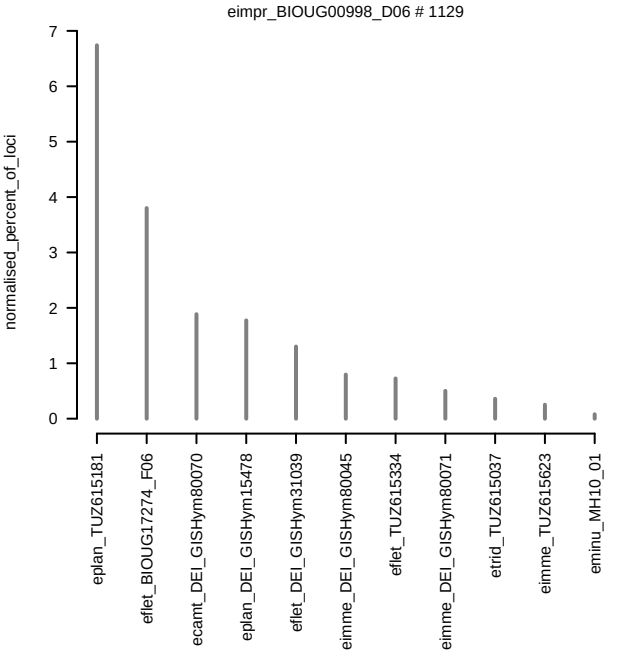
eimpr_BIOUG00998_D06 # 1129
normalised_percent_of_loci
0
1
2
3
4
5
6
7
eplan_TUZ615181
eflet_BIOUG17274_F06
ecamt_DEI_GISHym80070
eplan_DEI_GISHym15478
eflet_DEI_GISHym31039
eimme_DEI_GISHym80045
eflet_TUZ615334
eimme_DEI_GISHym80071
etrid_TUZ615037
eimme_TUZ615623
eminu_MH10_01

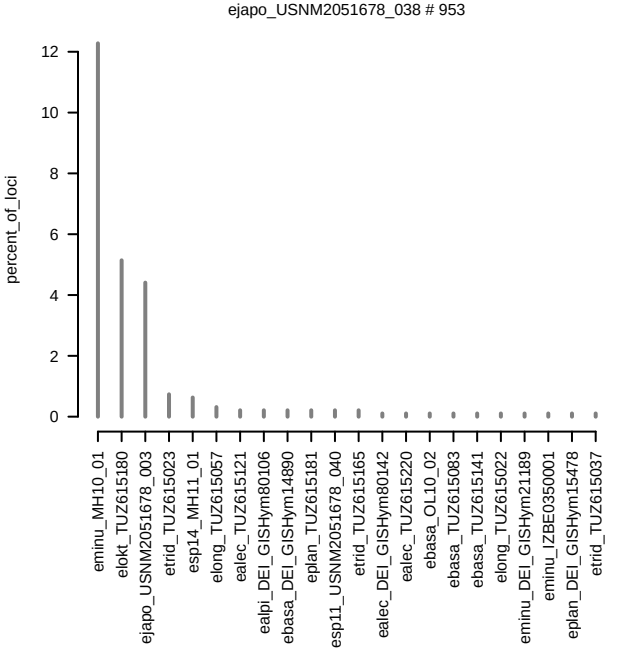
ejapo_USNM2051678_038 # 953
percent_of_loci
0
2
4
6
8
10
12
eminu_MH10_01
elokt_TUZ615180
ejapo_USNM2051678_003
etrid_TUZ615023
esp14_MH11_01
elong_TUZ615057
ealec_TUZ615121
ealpi_DEI_GISHym80106
ebasa_DEI_GISHym14890
eplan_TUZ615181
esp11_USNM2051678_040
etrid_TUZ615165
ealec_DEI_GISHym80142
ealec_TUZ615220
ebasa_OL10_02
ebasa_TUZ615083
ebasa_TUZ615141
elong_TUZ615022
eminu_DEI_GISHym21189
eminu_IZBE0350001
eplan_DEI_GISHym15478
etrid_TUZ615037

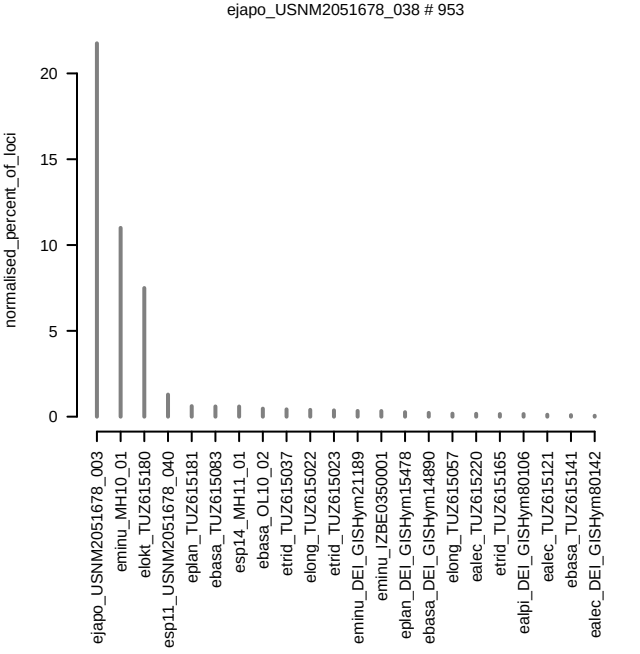
ejapo_USNM2051678_038 # 953
normalised_percent_of_loci
0
5
10
15
20
ejapo_USNM2051678_003
eminu_MH10_01
elokt_TUZ615180
esp11_USNM2051678_040
eplan_TUZ615181
ebasa_TUZ615083
esp14_MH11_01
ebasa_OL10_02
etrid_TUZ615037
elong_TUZ615022
etrid_TUZ615023
eminu_DEI_GISHym21189
eminu_IZBE0350001
eplan_DEI_GISHym15478
ebasa_DEI_GISHym14890
elong_TUZ615057
ealec_TUZ615220
etrid_TUZ615165
ealpi_DEI_GISHym80106
ealec_TUZ615121
ebasa_TUZ615141
ealec_DEI_GISHym80142

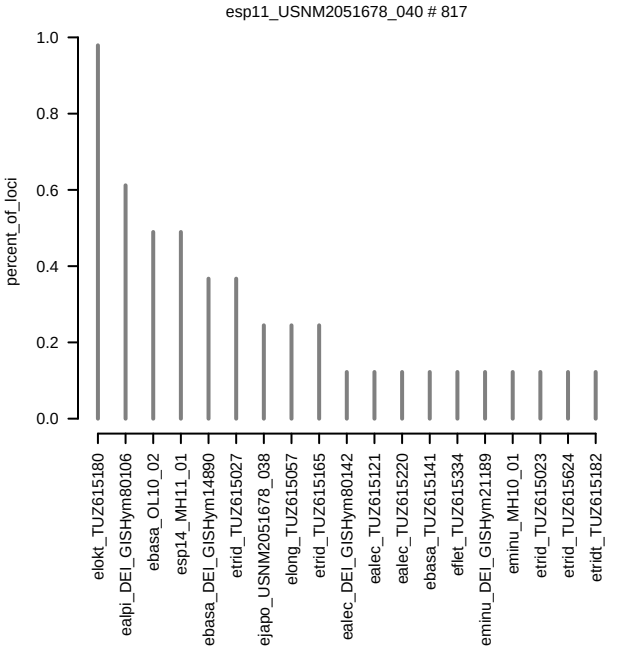
esp11_USNM2051678_040 # 817
percent_of_loci
1.0
0.8
0.6
0.4
0.2
0.0
elokt_TUZ615180
ealpi_DEI_GISHym80106
ebasa_OL10_02
esp14_MH11_01
ebasa_DEI_GISHym14890
etrid_TUZ615027
ejapo_USNM2051678_038
elong_TUZ615057
etrid_TUZ615165
ealec_DEI_GISHym80142
ealec_TUZ615121
ealec_TUZ615220
ebasa_TUZ615141
eflet_TUZ615334
eminu_DEI_GISHym21189
eminu_MH10_01
etrid_TUZ615023
etrid_TUZ615624
etridt_TUZ615182

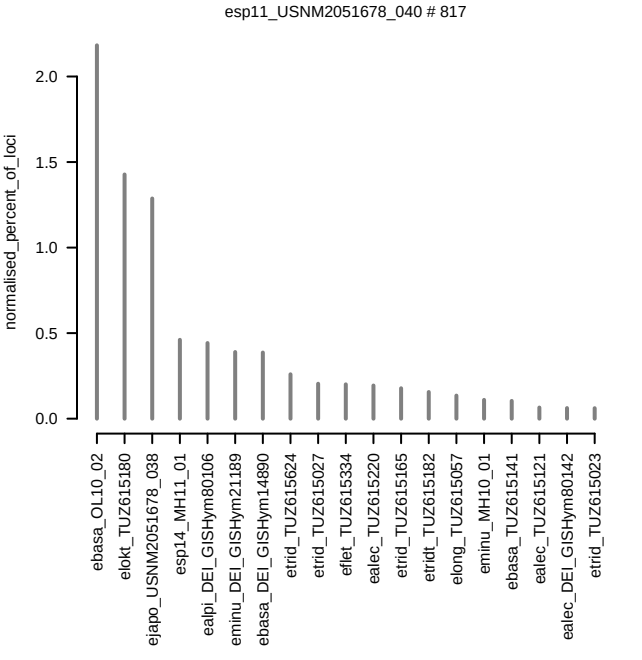
esp11_USNM2051678_040 # 817
normalised_percent_of_loci
2.0
1.5
1.0
0.5
0.0
ebasa_OL10_02
elokt_TUZ615180
ejapo_USNM2051678_038
esp14_MH11_01
ealpi_DEI_GISHym80106
eminu_DEI_GISHym21189
ebasa_DEI_GISHym14890
etrid_TUZ615624
etrid_TUZ615027
eflet_TUZ615334
ealec_TUZ615220
etrid_TUZ615165
etridt_TUZ615182
elong_TUZ615057
eminu_MH10_01
ebasa_TUZ615141
ealec_TUZ615121
ealec_DEI_GISHym80142
etrid_TUZ615023

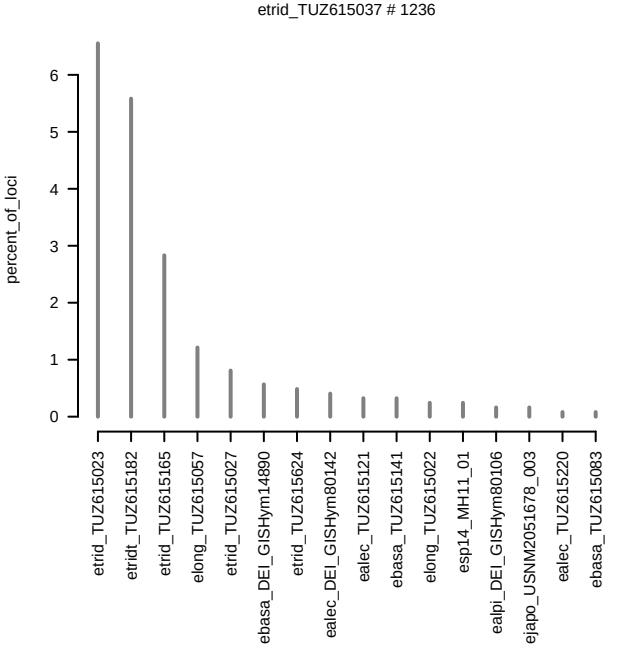
etrid_TUZ615037 # 1236
percent_of_loci
6
5
4
3
2
1
0
etrid_TUZ615023
etridt_TUZ615182
etrid_TUZ615165
elong_TUZ615057
etrid_TUZ615027
ebasa_DEI_GISHym14890
etrid_TUZ615624
ealec_DEI_GISHym80142
ealec_TUZ615121
ebasa_TUZ615141
elong_TUZ615022
esp14_MH11_01
ealpi_DEI_GISHym80106
ejapo_USNM2051678_003
ealec_TUZ615220
ebasa_TUZ615083

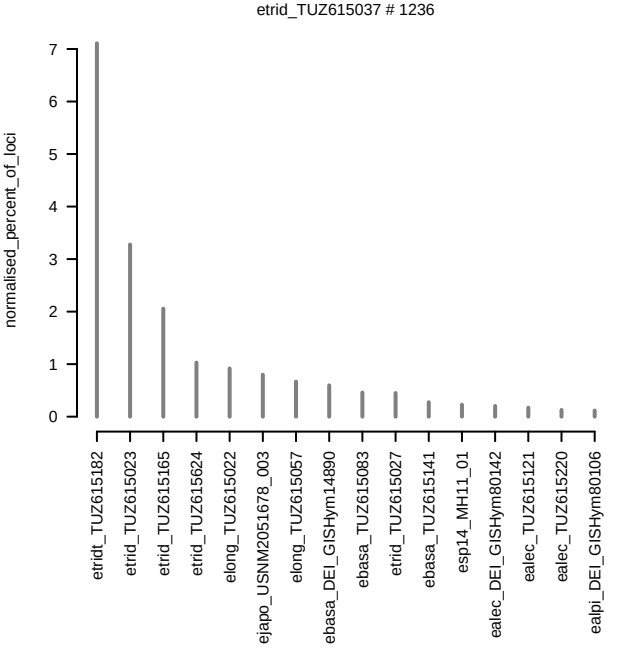
etrid_TUZ615037 # 1236
normalised_percent_of_loci
7
6
5
4
3
2
1
0
etridt_TUZ615182
etrid_TUZ615023
etrid_TUZ615165
etrid_TUZ615624
elong_TUZ615022
ejapo_USNM2051678_003
elong_TUZ615057
ebasa_DEI_GISHym14890
ebasa_TUZ615083
etrid_TUZ615027
ebasa_TUZ615141
esp14_MH11_01
ealec_DEI_GISHym80142
ealec_TUZ615121
ealec_TUZ615220
ealpi_DEI_GISHym80106

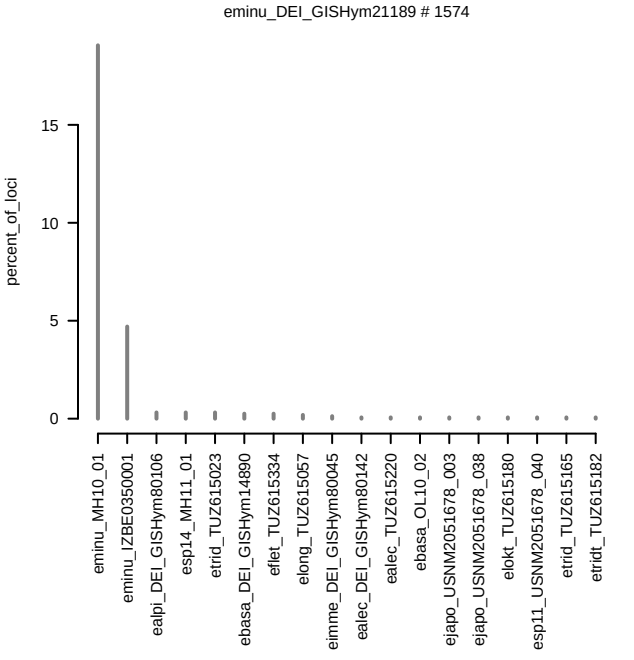
eminu_DEI_GISHym21189 # 1574
percent_of_loci
0
5
10
15
eminu_MH10_01
eminu_IZBE0350001
ealpi_DEI_GISHym80106
esp14_MH11_01
etrid_TUZ615023
ebasa_DEI_GISHym14890
eflet_TUZ615334
elong_TUZ615057
eimme_DEI_GISHym80045
ealec_DEI_GISHym80142
ealec_TUZ615220
ebasa_OL10_02
ejapo_USNM2051678_003
ejapo_USNM2051678_038
elokt_TUZ615180
esp11_USNM2051678_040
etrid_TUZ615165
etridt_TUZ615182

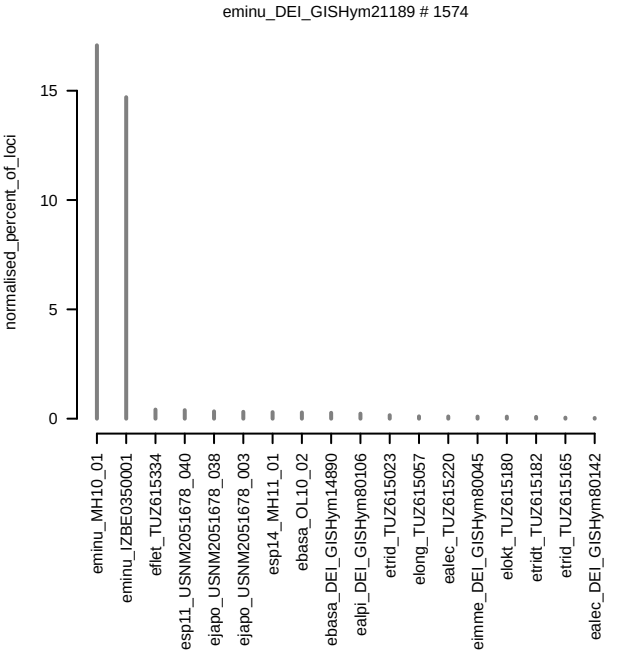
eminu_DEI_GISHym21189 # 1574
normalised_percent_of_loci
0
5
10
15
eminu_MH10_01
eminu_IZBE0350001
eflet_TUZ615334
esp11_USNM2051678_040
ejapo_USNM2051678_038
ejapo_USNM2051678_003
esp14_MH11_01
ebasa_OL10_02
ebasa_DEI_GISHym14890
ealpi_DEI_GISHym80106
etrid_TUZ615023
elong_TUZ615057
ealec_TUZ615220
eimme_DEI_GISHym80045
elokt_TUZ615180
etridt_TUZ615182
etrid_TUZ615165
ealec_DEI_GISHym80142

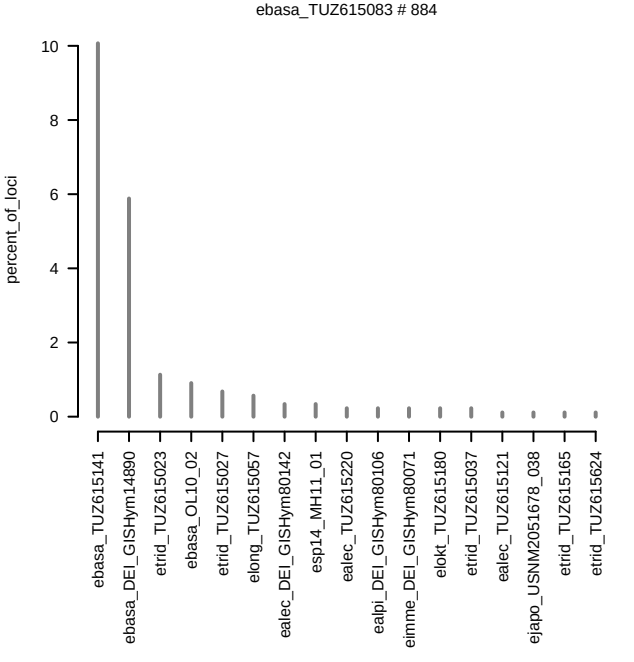
ebasa_TUZ615083 # 884
percent_of_loci
0
2
4
6
8
10
ebasa_TUZ615141
ebasa_DEI_GISHym14890
etrid_TUZ615023
ebasa_OL10_02
etrid_TUZ615027
elong_TUZ615057
ealec_DEI_GISHym80142
esp14_MH11_01
ealec_TUZ615220
ealpi_DEI_GISHym80106
eimme_DEI_GISHym80071
elokt_TUZ615180
etrid_TUZ615037
ealec_TUZ615121
ejapo_USNM2051678_038
etrid_TUZ615165
etrid_TUZ615624

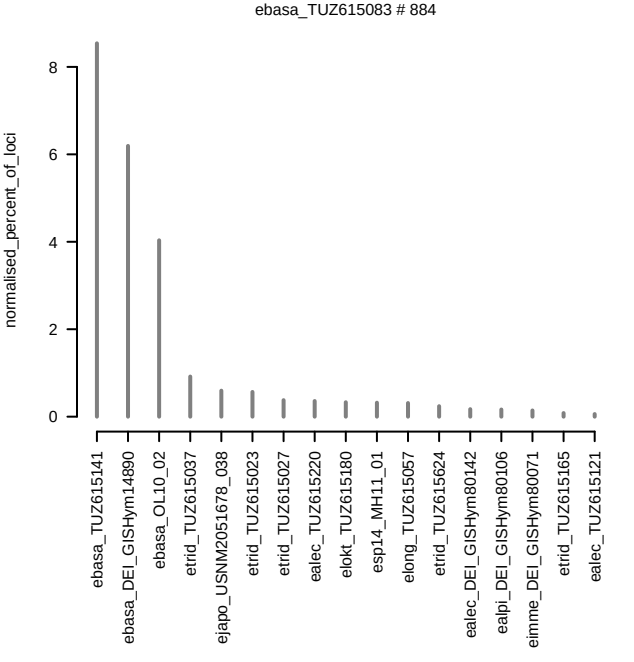
ebasa_TUZ615083 # 884
normalised_percent_of_loci
0
2
4
6
8
ebasa_TUZ615141
ebasa_DEI_GISHym14890
ebasa_OL10_02
etrid_TUZ615037
ejapo_USNM2051678_038
etrid_TUZ615023
etrid_TUZ615027
ealec_TUZ615220
elokt_TUZ615180
esp14_MH11_01
elong_TUZ615057
etrid_TUZ615624
ealec_DEI_GISHym80142
ealpi_DEI_GISHym80106
eimme_DEI_GISHym80071
etrid_TUZ615165
ealec_TUZ615121

eplan_DEI_GISHym15478 # 2002
percent_of_loci
0
2
4
6
8
ecamt_DEI_GISHym80070
eimme_DEI_GISHym80071
eimme_TUZ615623
eplan_TUZ615181
eimme_DEI_GISHym80045
eflet_TUZ615334
eflet_BIOUG17274_F06
eflet_DEI_GISHym31039
eimpr_BIOUG00998_D06
etrid_TUZ615624
etridt_TUZ615182
ebasa_DEI_GISHym14890
ejapo_USNM2051678_038
elokt_TUZ615180
eminu_MH10_01
etrid_TUZ615027

eplan_DEI_GISHym15478 # 2002
normalised_percent_of_loci
0
2
4
6
ecamt_DEI_GISHym80070
eplan_TUZ615181
eflet_TUZ615334
eimpr_BIOUG00998_D06
eflet_BIOUG17274_F06
eimme_DEI_GISHym80071
eimme_TUZ615623
eimme_DEI_GISHym80045
eflet_DEI_GISHym31039
etrid_TUZ615624
ejapo_USNM2051678_038
etridt_TUZ615182
elokt_TUZ615180
ebasa_DEI_GISHym14890
eminu_MH10_01
etrid_TUZ615027

Supplementary Data S6

Proportion of two-fold degenerate positions calculated from initial de novo assembly (29 859 loci, clustering threshold of 80% similarity; Supplementary Data S1). f - female, m - male.

seqID	sex	c80m4_emp_35
ebasa_TUZ615083	f	0.096977702
eplan_DEI_GISHym15478	f	0.110936547
eminu_DEI_GISHym21189	f	0.119766666
ealec_TUZ615220	f	0.140531012
eplan_TUZ615181	f	0.143195605
eimpr_BIOUG00998_D06	f	0.147432826
elokt_TUZ615180	f	0.184152156
ecamt_DEI_GISHym80070	f	0.352133659
ebasa_DEI_GISHym14890	f	0.368967193
etrid_TUZ615023	larva	0.479105879
etrid_TUZ615165	m	0.050117946
etrid_TUZ615624	m	0.050510643
ealec_TUZ615121	m	0.050542335
ealec_TUZ615036	m	0.056506316
ealec_DEI_GISHym80142	m	0.056811945
elong_TUZ615057	larva	0.05810912
eminu_IZBE0350001	m	0.060623912
ealpi_DEI_GISHym80106	m	0.061000681
eflet_DEI_GISHym31039	m	0.064387317
eimme_DEI_GISHym80071	m	0.067963696
etridt_TUZ615182	m	0.069430662
eminu_MH10_01	m	0.07009008
eimme_TUZ615623	m	0.075250443
ebasa_OL10_02	m	0.081340147
esp14_MH11_01	m	0.081750005
elong_TUZ615022	m	0.082851534
etrid_TUZ615037	m	0.090150841
eflet_BIOUG17274_F06	m	0.092170884
eimme_DEI_GISHym80045	m	0.097541328
esp11_USNM2051678_040	m	0.114109199
ejapo_USNM2051678_038	m	0.115543282
ejapo_USNM2051678_003	m	0.139947405
ebasa_TUZ615141	m	0.140099994
eflet_TUZ615334	m	0.169532302
etrid_TUZ615027	larva	0.055646596

Supplementary Data S7

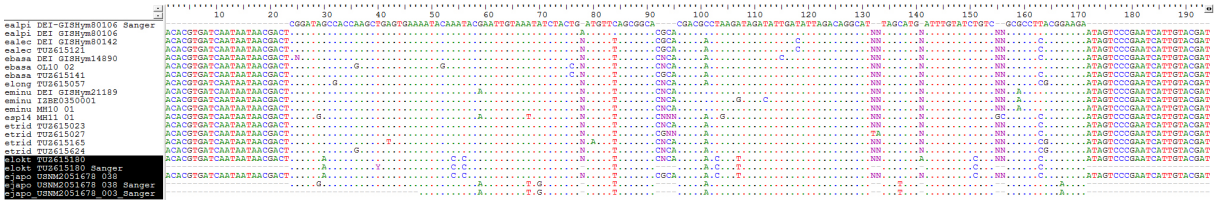

Anonymous ddRAD locus that was chosen for PCR amplification and Sanger sequencing. *Empria loktini* and *E. japonica* are highlighted. “Sanger” refers to PCR amplified Sanger sequences and the others are from *de novo* ddRAD assembly of *longicornis* group that includes only loci present at least in *E. loktini*, one *E. japonica*, and two other specimens. Note that Sanger sequence of *E. japonica* USNM2051678_038 is different from ddRAD sequence, latter of which is identical to *E. loktini* instead.

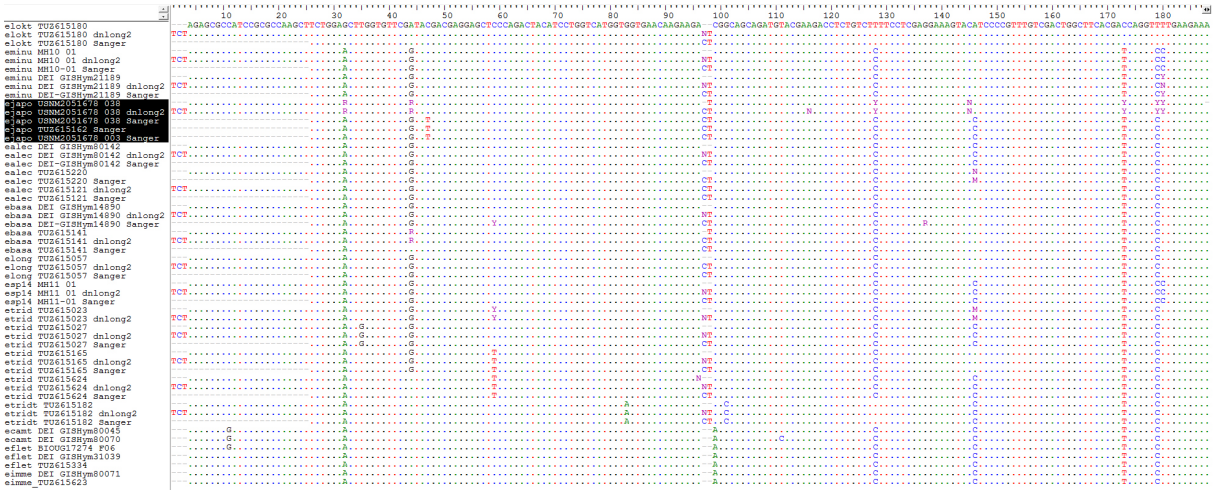

Second ddRAD locus that was chosen for PCR amplification and Sanger sequencing (ZC3H14 gene). *Empria japonica* is highlighted. “dnlong2” refers to *de novo* ddRAD assembly of *longicornis* group that includes only loci present at least in *E. loktini*, one *E. japonica*, and two other specimens, “Sanger” refers to PCR amplified Sanger sequences, and the others are from initial ddRAD assembly (*de novo*, 29 859 loci; Supplementary Data S1). Note that Sanger sequence of *E. japonica* USNM2051678_038 is different from ddRAD sequences, latter of which are identical to 9 (out of 23) other specimens. Based on two-fold degenerate positions, the ddRAD sequences of USNM2051678_038 are apparently combination of two different sequences, one of which is identical to *E. loktini* and the other to *E. minuta* MH10-01.

Supplementary Data S8. Specimens of *Empria* analyzed in this study and a summary of the ddRAD data in *de novo* and reference assembly. Removed individuals due to low quality of sequencing results or potential contamination issues were marked with asterisk in Sample ID.

Species	Sample ID	Total reads (million)	***de novo* assembly**				**Reference assembly**				
			Clusters at 95%[a]	Mean depth	Retained loci[b]	Recovered loci	Mapped reads	Clusters total	Clusters depth	Reads consensus	Recovered loci in assembly
(a) *Empria longicornis* group											
Empria alector	DEI-GISHym80142	4.78	25958	68.5	25324	11350	43907	13598	5413	4925	2025
Empria alector	TUZ615036	0.34	3270	23.4	3193	2336	1966	743	277	268	135
Empria alector	TUZ615121	4.81	23923	95.0	23456	12798	28829	8490	3537	3255	1688
Empria alector	TUZ615220	2.18	7291	170.4	7130	5203	NA	NA	NA	NA	NA
Empria alpina	DEI-GISHym15214 *	0.06	992	26.3	915	529	NA	NA	NA	NA	NA
Empria alpina	DEI-GISHym80011 *	0.15	1176	55.9	1091	594	NA	NA	NA	NA	NA
Empria alpina	DEI-GISHym80106	4.24	24001	69.3	23513	9841	34679	9359	4014	3747	1271
Empria basalis	DEI-GISHym14890	0.72	11116	29.8	10765	7764	6078	2233	882	836	479
Empria basalis	OL10-02	1.01	2932	164.5	2754	1824	2129	963	282	268	138
Empria basalis	TUZ615083	0.09	2189	22.3	2117	1580	879	531	165	158	82
Empria basalis	TUZ615141	0.86	12981	26.9	12661	9621	7856	3106	1242	1180	657
Empria basalis	TUZ615625 *	0.06	870	8.8	804	554	NA	NA	NA	NA	NA
Empria japonica	TUZ615162 *	0.02	788	15.3	755	477	NA	NA	NA	NA	NA
Empria japonica	USNM2051678_003	0.79	3324	36.2	3132	1583	4263	926	331	311	131
Empria japonica	USNM2051678_038 *	3.30	4455	430.3	4283	1945	41018	1262	466	424	168
Empria loktini	TUZ615180	3.73	16249	93.2	15940	6313	14176	4379	2039	1899	602
Empria longicornis	DEI-GISHym14886 *	0.99	1041	539.2	1014	503	NA	NA	NA	NA	NA
Empria longicornis	TUZ615022	2.35	3499	321.0	3427	2446	4558	648	320	313	158
Empria longicornis	TUZ615057	7.94	32886	96.2	32344	13430	41605	9137	5099	4747	1727
Empria minuta	DEI-GISHym21189	0.47	6280	34.5	6160	3435	3383	1054	629	605	295
Empria minuta	IZBE0350001	0.99	5861	94.3	5775	3430	2071	886	548	530	292
Empria minuta	MH10-01	2.47	21488	52.0	21141	10497	13372	3335	2364	2273	976
Empria montana	DEI-GISHym80040 *	0.08	237	9.3	233	131	NA	NA	NA	NA	NA
Empria sp.11	USNM2051678_040	0.34	3466	8.3	3401	1856	821	540	288	274	111
Empria sp.14	DEI-GISHym15231 *	0.21	269	70.2	259	110	NA	NA	NA	NA	NA
Empria sp.14	MH11-01	1.34	17644	41.6	17370	10184	9544	3411	2147	2065	936
Empria tridens	DEI-GISHym20872 *	0.09	484	126.0	471	303	NA	NA	NA	NA	NA
Empria tridens	TUZ615023	2.46	28797	37.3	28327	16107	21444	6939	4098	3944	1893
Empria tridens	TUZ615027	2.23	25524	45.6	25189	15028	21074	6332	3672	3520	1679
Empria tridens	TUZ615037	0.18	3436	19.6	3345	2296	NA	NA	NA	NA	NA
Empria tridens	TUZ615165	7.32	18133	149.1	17923	12029	12194	4322	2375	2270	1182
Empria tridens	TUZ615624	1.18	7095	60.0	6961	4417	3067	1570	784	745	360
Empria tridens	USNM2057434_19 *	0.24	1722	65.5	1662	962	NA	NA	NA	NA	NA
Empria tridentis	TUZ615182	2.93	19454	77.6	19143	8139	23160	4347	2562	2434	648

	AVERAGE	**1.79**	**9966**	**93.6**	**9764**	**5283**	**14873**	**3831**	**1893**	**1782**	**767**
(b) *Empria immersa* group											
Empria camtschatica	DEI-GISHym20706 *	0.09	1459	30.6	1367	1027	NA	NA	NA	NA	NA
Empria camtschatica	DEI-GISHym80070	1.22	12373	22.3	12018	8189	6828	2829	1145	1080	542
Empria fletcheri	BIOUG00998-E05 *	0.09	2114	16.3	1989	1383	NA	NA	NA	NA	NA
Empria fletcheri	BIOUG17274-F06	11.77	8052	743.4	7825	5294	NA	NA	NA	NA	NA
Empria fletcheri	DEI-GISHym31039	0.51	8273	27.7	8106	5647	4896	1970	745	713	345
Empria fletcheri	TUZ615113 *	0.56	545	704.1	497	291	533	349	58	54	11
Empria fletcheri	TUZ615334	0.27	7261	15.0	6969	4929	3115	1806	632	602	296
Empria immersa	DEI-GISHym80045	0.98	14671	19.9	14310	9770	9243	3864	1582	1501	738
Empria immersa	DEI-GISHym80071	4.09	23954	71.2	23543	11263	23754	6763	3268	3084	823
Empria immersa	TUZ615623	2.96	20559	54.8	20210	10731	15560	4795	2505	2379	794
Empria improba	BIOUG00998-B05 *	0.17	1322	47.3	1262	492	698	327	121	107	28
Empria improba	BIOUG00998-D05 *	0.39	931	57.4	895	324	NA	NA	NA	NA	NA
Empria improba	BIOUG00998-D06	0.48	3416	57.3	3317	1936	1405	742	323	309	114
Empria plana	BIOUG00998-C05 *	0.58	2248	175.7	2181	896	NA	NA	NA	NA	NA
Empria plana	DEI-GISHym15478	0.66	6115	168.6	5977	3474	1201	3	1	NA	NA
Empria plana	TUZ615181	1.84	5519	50.7	5330	2948	969	198	108	102	65
	AVERAGE	**1.67**	**7426**	**141.4**	**7237**	**4287**	**6200**	**2364**	**1049**	**993**	**376**

[a]Clusters that passed filtering for 3x minimum coverage.

[b]Loci retained after passing coverage and paralog filters.

NA, not applicable.

Supplementary Data S9

Maximum likelihood tree (NaK+POL2+ZC3H14) including *E. montana*

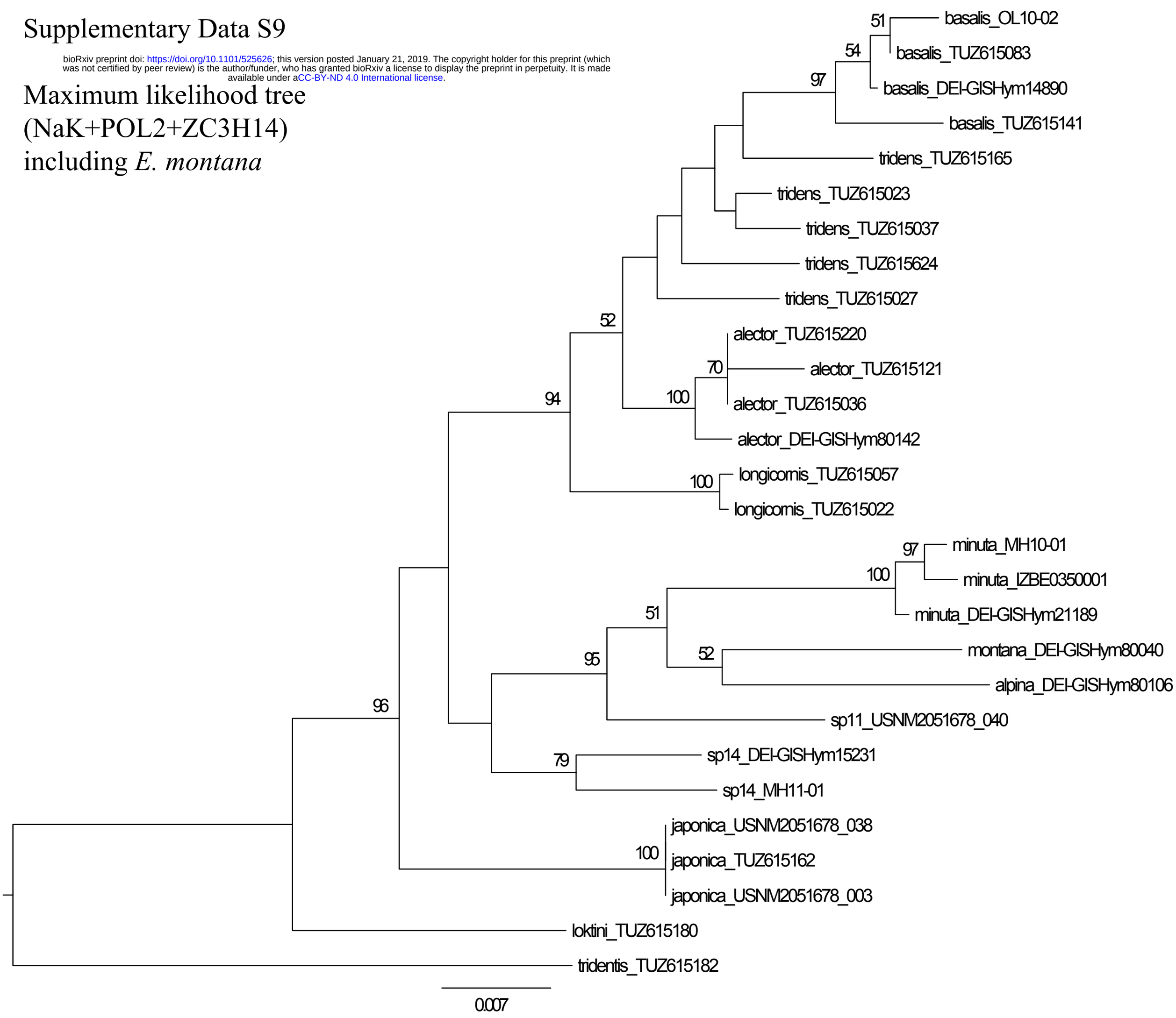

Supplementary Data S10

Maximum likelihood tree of mitochondrial COI including *E. montana* (mont) and additional sequences from Genbank

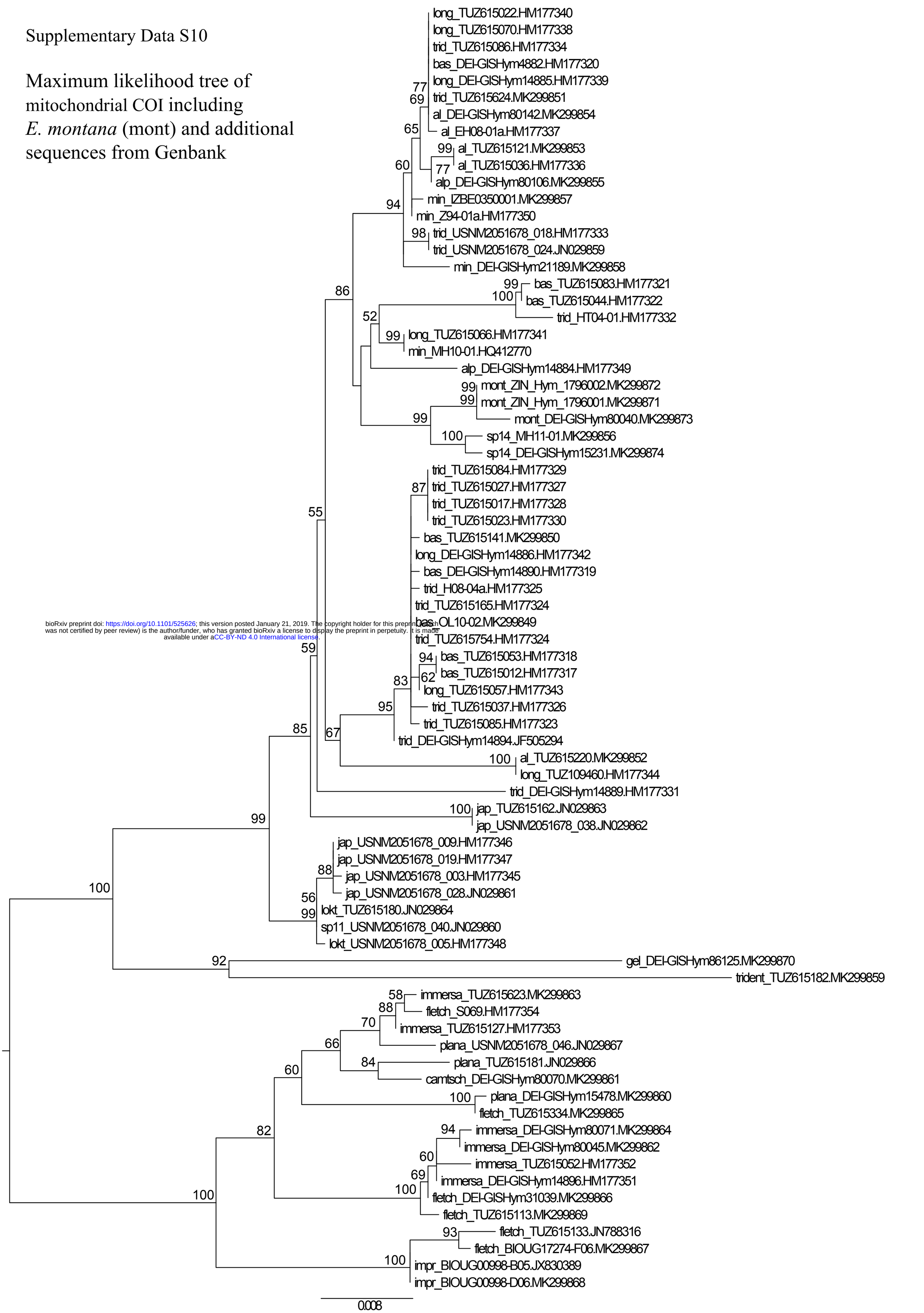

Supplementary Data S11

(a) *E. longicornis* group

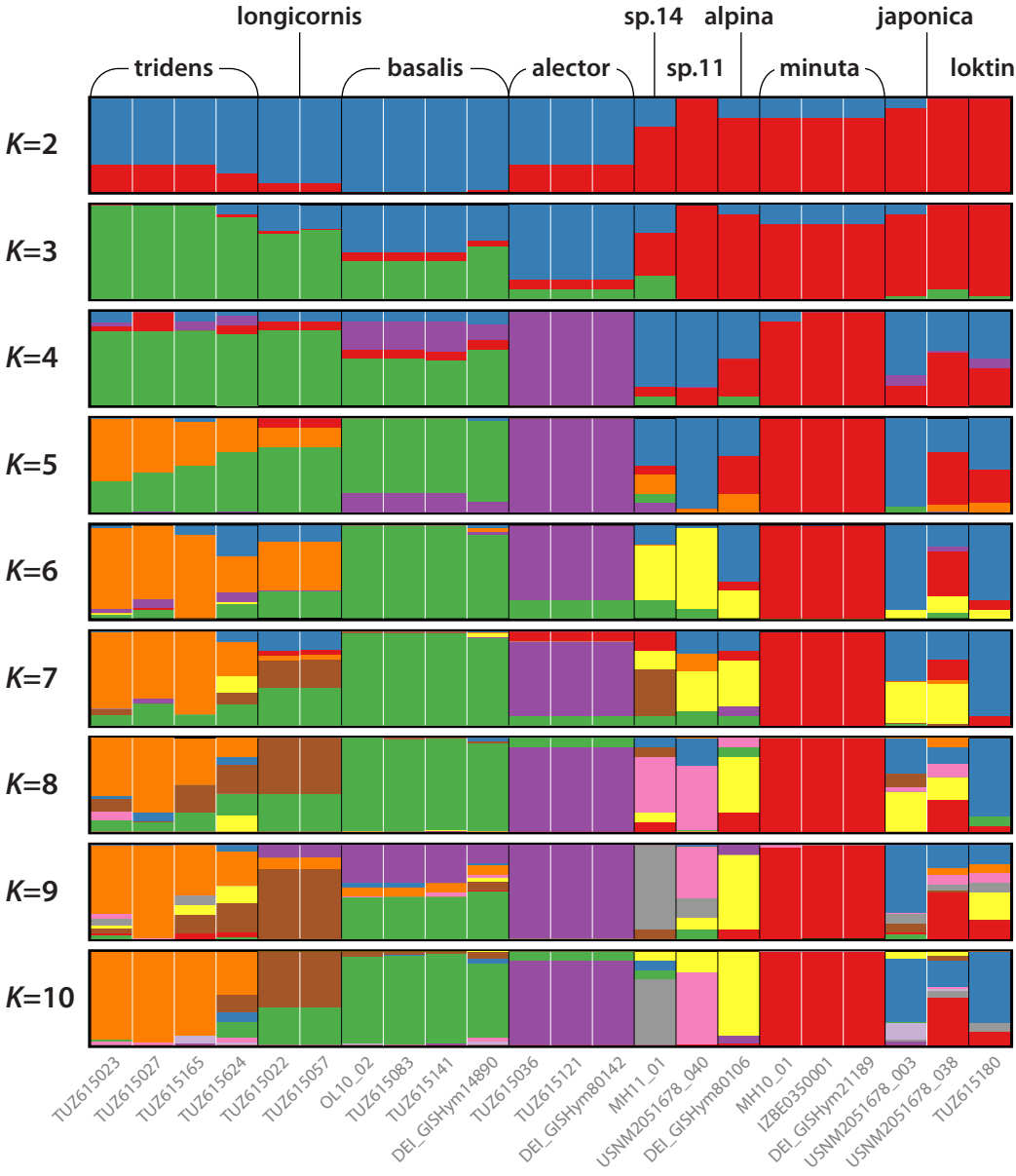

(b) *E. immersa* group

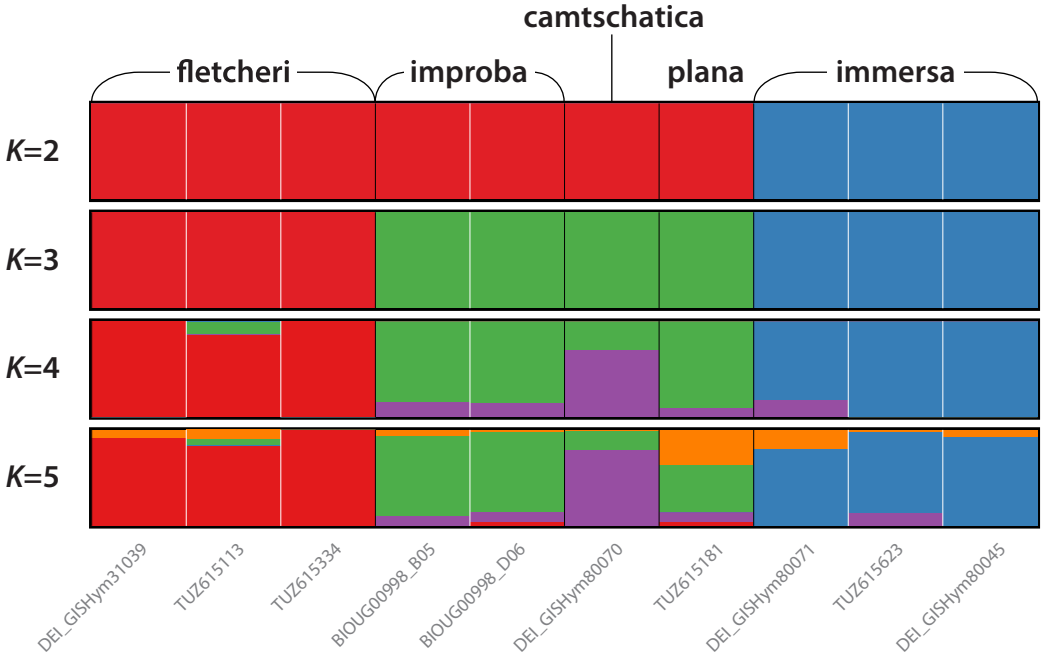

Supplementary Data S12

(a) *E. longicornis* group

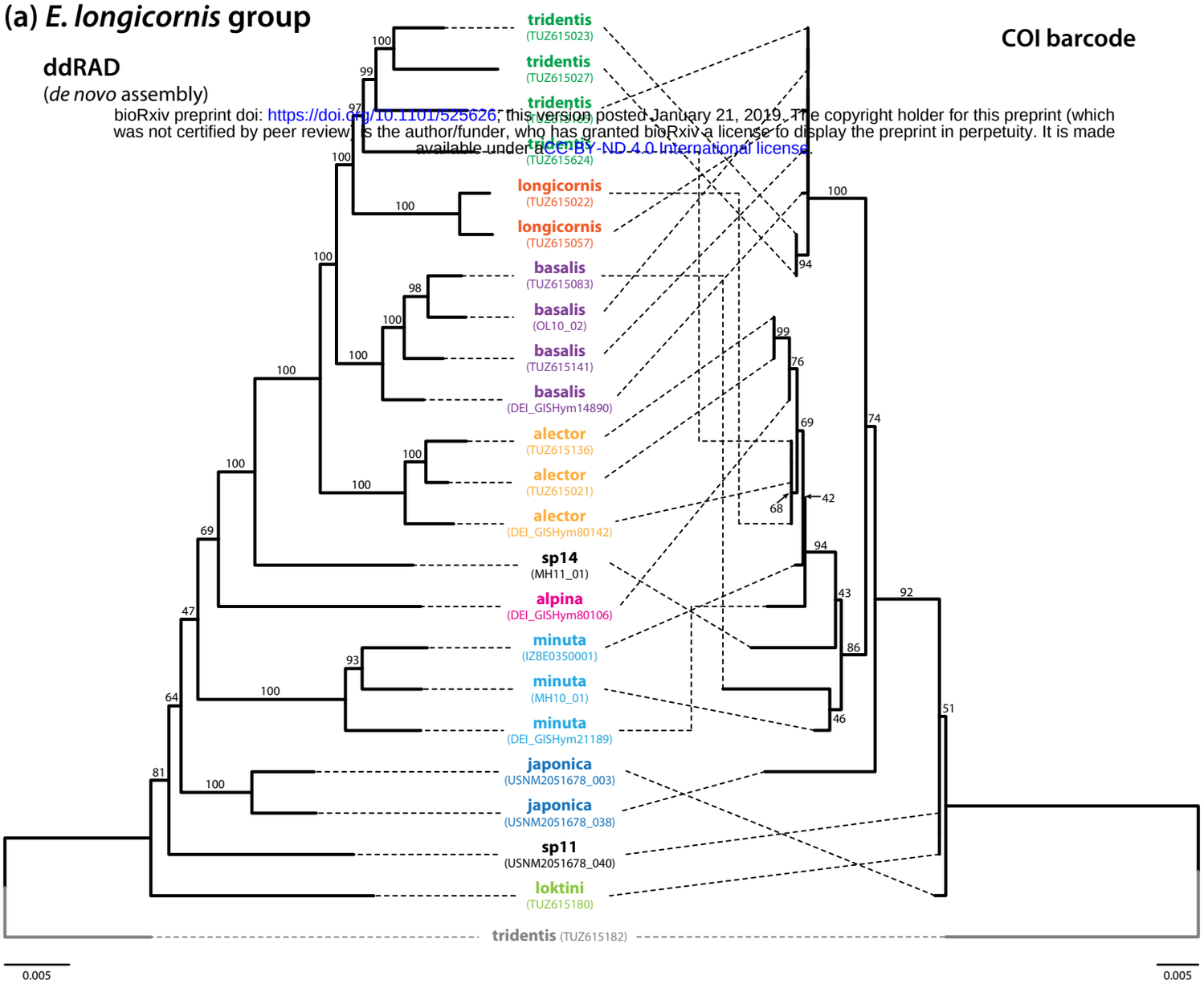

(b) *E. immersa* group